Lsz
9 000004 122402

OF 1915

ANALELE UNIVERSITATII BUCURESTI

fizica

Theoretical Physics • Nuclear Physics • Plasma Physics • Optics and Spectroscopy • Polymeres Physics • Liquid State Physics • Solid State Physics • Biophysics • Electron Physics

ANUL XXX—1981

FIZICA

COMITETUL DE REDACȚIE

Redactor responsabil : Prof. dr. doc. *Gheorghe Brătescu*
Redactor responsabil adj. : Prof. dr. *Ion Petrea*
Membri : Prof. dr. doc. *Vasile Mihu*
Prof. dr. *Grecu Voicu*
Conf. dr. *Constantin Vrejoiu*
Conf. dr. *Dumitru Ciobotaru*
Secretar de redacție : Conf. dr. *Ion Licea*

REDACȚIA
TIPOGRAFIA UNIVERSITĂȚII BUCUREȘTI
Șos. Panduri, nr. 90
Telefon 13 40 00/122

OF 1915

ANALELE UNIVERSITĂȚII BUCUREȘTI

1989

FIZICĂ

1981

BUDAPESTI MŰSZAKI ÉS GAZDASÁGTUDOMÁNYI EGYETEM
Országos Műszaki Információs Központ és Könyvtár
2001

SUMAR • CONTENTS

THEORETICAL PHYSICS

S. TURBATU : Aperiodic Unsteady Transonic Flow Around Bodies of Revolution 3

NUCLEAR PHYSICS

G. VLADUCA : A possible Extension of the HRTW Model for Fissionable Compound Nucleus 9

PLASMA PHYSICS

G. G. BRĂTESCU, MAGDA CAZAN-CORBASCA, CRISTINA DAMACUS : Coefficients d'ionisations dans les vapeurs de l'alcool butilique normal $CH_3-(CH_2)_3-OH$ 13
I. IOVA, MIHAELA ILIE, M. DOBRE : L'effet cavitaire en géométrie cylindrique à injections electronique et ionique dans He ET Ne 19

OPTICS and *SPECTROSCOPY*

N. GR. POPESCU, A. DUMITRICĂ G,. G. BRĂTESCU, T. TUDOR : Electrooptic Light Modulation with Crystals of Class 42 m 25

POLYMERS PHYSICS

I. C. PETREA, LIVIA MARIA IONESCU, E. BARNA, CARMEN RĂDULESCU, C. RĂDULESCU : Sur l'effet memoire dans le polyethylene „Ropol" 35
I. C. PETREA, E. BARNA, C. BUNEA : Configurational Sequence Rules in the Polymeric Tacticity 43

LIQUID STATE PHYSICS

N. FLOREA, V. DIMA : La fonction radiale de distribution, les nombres moyens de coordination et la compressibilite adiabatique des liquides (benzène) 51

C. A. STĂNESCU : A Parametric Solution of the Binary Molecular Models 59

SOLID STATE PHYSICS

H. V. ALEXANDRU, I. DIMA : Crystal Growth Mechanisms in Solutions. 65

V. DOLOCAN, ELENA DOLOCAN : Optical Constants of Bismuth Trioxide Thin Films 71

MOHAMED ISMAIL ABD EL ATI, I. SPÂNULESCU, I. DIMA : The Electrophysical Properties of PbTe and CdTe Thin Films 75

HAMDIA I. ZAYED, I. MUNTEANU, I. DIMA : Photoelectrical Properties of Indium Monoselenide 83

C. CIUCU, S. GEORGESCU : Crystal Field Splitting of the Ground Level $4I_{9/2}$ of Nd^{3+} : YAG 93

BIOPHYSICS

V. GHEORGHE, GABRIELA ANGEL, VIORICA TRANDAFIR, OLGA IONESCU: Fluorimetric Evaluation of Tyrosine Content of Solubilized Collagen 101

ELECTRON PHYSICS

S. I. SPÂNULESCU, V. GHEORGHE, I. SPÂNULESCU : A New Method for Detecting the Second Derivative in Innelastic Electron Tunneling Spectroscopy 107

Budapesti Műszaki Egyetem
Központi Könyvtára
P 151 1982

ANALELE UNIVERSITĂŢII BUCUREŞTI, FIZICA, XXX, 1981, PAG. 3–8

BME KÖZPONTI KÖNYVTÁRA
F
8482
FOLYOIRAT OSZTÁLY

APERIODIC UNSTEADY TRANSONIC FLOW AROUND BODIES OF REVOLUTION

S. TURBATU

Faculty of Physics — University of Bucharest*

ABSTRACT

Subject of the paper are aperiodic unsteady transonic flows. Such flows do exist if a body spontaneously changes its position or shape. An extension of the parabolic method for this case is presented including the solution for a spontaneously produced slender body of revolution. A special case is discussed, the limit $t \to \infty$.

1. Introduction

The study of transonic fluid flows is now as before very actual. Unsteady transonic flow is a specialized area of research which is of considerable interest for basic fluid dynamical reasons and in many engineering problems as well. The study of unseady flows helps one to achieve an improved understanding of steady flows, in particular as to the permanence and realizability of a particular steady flow and how typical transonic nonlinear effects develop in time. The engineering interest derives primarily from the problem of stability of a rigid or flexible flight vehicle; the transonic region is usually found to be the one most susceptible to flutter and other dynamic instability phenomena.

In this paper the perturbation velocity potential for slender bodies of revolution in aperiodic unsteady transonic flow is deduced. Such flows do exist if a body spontaneously changes its position or shape. An extension of the parabolic method for this case is presented including the solution for a spontaneously produced slender body of revolution.

---

* National Center of Physics, P.O.B. MG-11, Bucharest-Măgurele, Romania.

BUDAPESTI MŰSZAKI EGYETEM 1848 KÖZPONTI KÖNYVTÁRA

2. Basic equations and the solution

As is well known, the flow around an obstacle in the nearly sonic free stream is governed by a nonlinear differential equation of mixed type. With the flow directed along the positive y-axis the complete nonlinear differential equation was simplified by assuming the flow to be a small perturbation from a uniform stream near the speed of sound. The resulting equation for unsteady transonic flow is [1]:

$$[1 - M_\infty^2 - M_\infty^2(\gamma + 1)\varphi_x]\varphi_{xx} + \varphi_{yy} + \varphi_{zz} - 2M_\infty^2\, \varphi_{xt} - M_\infty^2 \varphi_{tt} = 0, \quad (1)$$

where M_∞ is the free-stream MACH number : γ is the ratio of specific heats ; x, y, z and t are nondimensional variables such that the body length is $l = 1$; $\varphi(x, y, z ; t)$ the perturbation velocity potential with

$$\varphi_x = \frac{u - u_\infty}{u_\infty}, \quad \varphi_y = \frac{v}{u_\infty}, \quad \varphi_z = \frac{w}{u_\infty}.$$

Here the subscript indicates differentiation.

With the slender body of revolutin orientated along the x-axis and $M_\infty = 1$ we can write the equation (1) as

$$-(\gamma + 1)\, \varphi_x \varphi_{xx} + \varphi_{rr} + \frac{1}{r}\, \varphi_r - 2\, \varphi_{xt} - \varphi_{tt} = 0\,, \quad (2)$$

where

$$r = (y^2 + z^2)^{\frac{1}{2}}.$$

Following the parabolic method introduced in [3]:

$$\varphi_{xx}(x\,; r\,; t) = \text{const.} = a > 0 \quad (3)$$

one can reduce equation (2) to

$$-A\varphi_x + \varphi_{rr} + \frac{1}{r}\,\varphi_r - 2\varphi_{xt} - \varphi_{tt} = 0, \quad (4)$$

where

$$A = a(\gamma + 1).$$

The boundary conditions require that u, v, and w vanish far upstream of the body, and that the flow be tangential to the body surface. The latter condition is approximated in transonic flow theory in exactly the same way as in linear theory. Thus, the appropriate relation for axisymmetric flow past a slender body of revolution having an axial distribution of cross-section area $F(x)$ and $t > 0$ is given by [4]:

$$\lim_{r\to\infty} r\varphi_r(x\,;\,r\,;\,t) = \begin{cases} \dfrac{1}{2\pi} F'(x)\;, & 0 \leqslant x \leqslant 1: \\ 0\;, & x > 1. \end{cases} \tag{5}$$

Applying the LAPLACE transformation

$$\mathscr{L}\{\varphi(x,r\,;\,t)\} = \int_0^\infty \varphi(x,\,r\,;\,t)\mathrm{e}^{-st}\,\mathrm{d}t = \Phi(x,\,r\,;\,s) \tag{6}$$

to equations (4), (5) one gets

$$\Phi_{rr} + \frac{1}{r}\,\Phi_r - K\,\Phi_x - s^2\Phi = 0, \tag{7}$$

$$\lim_{r\to\infty} r\,\Phi_r\,(x, r\,;\,s) = \frac{F'(x)}{2\pi s},\quad 0 \leqslant x \leqslant 1, \tag{8}$$

where

$$K = A + 2s\,. \tag{9}$$

With the substitution

$$\Phi(x, r, s) = \Psi(x, r\,;\,s)\,\mathrm{e}^{-\frac{s^2x}{K}}, \tag{10}$$

the equation (7) one may write

$$\Psi_{rr} + \frac{1}{r}\,\Psi_r - K\,\Psi_x = 0. \tag{11}$$

The solution of equation (11) is

$$\Psi(x, r\,;\,s) = \int_0^x \frac{g^*(\xi\,;\,s)}{x-\xi}\,\exp\left(-\frac{Kr^2}{4(x-\xi)}\right)\mathrm{d}\xi. \tag{12}$$

We return to the function Φ and we have

$$\Phi\,(x, r\,;\,s) = \int_0^x \frac{g(\xi\,;\,s)}{x-\xi}\,\exp\left(-\frac{Kr^2}{4(x-\xi)}\right)\mathrm{d}\xi, \tag{13}$$

where

$$g(x,\,s) = g^*(x,\,s)\mathrm{e}^{-\frac{s^2x}{K}}$$

The function g will be determined by the boundary condition (8). From (13) we obtain

$$r\Phi_r(x, r\,; s) = -\frac{Kr^2}{2}\int_0^x \frac{g(\xi\,; s)}{(x-\xi)^2}\exp\left(-\frac{Kr^2}{4(x-\xi)}\right) d\xi. \tag{14}$$

We now make the substitution

$$x - \xi = r^2\tau.$$

and (14) becomes

$$r\Phi_r(x, r\,; s) = -\frac{K}{2}\int_0^{\frac{x}{r^2}} \frac{g(x-r^2\tau\,; s)}{\tau^2}\exp\left(\frac{-K}{4\tau}\right) d\tau$$

and hence

$$\lim_{r\to 0} r\Phi_r(x, r\,; s) = -2g(x\,; s).$$

With the aid of (8) we have

$$g(x\,; s) = -\frac{F'(x)}{4\pi s}, \quad 0 \leqslant x \leqslant 1. \tag{15}$$

Using equation (15) then, equation (13) can be written as

$$\Phi(x,r\,; s) = -\frac{1}{4\pi}\int_0^x \frac{F'(x)}{(x-\xi)s}\exp\left(-\frac{Kr^2}{4(x-\xi)}\right) d\xi. \tag{16}$$

This is the solution of the boundary problem defined by the equations (7), (8)

The inversion to the perturbation velocity potential φ is easily carried out by aid of the following formulas [2]:

$$\mathscr{L}^{-1}\{s^{-\frac{1}{2}}\} = (\pi t)^{-\frac{1}{2}},$$

$$\mathscr{L}^{-1}\left\{s^{-\frac{1}{2}}\exp\left(-\frac{r^2 s}{2(x-\xi)}\right)\right\} = \begin{cases} \pi^{-\frac{1}{2}}\left(t - \dfrac{r^2}{2(x-\xi)}\right)^{-\frac{1}{2}}, & t > \dfrac{r^2}{2(x-\xi)}; \\ 0, & t < \dfrac{r^2}{2(x-\xi)}. \end{cases}$$

Then from equation (16) and using the convolution theorem for LAPLACE transform, we obtain [6]:

$$\varphi(x, r\,;\, t) = -\frac{1}{4\pi^2 i}\int_0^x \frac{F'(\xi)}{x-\xi}\exp\left(-\frac{Ar^2}{4(x-\xi)}\right)\times$$

$$\times \ln\frac{r+\sqrt{2t(x-\xi)}}{r-\sqrt{2t(x-\xi)}}\,\mathrm{d}\xi, \quad t > \frac{r^2}{2(\xi x-\xi)} \tag{17}$$

This is the solution of the boundary value problem defined by equations (4), (5).

3. A special case

In the particular case $t \to +\infty$ and $a = a^*$ the potential φ reduces to the potential φ^* for a steady flow given in [3], [5]:

$$\lim_{t\to\infty} \varphi(x, r\,;\, t) = \varphi^*(x, r) = -\frac{1}{4\pi}\int_0^x \frac{F'(\xi)}{x-\xi}\exp\left(-\frac{Ar^2}{4(x-\xi)}\right)\mathrm{d}\xi, \tag{18}$$

where

$$a^* = \varphi^*_x(x, r) = \text{const.} > 0.$$

With the substitution

$$\frac{Ar^2}{4(x-\xi)} = u$$

and by the Taylor expansion of $F'\left(x - \dfrac{Ar^2}{4u}\right)$,

$$\varphi^*(x, r) = -\frac{1}{4\pi}\sum_{n=0}^{\infty}\frac{(-1)^n}{n!}F^{(n+1)}(x)\left(\frac{Ar^2}{4}\right)^n \times$$

$$\times \int_{\frac{Ar^2}{4x}}^{+\infty}\frac{e^{-u}}{u^{n+1}}\,\mathrm{d}u, \quad 0 < x < 1. \tag{19}$$

Integrations in (19) can be much simplified by the recurrence relation

$$J_{n+1} = \frac{1}{n!}\left(\sum_{k=0}^{n-1}(-1)^k(n-k-1)!\;\frac{\exp\left(-\dfrac{Ar^2}{4x}\right)}{(Ar^2/4x)^{n-k}} + \right.$$

$$\left. + (-1)^n J_1\right)_i \quad n \in N,$$

where

$$J_{\mathrm{n}} = \int_{\frac{Ar^2}{4x}}^{+\infty} \frac{e^{-u}}{u^n}\, \mathrm{d}u\,,$$

and

$$J_1 = Ei\left(\frac{Ar^2}{4x}\right) = -\,C - \log\frac{Ar^2}{4x} + \frac{Ar^2}{4x} + $$

$$+\,0\left(\left(\frac{Ar^2}{4x}\right)^2 \log\frac{Ar^2}{4x}\right).$$

Consequently

$$\varphi^*(x.\ r) = \frac{1}{4\pi} F'(x) \log\frac{e^{\mathrm{C}}\, Ar^2}{4x} - \frac{1}{4\pi} \sum_{n=1}^{\infty} F^{(n+1)}_{(x)} \cdot \frac{(-1)^n}{n\cdot n\,!}\, x^n +$$

$$+\,0(t^4 \log t) \qquad 0 < x < 1,$$

where C is Euler's Constant.

REFERENCES

1. M. T. LANDAHL. *Unsteady transonic flow*, Pergamon Press (1961)

2. F. OBERHETTINGER – L. BADII, *Tables of Laplace transforms*, Springer-Verlag, Berlin Heidelberg New-York (1973)

3. K. OSWATITSCH – F. KEUNE, *Proc. Conf. on High Speed Aeronautics*, Polytech. Inst. Brooklyn (1955).

4. J. ZIEREP, *Theorie der Schallnahen und der Hyperschallströmungen*. G. Braun, Karlsruhe (1966)

5. I. HOSOKAWA, Jour. Phys. Soc. Japan, vol. 15, No. 1, (1960)

6. S. TURBATU, *Symposium Transsonicum II*, Springer-Verlag, Berlin Heidelberg New-York, (1976).

Received, 5, December, 1980

ANALELE UNIVERSITĂŢII BUCUREŞTI, FIZICA, XXX, 1981, PAG. 9–12

A POSSIBLE EXTENSION OF THE HRTW MODEL FOR FISSIONABLE COMPOUND NUCLEUS

G. VLADUCA

Faculty of Physics, University of Bucharest *

ABSTRACT

A possible version of the HRTW's formalism for the nuclear reactions, leading to a fissionable compound nucleus, in wich the unitarity of the S-matrix is taken into account, is described.

The statistical model of nuclear reactions has been applied for many years to the analysis of experimental data either in his original form [1] or in the modified version given by Moldauer [2].

Engelbrect and Weidenmüller [3] have shown that these theories could be consistently derived only in the limit of weak absorption in all channels. Relatively recently the statistical model was extended by Hofmann, Richert, Tepel and Weidenmüller [4] (HRTW) to describe the medium and strong absorption too.

The purpose of this note is to study a possible extension of the HRTW model for fissionable compound nucleus. In this case it is necessary to consider competition of particle, gamma-ray and fission decay.

Using the HRTW's ideas we hope that the fluctuation (or energy averaged compound nucleus) cross section $<\sigma_{ab}^{fl}>$ factorizes into a part depending on the entrance and one depending on the exit channel only. Thus, up to geometrical and kinematical factors and for a single value of the spin J and parity π of the compound nucleus, the fluctuation cross sections for elastic, inelastic and gamma-ray of fission decay, will be :

$$\langle\sigma_{aa}^{fl}\rangle = \frac{P_a^2}{N(J,\pi)} G_a \tag{1}$$

$$\langle\sigma_{ab}^{fl}\rangle\rangle = \frac{P_a \cdot P_b}{N(J,\pi)} \tag{2}$$

$$\langle\sigma_{ai}^{fl}\rangle = \frac{P_a T_i}{N(J,\pi)} \tag{3}$$

---

* National Centre of Physics, Măgurele-Bucharest P.O.Box. 5211

where a, b, c...denote the open particle channels and T_i^γ or T_i^f are the gamma-ray or fission transmission coefficients. The denominator $N(I, \pi)$ is defined as the sum of transmission coefficents for all open channels :

$$N(I, \pi) = \sum_b P_c + \sum_i T_i \tag{4}$$

For the elastic case an enhancement factor Ga has been introduced since the partial widths for entrance and exit channel are identical and-hence, correlated. The equations (1) ÷ (3) indicate how the additional flux drained into elastic channel by enhancement is taken from the various reaction channels. These equations are of a similar structure as those of Hauser-Feshbach and therefore we could think of the factors P_a as effective particle transmission coefficients.

In the following we shall assume that the transmission coefficients T_i for gamma and fission decay are well defined and thus our aim is to determine the P_a factors. By using the unitarity relation :

$$T_a = \sum_b \langle \sigma_{ab}^{fl} \rangle + \sum_i \langle \sigma_{ai}^{fl} \rangle \tag{5}$$

where T_a is the optical model transmission coefficients, we find :

$$T_a = P_a \left[1 + \frac{P_a}{N(I, \pi)} (G_a - 1) \right] \cdot \tag{6}$$

It has been demonstrated [4] that the quadratic equation (6), in the case of particle channels ($\sum_i T_i = 0$), has a unique positive solution, and, thus $\langle \sigma_{ab}^{fl} \rangle$ is an unique function of the optical transmission coefficients and enhancement factors G_a. In turn, G_a are mainly functions of T_a and depend weakly on transmission coefficients in other particle channels. The equation (6) is solved iteratively, by replasing, as a first approximation $P_a/\sum_c P_c$ by $T_a/\sum_c T_c$:

$$P_a^{HRTW} = T_a \left[1 + \frac{T_a}{\sum_c T_c} (G_a - 1) \right]^{-1} \tag{7}$$

with :

$$G_a - 1 = 2[1 + T_a^{0.3 + 1.5 T_a \Sigma_c T_c}]^{-1} + 2[(T_a - \bar{T}) / \sum_c T_c]^2 \tag{8}$$

$$\bar{T} = \sum_c T_c / \mathcal{N} \tag{9}$$

where $\mathcal{N}$ is the number of open particle channel.

Phenomenological equation (8) has been empiricaly chosen so that the results for the fluctuation cross sections are in good agrement with computer-generated „experiments'' obtained from a random matrix model. Following the same procedure and assuming that G_a remain unchanged, with :

$$P_a/\sum_c P_c \simeq T_a/\sum_c T_c \tag{10}$$

as a first approximation for particle channels only, the unitarity relation (6) may be solved iteratively giving :

$$P_a^{(n+1)} = 2\frac{P_a^{(n)}}{\sum_c P_c^{(n)}}(\sum_i T_i)\left[\left(1+\frac{P_a^{(n)}}{\sum_c P_c^{(n)}}\cdot\frac{\sum_i T_i}{T_a}\right)\times\right.$$
$$\left.\times\left(1+\frac{4(P_a^{(n)})^2 T_a(\sum_i T_i)(G_a-1)}{(T\sum_c P_c^{(n)}+P_a\sum_i T_i)^2}\right)^{1/2}-\left(1-\frac{P_a^{(n)}}{\sum_c P_c^{(n)}}\cdot\frac{\sum_i T_i}{T_a}\right)\right]^{-1} \tag{11}$$

with :

$$P_a^{(0)} = T_a \tag{12}$$

The iteration procedure is continued till the fluctuation cross sections stabilise within a prescribed margin of error.

A more simplified expression for coefficients $P_a^{(n+1)}$ can be obtained in the case :

$$\frac{4(P_a^{(n)})^2 T_a(\sum_i T_i)(G_a-1)}{(T_a\sum_c P_c^{(n)}+P_a^{(n)}\sum_i T_i)^2} \ll 1 \tag{13}$$

Significant deviations from relation (13) may occur only in the case when one particle chanel dominates the absorption, $P_a^{(n)} > \sum_{c\neq a} P_c^{(n)}$, or $\sum_i T \gg \sum_c P_c^{(n)}$. Otherwise the inequality (13) is holds true and one obtains :

$$P_a^{(n+1)} = T_a\left[1+\frac{P_a^{(n)}}{\sum_c P_c^{(n)}+\frac{P_a^{(n)}}{T_a}\sum_i T_i}(G_a-1)\right]^{-1}. \tag{14}$$

The relation (14) is more convenient for calculations and coefficients $P_a^{(n+1)}$ thus obtained are a good approximation of those derived from (11).

When the number of open channels is large, the first approximation is an adequate one. In this case one obtains :

$$P_a^{(1)} = T_a\left[1 + \frac{T_a}{\sum_c T_c + \sum_i T_i}(G_a - 1)\right]^{-1} \tag{15}$$

One can note the similar structure of equation (15) and (7). This suggests the possible alternative of using the HRTW's equations (7) ÷ ÷ (9) by replasing the sum $\sum_c T_c$ by $\sum_c T_c + \sum_i T_i$. It is interesting to observe that by this substitution $(G_a - 1)$ in (8) will decrease somewhat and consequently $P_a^{(1)}$ in equation (15) increase. Mathematically this increase is in the favourable direction, $P_a^{(1)}$ thus calculated being a better approximation of $P_a^{(1)}$ given by equation (11). From another point of vue, this substitution is also preferable since calculation is easier to handle and HRTW's statistical model could be applied just by replasing $\sum_c T_c$ by $\sum_c T_c + \sum_i T_i$ for the case of fissionable compound nucleus also.

To conclude, we propose to use the HRTW'S statistical model in this version when the cases under considerations fulfill the necessary requirements of using the first approximation (15) — the most frequently case- or the relations (11) or (14) with G_a from (8), in the cases where the number of channels is small.

We think that formulae (1)÷(3), in which the effective transmision coefficients P_a are computed following the procedure just described, where the unitarity of the S-matrix is taken into account, are to be used in the theoretical analysis of the experimental data. Clearly, a direct comperison with experimental data would be desirable and welcomed.

REFERENCES

1. W. HAUSER, H. FESHBACH, Phys. Rev., *87*, 366 (1952)
2. P. A. MOLDAUER, Phys. Rev., *135*, B642 (1964)
3. C. A. ENGELBRECHT, H. A. WEIDENMÜLLER, Phys. Rev., *C8*, 859 (1973)
4. H. M. HOFMANN, J. RICHERT, J. W. TEPEL, H. A. WEIDENMÜLLER, Ann. Phys., *90*, 403 (1975)

Received, February 18, 1981

ANALELE UNIVERSITĂŢII BUCUREŞTI, FIZICA, XXX, 1981, PAG. 13–17

COEFFICIENTS D'IONISATIONS DANS LES VAPEURS DE L'ALCOOL BUTILIQUE NORMAL $CH_3-(CH_2)_3-OH$

G.G. BRĂTESCU, MAGDA CAZAN-CORBASCA

Faculté de Physique, Université de Bucarest*

CRISTINA DAMACUS

L'entreprise d'appareils et outils pour la recherche scientifique **

RÉSUMÉ

On a calculé les valeurs des coefficients α et γ de Townsend et tracé les courbes $\frac{\alpha}{p_0} = f\left(\frac{E}{p_0}\right)$; $\eta^{-1} = f\left(\frac{E}{p_0}\right)$ et $\gamma = f\left(\frac{E}{p_0}\right)$ dans les vapeurs de l'alcool butilique normal, pour des electrodes de Al et Ni. On a comparé les résultats obtenus avec ceux de l'alcool propilique normal.

1. Introduction

Les résultats publiés dans cet ouvrage se situent dans le domaine des recherches effectuées sur les vapeurs des divers alcools [1 – 3].

On a caculé les valeurs des coefficients d'ionisation en volume, de Townsend, α, et on a tracé les courbes $\frac{\alpha}{p_0} = f\left(\frac{E}{p_0}\right)$ et $\eta^{-1} = f\left(\frac{E}{p_0}\right)$, où p_0 est la pression reduite du gaz à 0°C, E, l'intensité du champ électrique et $\eta = \frac{\alpha}{E}$.

Les coefficients α ont été calculés en employant la relation [4, 5]

$$\frac{\alpha}{p_0} = A\, e^{-\frac{B}{\frac{E}{p_0}}} \qquad (1)$$

---

* Centre National de Physique, Măgurele – Bucarest, B.P. 5211

** Rue de la Fabrique, sect. VII – Bucarest où le coefficient A est provenu de la littérature [6] et le coefficient B a été calculé des données expérimentales obtenues par les auteurs [7], à l'aide de la relation [8]

$$B = \frac{V_{\min}}{(p\, d)_{\min}} \tag{2}$$

où $V_{\min}$ est le potentiel explosif minime, p — la pression du gaz et d-la distance entre les électrodes.

Dans un ouvrage antérieur [2] sont données des detailles concernant l'installation expérimentale.

On a calculé aussi les valeurs des coefficients d'ionisation superficielle de Townsend, γ, en employant la relation [8]

$$V = \eta^{-1} \ln\left(1 + \frac{1}{\gamma}\right) \tag{3}$$

On compare les résultats obtenus sur l'alcool butilique à ceux obtenus antérieurement dans le cas de l'alcool propilique [2].

2. Résultats

Les figures (1) et (2) représentent les courbes $\frac{\alpha}{p_0} = f\left(\frac{E}{p_0}\right)$ et $\eta^{-1} = f\left(\frac{E}{p_0}\right)$ dans les vapeurs de l'alcool butilique par comparaison à celles obtenues dans les vapeurs de l'alcool propilique, pour des électrodes de Al et de Ni.

Les figures (3) et (4) représentent les courbes $\gamma = f\left(\frac{E}{p_0}\right)$ dans les vapeurs de l'alcool butilique, comparées, de même, avec celles obtenues dans les vapeurs de l'alcool propilique pour des électrodes de Al et de Ni.

On a effectué des déterminations pour les valeurs du raport $\left(\frac{E}{p_0}\right)$ situées dans les domaines :

$400 \leqslant \frac{E}{p_0} \leqslant 4000$ V cm^{-1} Torr^{-1} pour le Al et

$700 \leqslant \frac{E}{p_0} \leqslant 3500$ V cm^{-1} Torr^{-1} pour le Ni.

On a obtenu pour le coefficient B les valeurs :

$B = 1293{,}78$ V cm^{-1} Torr^{-1} pour les électrodes de Al et $B = 1797{,}10$ V cm^{-1} Torr^{-1} pour les électrodes de Ni.

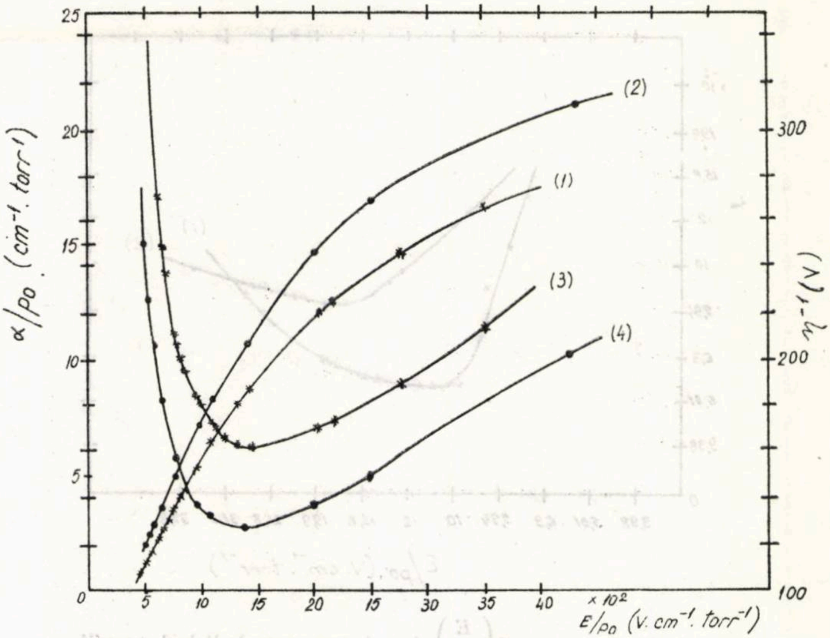

Fig. 1. Les courbes $\frac{\alpha}{p_0} = f\left(\frac{E}{p_0}\right)$ et $\eta^{-1} = f\left(\frac{E}{p_0}\right)$ dans les vapeurs de l'alcool propilique (1), (3) et butilique (2), (4) pour l'éectronde de Al.

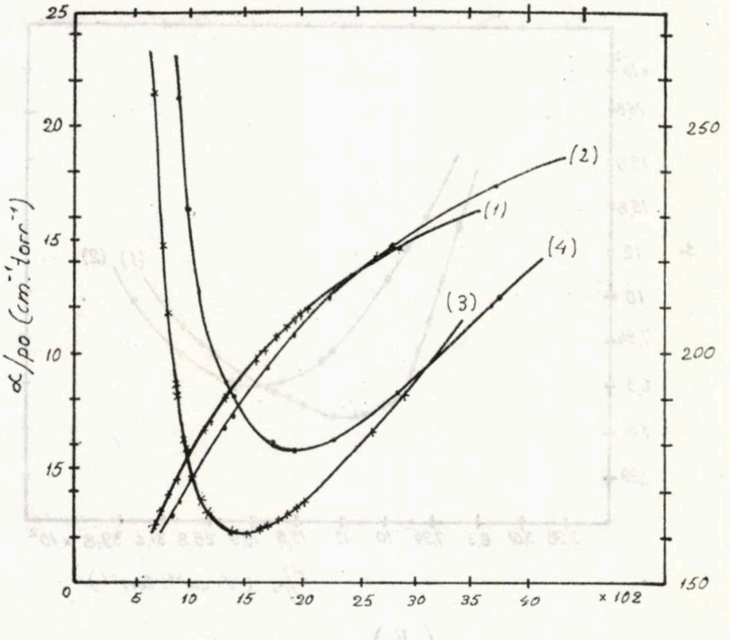

Fig. 2. Les courbes $\frac{\alpha}{p_0} = f\left(\frac{E}{p_0}\right)$ et $\eta^{-1} = f\left(\frac{E}{p_0}\right)$ dans les vapeurs de l'alcool propilique (1), (3) et butilique (2), (4) pour l'électrode de Ni.

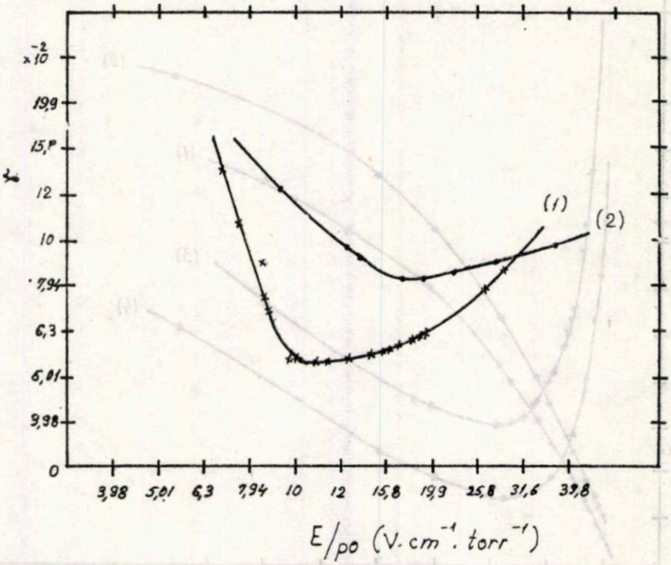

Fig. 3. Les courbes $\gamma = f\left(\frac{E}{p_0}\right)$ dans les vapeurs de l'alcool propilique (1) et butilique (2) pour l'électrode de Al.

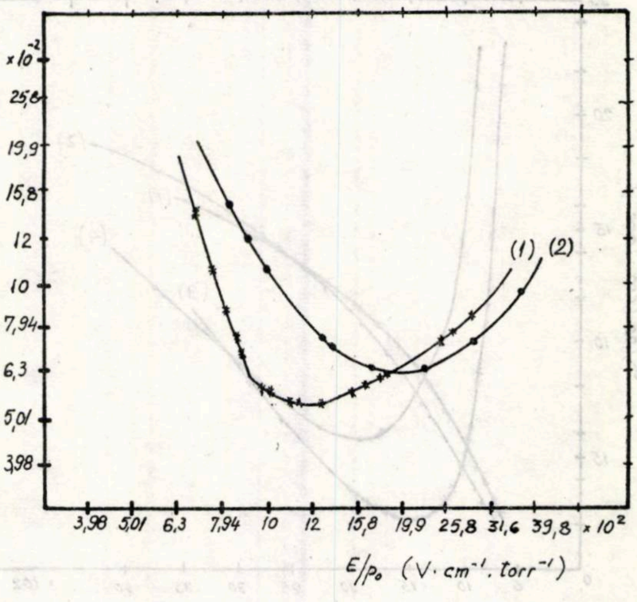

Fig. 4. Les courbes $\gamma = f\left(\frac{E}{p_0}\right)$ dans les vapeurs de l'alcool propilique (1) et butilique (2) pour l'électrode de Ni.

3. Conclusions

On constate que les valeurs du coefficient α dans le cas de l'alcool butilique sont très proches de celles obtenues à l'alcool propilique, la structure moléculaire des deux substances étant ressemblante.

Dans les leux cas, les courbes $\frac{\alpha}{p_0} = f\left(\frac{E}{p_0}\right)$, $\eta^{-1} = f\left(\frac{E}{p_0}\right)$ et $\gamma = f\left(\frac{E}{p_0}\right)$ ont l'allure ressemblante des courbes obtenues en d'autres substances organiques [8].

Dans les substances organiques, celles-ci ayant la structure moléculaire complexe, ont lieu un grand nombre de processus élémentaires dans le volume du gaz [4, 9].

Malgré le grand nombre d'impacts entre les électrons, qui se déplacent dans la direction du champ électrique appliqué entre les électrodes, et les molécules du gaz, le rendement d'ionisation est bas, parceq'une partie de l'énergie reçue par les électrons de l'extérieur se consomme dans une serie de processus non suivis d'ionisation comme : excitations, dissociations, etc.

Le coefficient γ dans les substances organiques prend généralement des valeurs basses, l'extraction de la cathode étant faite à un bas rendement.

On peut expliquer cela par le fait que le nombre des ions positifs qui arrivent à la cathode est petit, une partie de ces ions crées dans le gaz, n'ayant pas l'énergie suffisante pour arriver à la cathode et pour extraire des électrons, fait valable aussi pour les photons et les atoms métastables.

Les auteurs considèrent que les explicationes données sont valables aussi dans le cas de l'alcool butilique.

BIBLIOGRAPHIE

1. A. T. NICOLAU, E. PASCU, M, CAZAN – CORBASCA, P. POPESCU. Studii şi cercetări de Fizică, *20*, 799 (1968)
2. G. G. BRĂTESCU, M. CAZAN-CORBASCA, Anal. Univ. Bucureşti, Fizică, *27*, 11 (1978)
3. G. G. BRĂTESCU, M. CAZAN-CORBAŞCA, Anal. Univ. Bucureşti, Fizică, *29*, 9 (1980)
4. G. G. BRĂTESCU, *Fizica Plasmei*, Ed. Didactică şi Pedagogică, Bucureşti, p. 407, 409 (1970)
5. L. LOEB, *Basic Processes in Gaseous Electronics*, University of California, Press Berkley and Los Angeles, p. 647, (1955)
6. M. NARAYANA SWAMY, J. A. HARRISON, Brit. J. Appl. Phys., *18*, 781 (1967)
7. G. G. BRĂTESCU, M. CAZAN-CORBASCA, C. MARMANDIU, Buletinul Inst. de Petrol şi Gaze, Ploieşti, *8*, 73 (1978)
8. E. BĂDĂRĂU, I. POPESCU, Gaze Ionizate, Ed. Tehnică, Bucureşti, p. 21, 35 (1965)
9. M. VALERIU, Thèse, Univ. Bucarest, 1943.

Reçue 5 Janvier 1981

BUDAPESTI MŰSZAKI EGYETEM 1848 KÖZPONTI KÖNYVTÁRA *

ANALELE UNIVERSITĂŢII BUCUREŞTI, FIZICA, XXX, 1981, PAG. 19–33

L'EFFET CAVITAIRE EN GÉOMÉTRIE CYLINDRIQUE À INJECTIONS ELECTRONIQUE ET IONIQUE DANS He ET Ne

I. IOVA, MIHAELA ILIE

Faculté de Physique Université de Bucarest*

M. DOBRE

Institute Polytechnique de Bucarest, Departement de Physique

RÉSUMÉ

On étudie une nouvelle forme de la decharge electriques luminescente en He et Ne, a une grande amplification du courant et des radiations. realisé par des injections électroniques ou ioniques, dans des cavités crées par des electrodes cylindriques coaxiales.

1. Les bases physiques de l'effet de la ,,cathode creuse"

On appelle ,,cathode creuse", la cathode dont la surface de travail a une courbure negative, ou celle constituée d'un système de surfaces qui créent une cavité dans laquelle se localise la décharge electrique. Il est connu que les électrons primaires, accélérés dans l'espace sombre cathodique, ont des propriétés de faisceau perpendiculaire à la surface de la cathode. A cause de ca, l'utilisation, d'une cathode concave a un effet de focalisation des électrons primaires, ce qui conduit à une grande augmentation d'ionisation en lumière négative. Cela fait que, pour l'entretien du même courant de décharge, une chute cathodique beaucoup plus petite soit nécessaire ou, autrement dit, pour une même chute cathodique, le courant soit de quelques ordres de grandeur plus grand que dans le cas de la cathode plane.

Cet article a pour sujet l'etude de l'effet cavitaire dans une décharge électrique en régime luminescent, par un gaz monoatomique (Ne), en utilisant des électrodes, de géométrie cylindriques, coaxiales (Fig. 1)

---

* Centre National de Physique, Măgurele, Bucarest, B.P. 5211

Au point de vue qualitatif, l'effet de la „cathode creuse" s'explique ainsi : à cause de la géometrie speciale, se produit une superposition de l'action ionisante des électrons primaires, dans la lumière négative comune des deux électrods. L'augmentation de l'ionisation en lumière négative est due également au fait que, les électrons primaires à haute énergie, une fois injectés dans le plasma de la lumière négative, sont retenus là bas, par les hautes barrières de potentiel de la chute cathodique.

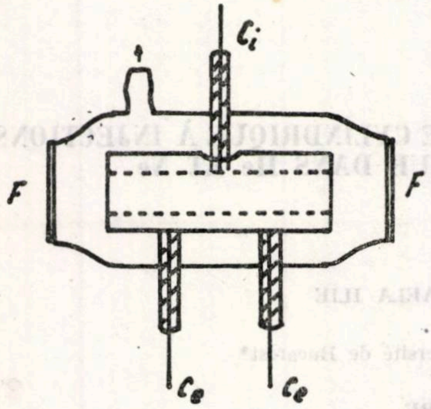

Fig. 1. Le schema du tube de la décharge électrique, avec des électrodes cylindriques coaxiales

La géométrie de la cathode concave réduit beaucoup les pertes de porteurs de charge, par diffusion ambipolaire.

En principe, le mécanisme des excitations et des ionisations dans les parties cathodiques, dans les conditions de l'effet de la „cathode creuse" est le même que celui de la décharge luminescente anormale. Ainsi, en utilisant les paramètres Vc, j/p_0^2, p_0d, dans le cas de la décharge anormale, on obtient la relation de similitude [1], [2] :

$$\frac{j}{p_0^2} = \frac{1}{\sqrt{18}}\left(\frac{5}{3\pi}\right)^{3/2}\left(\frac{\mathrm{e}}{m_p Q_t}\right)^{1/2} V_c^{3/2}\ (\mathrm{p}_0\,\mathrm{d})^{-5/2}$$

où e et m_p sont respectivement la charge et la masse d'ion Q_t la section efficace de transfert resonnant de charge.

La vitesse des ions correspondante à Q_t, est égale avec la vitesse d'entraînement moyenne, v_m, des ions positifs dans l'espace sombre.

$$v_m = \frac{3}{4}\left(\frac{12\,\mathrm{e}}{\mathrm{m}_p\, Q_t} \cdot \frac{j}{p_0^2} \cdot \mathrm{p}_0\mathrm{d}\right)^{\frac{1}{2}}$$

Les valeurs experimentales obtenues pour Q_t sont en (bon) accord avec le calcul quantique qui mène à l'expression :

$$\sqrt{Q} = A - B \log v$$

où

$$A = \frac{3{,}1.\ 10^{14}}{\alpha\sqrt{I}}\ \mathrm{In}\ (3{,}86\ \mathrm{e}^{31}\ \alpha\sqrt{I})$$

$$B = \frac{7{,}1.\ 10^{14}}{\alpha\sqrt{\mathrm{I}}},$$

I étant l'énergie de première ionisation, et α — la correction adéquate de la fonction d'essai hydrogénoide :

$$\psi(r) = \frac{\alpha^{3/2}}{\sqrt{\pi}} \left(\frac{Z^*}{n^* a_0} \right)^{3/2} \exp\left(-\alpha \frac{Z^*}{n^* a_0} r \right)$$

Pour les calculs antérieurs on a considéré que dans le cas de la décharge anormale, les électrons primaires sont extraits de la cathode prépondérément par bombardement ionique et que, dans l'espace sombre, le procès prépondérent est celui de transfert résonnant de charge en modèle „estafette anisotrope'', la plupart des excitations et ionisations se produisant par collisions en lumière négative.

Vues les hypothèses antérieures et, également, le fait que le distribution des électrons d'après les énergies dans l'espace sombre, ne dépend pas de la géométrie de l'électrode, le modele peut être élargé a une géométrie cylindrique [3] [4] :

Dans ce cas, résulte la relation de similitude :

$$\frac{j}{p_0^2} = \frac{\mathrm{e}(1 + \gamma_i)}{\sqrt{8\pi^3 \, \mathrm{m}_p Q_t}} \cdot \frac{U_k^{2/3}}{p_0^{5/2}[F(R, r_0)]^{3/2}}$$

où γ_i est le nombre d'électrons extraits de la cathode par un ion, R-le rayon intérieur de la cathode, r_0 — le rayon de la lumière négative, U_k — — le potentiel à la cathode, et $F(R, r_0)$ — la fonction :

$$F(R, r_0) = \int_{r_0}^{R} \left[1 - \left(\frac{r_0}{r} \right]^{3/2} \right]^{2/3} \mathrm{d}r$$

Un nouveau type d'effet cathodique *cavitaire* en géométrie cylindrique est l'effet *cavitaire* à injection controlée électronique et ionique. On utilise un système de deux cavités cylindriques coaxiales. Le cylindre intérieur est fait en tamis, de telle manière, qu'en fonction de la polarité des connexions, dans la cavité pénètrent des électrons ou des ions, c'est-à-dire, qu'une injection électronique ou ionique se produise.

Dans le cas où l'électrode interieure joue le rôle d'anode (injection électronique), pour Ne, la relation de similitude s'écrit :

$$\frac{j}{p_0^2} = 8{,}82.\ 10^5 \frac{1}{\sqrt{Q_t \, p_0^{5/2}}} \left[\frac{U}{F(R, r_0)} \right]^{3/2}$$

Lorsque l'électrode intérieure fonctionne en régime de cathode (injection ionique), on remarque une forte amplification (exponentielle) du courant, qui n'est pas obtenue dans le cas de l'effet de la cathode cavitaire plane ou cylindrique, même en régime de décharge fort anormal.

Les recherches effectuées sur He [5] ont mis en évidence la grande intensité de courant dans le cas i.i. par rapport à i.e. Dans certaines conditions, ont été obtenues pourtant (pour de petites tensions), des intensités de la radiation plus basses pour i.i. par rapport à i.e.

2. Techniques expérimentales Des resultats. Discutions

On a utilisé un tube de cuartz, avec deux électrodes cylindriques coaxiales. Les décharges ont été réalisées en néon aux pressions $p_1 = 1,31$ torr et $p_2 = 3,53$ torr. En faisant l'analyse spectrale de la radiation, nous avons retenu pour analyse la raie atomique de 5852,48 Å parmi les plus intenses raies du Ne en visible.

En tracant le graphique $j/p_0 = f(U)$ pour le cas i.e. et i.i., (Fig 2 *a*, Fig. 2*b*, respectivement) on observe que l'amplification du courant est plus grande dans le cas i.i.

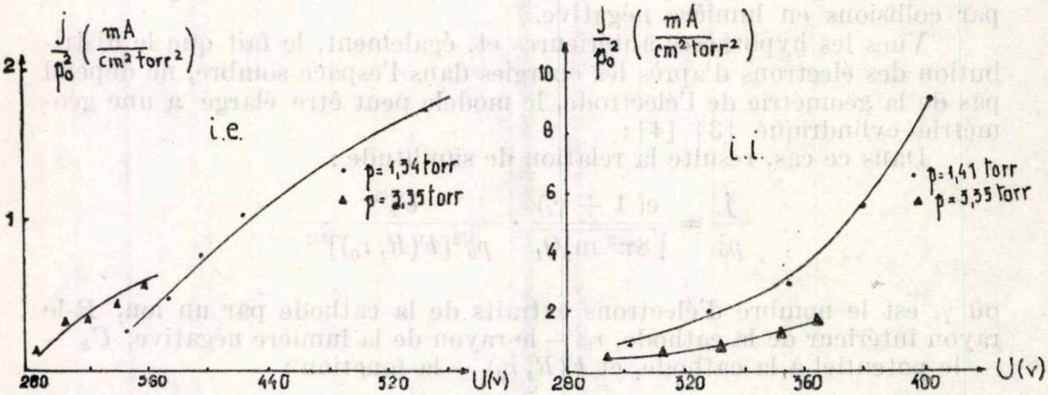

Fig. 2. La dependance $j/p_0^2 = f(U)$ pour les cas de l'injection électronique (a) et ionique (b)

De même, la tension d'allumage dans le cas i.i. est plus basse que pour i.e. Lors de l'augmentation de la pression, l'effet d'amplification et les valeurs absolues du j/p^2 diminuent, ce qui indique une plus grande efficience de l'effet pour les basses pressions.

Dans le cas i.e. apparait une tendence de saturation de l'effet, qui ne s'observe pas pour le cas i.e., dans le domaine des tensions exploré.

La comparaison avec les résultats obtenues en He indique une efficience plus élevée de l'effet cavitaire en He, ce qui, d'ailleurs, résulte et de la dépendance

$$j/p_0^2 \sim \frac{1}{\sqrt{m_p}}$$

Représentant l'intensité relative de la radiation lumineuse en fonction de la tension, (Fig. 3a, Fig. 3b), on observe la forte amplification de la radiation lumineuse dans le cas i.i., ainsi que le fait que l'intensité relative a des valeurs absolues beaucoup plus basses dans le cas i.e.

Ces résultats s'expliquent par le fait que i.e. peut être considérée un effet anodique, *cavitaire*, beaucoup plus faible que celui cathodique, tandis que i.i. est un effet cathodique „stimulé".

L'effet peut être utilisé au perfectionnement des sources spectrales pour la spectroscopie à haut pouvoir de résolution, au générateurs ioniques pour les éléments aux petits potentiels d'ionisation, aux sources d'oscillations de hautte fréquence, aux dispositifs de fusion des métaux, ainsi que, à l'excitation du milieu actif *laser*.

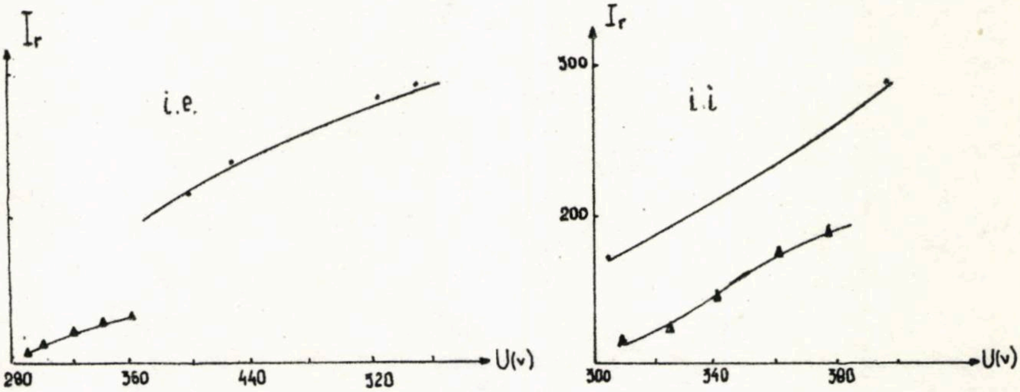

Fig. 3. L'intesité relative de la radiation Ne I λ 5842,48Å, en fonction de la tension, pour es deux cases : i.e. (a), i.i. (b)

RÉFÉRENCES

1. E. BĂDĂRĂU, I. I. POPESCU, *Gaze ionizate* Ed. Tehnică 1963, 1965
2. E, BĂDĂRĂU, I. I. POPESCU, I. IOVA Annalen der Physik *5*, 308 (1950)
3. I. IOVA, A. LUNK, N. DOBRE *Topics in Physics*, Central Institute of Physics Bucharest, p. 21 (1980)
4. I. IOVA, M. DOBRE, S. KATRIB „Revue Roumain de physique" *24* (9), 1979
5. I. IOVA, M. DOBRE, A. IOAN Sesiunea „Progrese în fizică" a ICEFIZ București 21 – 22 iunie 1979 ; Rev. Roum. Phys. *25*, 6, 657 (1980)

Reçue, 15 Décembre, 1980

ANALELE UNIVERSITĂȚII BUCUREȘTI FIZICA XXX 1981, PAG. 25–33

ELECTROOPTIC LIGHT MODULATION WITH CRYSTALS OF CLASS $\bar{4}2$ m

N. GR. POPESCU, A. DUMITRICA
Institute for Physics and Technology for Radiation Devices*
G .G. BRĂTESCU, T. TUDOR
Faculty of Physics, University of Bucharest **

ABSTRACT

The construction, performance characteristics and modulation possibility of various types of KDP and ADP light modulators with longitudinal and transverse electrooptic effect are discussed and presented. We used and experimental arrangement for verification of these modulators in intensity, phase and single-sideband suppressed-carrier modulation by direct optical detection or homodyne optical detection.

1. Electrooptic effect in crystals of class $\bar{4}2$ m

Electrooptic modulation utilizes the change of optical properties caused, in some materials, by an applied electric field. So, certain crystals and liquids become birefringent in the presence of an electric field. The most widely know electrooptic crystals are potassium dihydrogen phosphate (KDP) and ammonium dihydrogen phosphate (ADP), which are transparent at the visible and near infrared region of the spectrum. They are tetragonal crystals of class $\bar{4}2$m, which exchibit linear (Pockels) electrooptic effect.

The optical properties of a crystal are frequently described in terms of the index ellipsoid (or Indicatrix) ; for KDP, ADP and their isomorphes, the equation of the indicatrix, in the absence of an applied electric field, is :

$$\frac{x^2}{n_0^2} + \frac{y^2}{n_0^2} + \frac{z^2}{n_e^2} = 1 \tag{1}$$

---

* National Centre of Physics, P.O.B.ox 5 206, Măgurele, Bucharest.

* * National Centre of Physics. P.O. Box 5211 Măgurele, Bucharest.

where n_0 and n_e are the ordinary and extraordinary indices of refraction, respectively and x, y, z are along the crystallographic a, b, c axes [1], [2]. A change of refractive indices by application of an electric field induces a change in the indicatrix. If is convenient to express this change in terms of the modification in $1/n^2$, with application of the field :

$$\Delta\left(\frac{1}{n^2}\right)_{ij} = \sum_k r_{ijk} E_k \tag{2}$$

where E is the applied field, r_{ijk} are components of the linear electro-optic tensor and $i, j, k = 1 : 3$. Since, the indices i, j can be interchanged we can made the contraction $ij \Leftrightarrow m$, where m run from 1 to 6, as follows : $11 \Leftrightarrow 1$, $22 \Leftrightarrow 2$, $33 \Leftrightarrow 3$, $23 \Leftrightarrow 4$, $13 \Leftrightarrow 5$, $12 \Leftrightarrow 6$. For the crystals of class $\bar{4}2$m the only nonvanishing coefficients are (with the specified notations) $r_{41} = r_{52}$ and r_{63} [3].

When an electric field is applied along z axes, the indicatrix is :

$$\frac{x^2}{n_0^2} + \frac{y^2}{n_0^2} + \frac{z^2}{n_e^2} + 2r_{63} E_3 xy = 1 \tag{3}$$

By rotating the coordinates 45° around the z axes, equation (3) becomes :

$$\frac{x'^2}{(n_0 + \Delta n)^2} + \frac{y'^2}{(n_0 - \Delta n)^2} + \frac{z^2}{n_e^2} = 1 \tag{4}$$

where x' and y' are the new coordinate axis and

$$\Delta n = \frac{n_0^3 r_{63} E_3}{2} \tag{5}$$

When the electric field is applied along the x axes, the indicatrix is :

$$\frac{x^2}{n_0^2} + \frac{y^2}{n_0^2} + \frac{z^2}{n_e^2} + 2r_{41} E_1 yz = 1 \tag{6}$$

By rotating the coordinate axis with 45° around the x axes, equation (6) becomes :

$$\frac{x^2}{n_0^2} + y'^2\left[\frac{1}{2}\left(\frac{1}{n_0^2} + \frac{1}{n_e^2}\right) - r_{41} E_1\right] + z'^2\left[\frac{1}{2}\left(\frac{1}{n_0^2} + \frac{1}{n_e^2}\right) + r_{41} E_1\right] +$$

$$+ y'z'\left(\frac{1}{n_0^2} - \frac{1}{n_e^2}\right) = 1 \tag{7}$$

Light propagation inside a crystal may be described by means of the index ellipsoid. For a given direction of propagation there are two independent linearly polarized plane waves (the so called normal modes) which propagate with different phase velocities. The corresponding refractive indices may be found by intersecting the indicatrix by a plane normal to the direction of the light propagation and passing through the origin.

We shall consider here two of the configuration most commonly used in practice for producing electrooptic effect with crystals of class $\bar{4}2$m. If both the applied electric field and the direction of light propagation are along the z axes of the crystal, the electrooptic effect is a longitudinal one, the ellipse definig the normal modes is obtained from (4) by setting $z = 0$. The directions of polarization of these modes are along the x' and y' axes and their indices of refraction are :

$$\begin{aligned} n_{x'} &= n_0 + \Delta n \\ n_{y'} &= n_0 - \Delta n \end{aligned} \tag{8}$$

with Δn given by (5). If the electric field is applied along the x axes and the light propagates normal to the electric field and at 45° with respect to the y and z axes the effect is a transverse one and the ellipse defining the normal modes is obtained from (7) by setting $y' = 0$. The directions of polarization of these modes are along x and z' axes and their indices of refractions are [4] :

$$\begin{aligned} n_x &= n_0 \\ n_{z'} &= \sqrt{2}\left(\frac{1}{n_0^2} + \frac{1}{n_e^2}\right)^{-\frac{1}{2}} - \sqrt{2}\left(\frac{1}{n_0^2} + \frac{1}{n_e^2}\right)^{-\frac{3}{2}} r_{41} E_1 \end{aligned} \tag{9}$$

In the following we shall present the construction of some types of electrooptic modulators with crystals of class $\bar{4}2$ m and their use as phase intensity and single-sideband suppressed-carrier light modulators.

2. Modulators description

We have constructed two type of modulators, operating in longitudinal as well as in transverse electrooptic effect. For the construction, we have used samples cut from optical quality regions of KDP and ADP crystals. To prevent a depolarizing effect it was assured a good optical finish of the crystal end faces ; they were polished to a planeity of one-fourth wavelength of light and parallelism of 5″. The modulator with longitudinal effect, fig. 1, was constructed with four z-cut KDP crystals, mounted in series along the optical axes, for reducing the modulation voltage [5]. The voltage is applied to the crystals by means of four pairs of ring electrodes coated on end of the lateral faces of crystals. In order to obtain an uniform electric field, it is necessary that the length of the crystals be at least twice with respect to their transverse dimensions ; our samples have each 7 × 7 × 16 mm. The modulator with transverse effect consists of two ADP crystals with the dimensions 3 × 5 × 42 mm. The two crystals must be equal in length with $\lambda/2$ accuracy to ensure that the phase difference of the normal modes introduced by the natural birefringence to be less than 10°. This can be achieved by polishing the two crystals together. They are cut at 45° with respect to optical axes z, and the modulation field is applied on the crystal faces normal to x axes. The crystals are fixed on a amount which allows relative optical alignement one in respect to the other. The mount is introduced in a plastic case, provided with coated glass windows, fig. 2., To improve the optical performances, the cases has been filled with silicon oil.

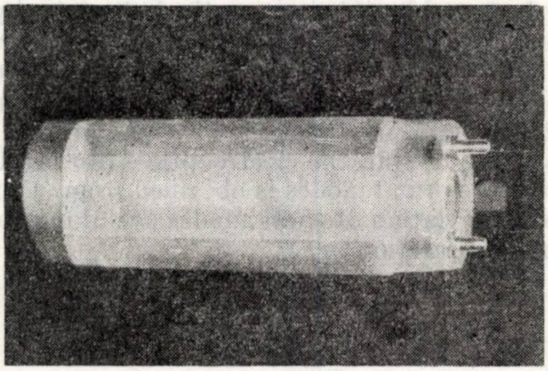

Fig. 1. The modulator with longitudinal effect.

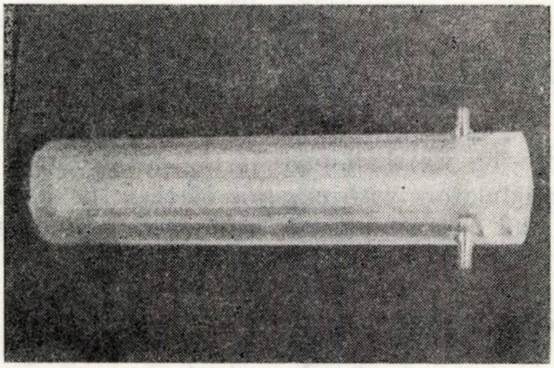

Fig. 2. The modulator with transverse effect.

3. Phase modulation

A phase modulation can be obtained both in longitudinal and in transverse effect, if the incident light propagates in the crystal as a normal mode. For example, in the modulator with longitudinal effect, the incident light must be polarized linearly along the x' or y' axes. In this case, for a incident wave $Ae^{i\omega t}$, the emergent wave may be written :

$$Ae^{i\left[\omega t-\frac{2\pi}{\lambda}(n_0\pm\Delta n)L\right]} \tag{10}$$

where Δn is given by (5) and L is the length of the whole modulator. For the modulator with transverse effect, the incident light must be polarized linearly along z' axes and for a incident monochromatic wave the emergent wave is :

$$Ae^{i\left[\omega t-\frac{2\pi}{\lambda}n_{z'}L\right]} \tag{11}$$

where $n_{z'}$, is given by (9). In both cases, the light emerges from the modulator conserving its polarization plane ; its phase depend linearly on the electric field intensity, by means of the indice of refraction, as results from (5) respectively (9).

The phase modulation signal was detected in a homodyne optical receiver (figs. 3 and 7). The light from a He-Ne laser was divided by means of the beam splitter O_1 ; one of the beams was modulated in the modulator M, and the other was used at detection as a local oscillator beam. The two beams were mixed on the surface of a ROL 21 photodiode. A carefull alignement was made to ensure that on the surface of the photodetector falls less than 1/10 fringe of the interference pattern of two beams — a condition for having a good detected signal [5], [6]. The signal was optimized by varing the optical path difference between the two beams so that the phase difference between the local oscillator beam and the unmodulated carrier beam becomes $\pi/2$ [6]. The arrangement was mounted on a stable table so that the conditions of the two beams alignement and detected signal optimization to be ensured.

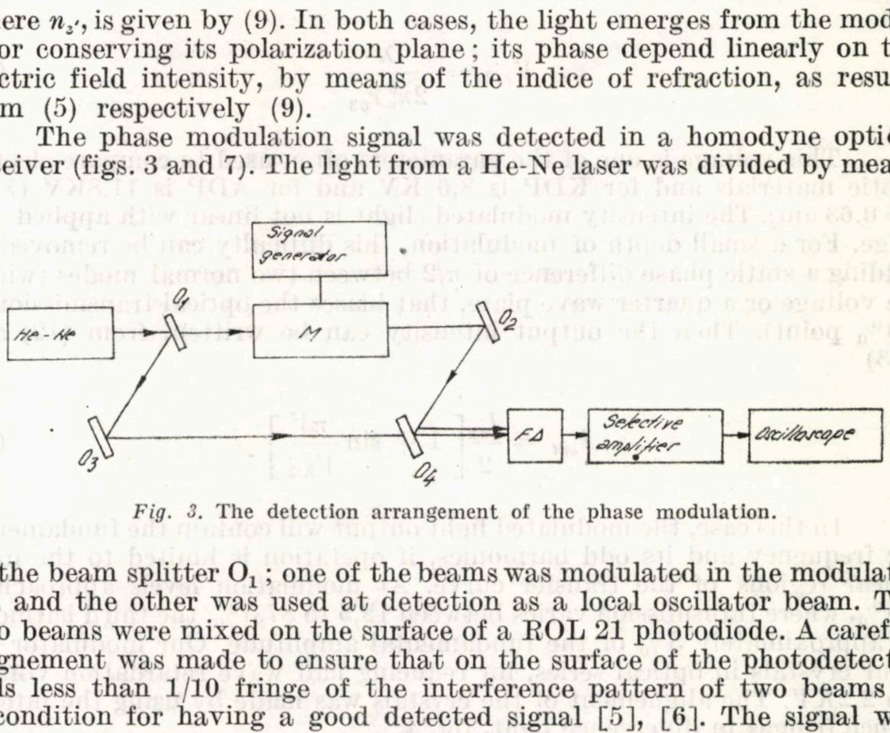

Fig. 3. The detection arrangement of the phase modulation.

4. Intensity modulation.

The intensity modulation can be obtained by interference of phase modulated normal modes and by control of light intensity with a polarizer. In the case of the modulator with longitudinal effect, the incident light must be polarized linearly along the x or y axes. If the output polarizer (analyzer) is positioned to have its polarization direction at $\pi/2$ to the input light polarization, the emergent light intensity is [8] :

$$I_{out} = I_{in} \sin^2\left[\frac{\pi n_0^3 r_{63} V_z}{\lambda}\right] \tag{12}$$

where $V_z = E_3 L$ is applied voltage to modulator. When the voltage across the crystal is increased, the light transmitted will also increase until a maximum transmission is reached. The applied voltage at maximum transmission is defined as half-wave retardation voltage $V\lambda/2$. From equation (12) we obtain :

$$V_{\lambda/2} = \frac{\lambda}{2 n_0^3 r_{63}} \tag{13}$$

This voltage is one of the parameters often used to compare electro-optic materials and for KDP is 8,6 KV and for ADP is 11,8KV ($\lambda = 0.63\ \mu$m). The intensity modulated light is not linear with applied voltage. For a small depth of modulation, this difficulty can be removed by adding a static phase difference of $\pi/2$ between two normal modes (with a dc voltage or a quarter-wave plate, that biases the optical transmission to 50% point). Then the output intensity can be written, from (12) and (13)

$$I_{out} = \frac{I_{in}}{2}\left[1 + \sin\frac{\pi V}{V_{\lambda/2}}\right] \tag{14}$$

In this case, the modulated light output will contain the fundamental ac frequency and its odd harmonics, if operation is limited to the more linear regions of the transfer curve. At modulation levels approaching 75%, where transmission varies between 12,5 to 87,5%, the third harmonic is approximately 3% of the fundamental amplitude. Our modulator has four crystals in optical series, for reducing half wave retardation voltage to 2,2KV. The alignement of the crystals was made by using the interference fringes in divergence light, fig. 4.

In the case of the modulator with transverse effect, the incident light must be polarized linearly at 45° to x axes. If the analyszer is crossed with the polarization direction of the incident light, the emergent intensity light is :

$$I_{out} = I_{in} \sin^2\frac{\varphi}{2} \tag*{15)}$$

where φ is phase retardation between the normal modes. From equation (9) we found, if neglect the constant term due to natural birefringence

$$\varphi=\frac{2\pi}{\lambda}\,\mathrm{L}\sqrt{2}\left(\frac{1}{n_0^2}+\frac{1}{n_e^2}\right)^{-3/2} r_{41}\;E_1 \tag{16}$$

The half wave retardation voltage is obtained from equation (15) and (16)

$$V_{\lambda/2}=\frac{\lambda}{2\sqrt{2}}\left(\frac{1}{n_0^2}+\frac{1}{n_e^2}\right)^{3/2}\frac{\mathrm{d}}{L} \tag{17}$$

where *d* is the electrode spacing.

Equation (17) shows that $V_{\lambda/2}$ can be reduced by choosing a small geometrical factor d/*L*. This why the transverse electrooptic effect is prefered when a large index of modulation is desired.

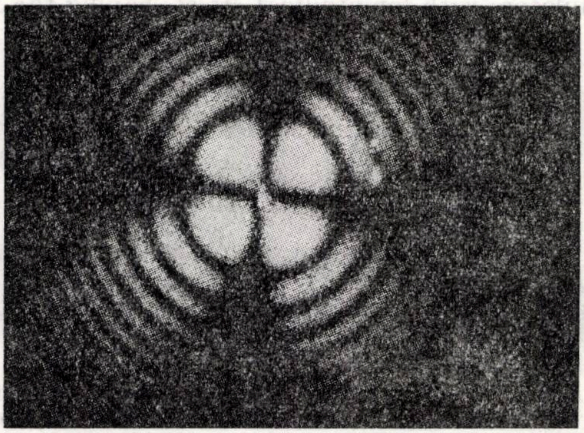

Fig. 4. The interference fringes of the modulator with longitudinal effect.

Our modulator has two crystals ; the second crystal is rotated by 180° in respect to the first, for compensate the natural birefringence due to the constant term from (9) (and the half wave retardation voltage is 260 V. The crystals alignement was made by using the interference fringes in divergence light, fig. 5. The temperature dependence of the natural bire-

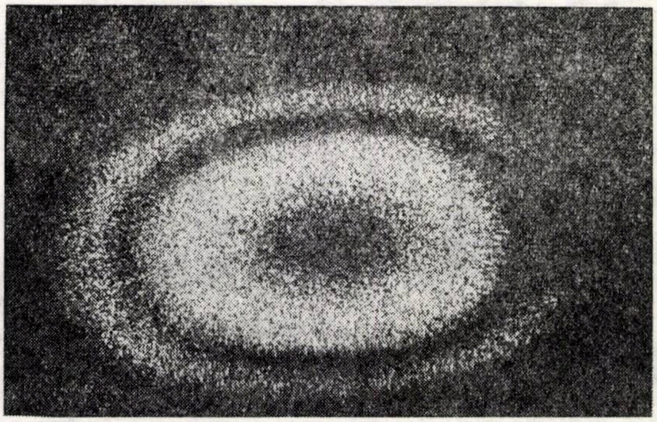

Fig. 5. The interference fringes of the modulator with transverse effect.

fingence can induce fluctuations of the depth of intensity modulation. This dependence can be reduced by thermal stabilization of the crystals or by a dc control voltage.

The detection of the intensity modulated light was made by direct optical detection with aphotodiode. We measured the half wave retardation voltages for the modulators with longitudinal and transverse effect, 2.2kV and respectively 260 V, in a good agreement with equation (13) and (17). The modulators were operated with signals in 0 – 6 Mc/s bandwith, with 60 % modulation index.

5. Single sideband suppressed-carrier modulation.

The single-sideband suppressed-carrier modulation can be obtained with two modulators with longitudinal effect, having the x axes oriented 45 degrees apart, fig. 6. The modulating voltages applied to these modulators are in phase quadrature. The incident light is passed through a left

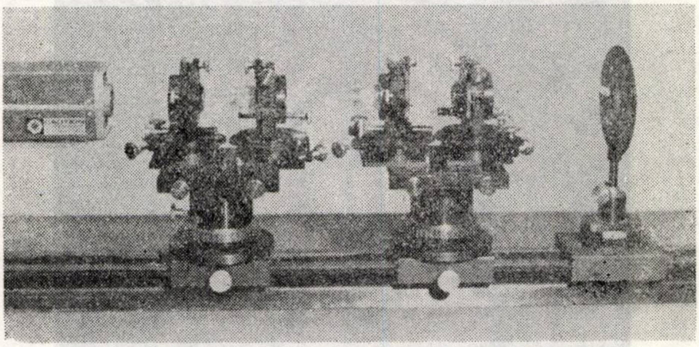

Fig. 6. The single-sideband, suppressed-carrier modulator.

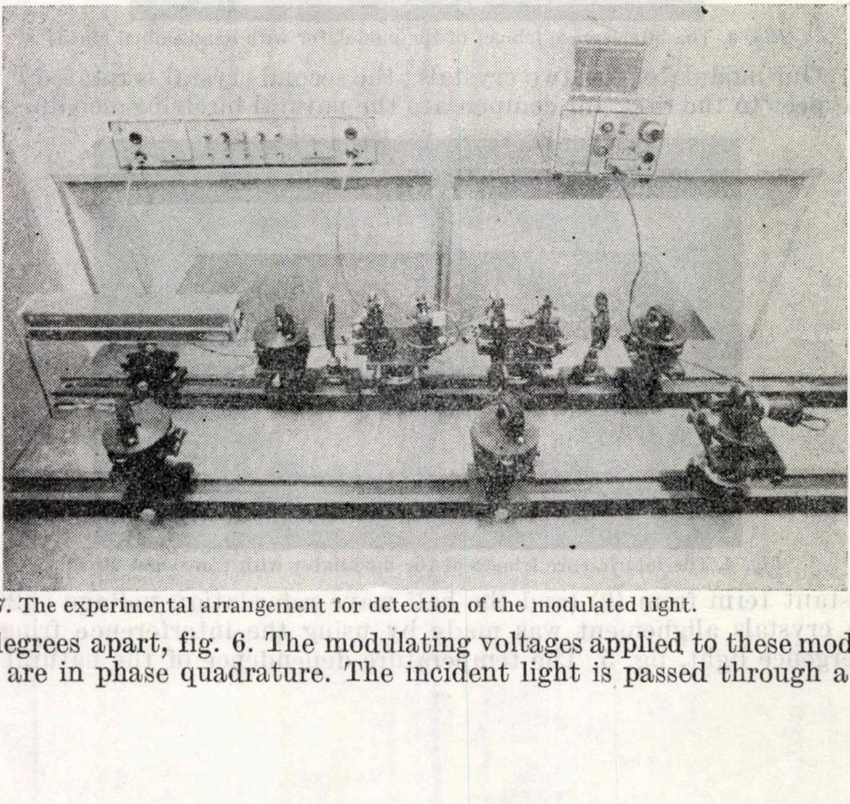

Fig. 7. **The experimental arrangement for detection of the modulated light.**

hand circular polarized consisting of a linear polarizer and a quarter-wave plate in order to obtain circular polarized light. After modulation, the light passes through an other right hand circular analyzer. The output light consists of a left-hand component and a right-hand component [9] The frequency of the right-hand component is the sum of the input light frequency and the modulation frequency, that is the upper sideband frequency [10]. The left-hand component is eliminated by passing the light through the right-hand circular analyzer. The single sideband suppressed-carrier modulation light was detected in a homodyne optical receiver, fig. 7. The conversion efficiency to the desired upper sideband is a function of the peak voltage. For peak voltage up to 4.5 kv, the intensity of this sideband is nearly linear with the peak voltage and is up to 40% from the incident light.

REFERENCES

1. J. F. NYE, *Physical Properties of Crystals*, Oxford University Press, (1967).
2. F. T. ARECCHI, E. O. SCHULZ-DUBOIS, *Laser Handbook*, North-Holland Publ. Co. (1972).
3. I. P. KAMINOW, E. H. TURNER, Proc. IEEE, *54*, 1374, (1966).
4. A. DUMITRICĂ, Rev. Roum. Phys., *20*, 995, (1975).
5. A. DUMITRICĂ, N. GR. POPESCU, St. cerc. Fiz., *27*, 399, (1975).
6. W. PRATT, *Laser Communication Systems*, J. Wiley, N. Y. (1969).
7. W. S. READ, R. G. TURNER, Appl. Opt., *4*, 1570 (1965).
8. I. P. KAMINOW, *An Introduction to Electrooptic Devices*, Acad. Press., N. Y. (1974).
9. L. E. DRAIN, B. C. MOSS, *Optoelectronics*, *4*, 429, (1972).
10. A. DUMITRICĂ, T. TUDOR, Rev. Roum. Phys., *26*, (1981).

Received, January 10, 1981.

ANALELE UNIVERSITĂŢII BUCUREŞTI, FIZICA, XXX, 1981, PAG. 35–42

SUR L'EFFET MEMOIRE DANS LE POLYETHYLENE „ROPOL"

I. C. PETREA, LIVIA MARIA IONESCU, E. BARNA
Faculté de Physique, Université de Bucarst *

CARMEN RĂDULESCU, C. RĂDULESCU
L'entreprise de câbles et matériaux électroisolants-Bucarest

RÉSUMÉ

Les expériences effectuées, dans des conditions d'irradiation, sur des échantillons étirés de polyéthylène ont mis en évidence l'existence d'une dose-seuil (55 Mrad).

Les auteurs font une analyse sur les possibilités de corrélation de certains paramètres mécaniques et de structure, en révélant quelques particularités d'effet-mémoire.

Introduction

La réticulation de certains polymères sous l'action des radiations mène à l'apparition des caractéristiques, différentes de celles qui sont propres à la réticulation provoquée par d'autres moyens. Dans le cas de la réticulation avec des agents chimiques, les ponts transversaux sont réalisés par des radicaux adéquats [1].

Les procès élémentaires concurants à la réticulation des systèmes macromoléculaires linéaires deviennent, en grande partie, responsables de l'implication macroscopique de l'effet-mémoire. Dans ces conditions se fait remarquer le retour d'un polymère irradié à la forme détenue avant l'application de certaines contraintes ou sollicitations externes.

Un rôle très important dans l'explication du mécanisme de cet effet le jouent les interdépendences cinético-moléculaires supposées par le mouvement micro- et macrobrownien des entités structurales remarqables dans le système polymère, ainsi que par les procès de transition conformationnelle ou de rotamérisation.

---

* Centre National de Physique, Măgurele B.P. 5211, Bucarest, Roumanie.

Les radiations de haute énergie influencent de manière statistique la cinétique des réactions secondaires au niveau intermacromoléculaire, y compris le procès de réticulation et les paramètres ou les coefficiènts spécifiques de celui-ci. Les mécanismes concurants (radicaliques, ioniques etc.) ne sont pas encore tout-à-fait expliqués et corrélés.

On observe que l'augmentation de la concentration des ponts C—C mène à une structuration plus accentuée des macrochaînes empaquetées de manière relativement dense, c'est-à-dire, à la perte de certains degrés de liberté, responsable d'une rigidisation de la structure d'ensemble avec des conséquences au niveau de certains paramètres macroscopiques. Ainsi augmente la valeur et le rapport des caractéristiques de frottement interne, viscoélasticité, etc.

Considérations théoriques

Le procès statistique de la réticulation d'un polymère par irradiation avec une dose r est subordonné à une loi de la forme :

$$q = q_0 r \tag{1}$$

compte tenu de l'observation que l'indice de réticulation q, c'est-à-dire la proportion d'unités monomères affectées par de ponts transversaux, est proportionnel avec la dose appliquée et dépend de la nature du polymère par l'intermède d'une constante de matériel q_0.

Dans les mêmes conditions d'irradiation, on peut encore faire appel à un autre paramètre caractéristique, notamment le coefficient de réticulation :

$$\delta = qn = q_0 n\, r \tag{2}$$

défini comme le nombre moyen d'unités monomères liées dans une macromolécule de degré moyen de polymérisation n.

La réticulation conditionne (par l'intermède de ses paramètres) la longueur des chaînes, ainsi que le changement des valeurs moyennes des masses molaires de ces segments de chaîne (et de leur degré de polymérisation).

L'augmentation des doses d'irradiation donne une prépondérence au caractère macroréticulaire du polymère.

De telles évolutions peuvent être suivies en étudiant la solubilisation des échantillons irradiés aux différentes doses. On observe que pour petites doses, le système manifeste une solubilité totale, tandis que la viscosité de la solution augmente avec la dose. L'apparition d'un gel insoluble est liée à l'évolution du réseau spatial. On constate aussi que l'augmentation de la dose mène à la diminution de la fraction soluble dans la masse du polymère. Dans ces termes on met en évidence la dose r_0 à laquelle apparaît le gel (point de gel) et qui, dans le cas du polyéthylène étudié, est $r_0 \simeq 2$ Mrad.

En cas d'une distribution globale de la masse moléculaire, le gel apparaît à $\delta = 1$ [2].

Les études de ce genre sont basées sur des expériences adequates photoélasticimètriques. On examine ainsi la biréfringence accidentelle des échantillons isotropes et transparents au début, en utilisant les lois de corrélation des paramètres caractéristiques pour l'etirement conditionné de ces échantillons.

La théorie de base du phénomène photoélastique suppose quelques conditions et critères d'étude [3].

— Les axes principaux de biréfringence accidentelle dans un point coïncident avec les directions principales de l'état des tensions intérieures dans ce point. Une vibration plane V pourra être décomposée dans deux vibrations perpendiculaires V_1 et V_2, suivant les directions des tensions principales :

$$V_1 = V \cos\alpha \, ; \qquad V_2 = V \sin\alpha \tag{3}$$

α étant l'angle formé par la vibration initiale V et la direction d'une des tensions principales. Les vibrations auront les vitesses v_1 et respectivement v_2, avec les indices de réfraction n_1 et n_2 ;

$$n_1 = \frac{c}{v_1} \text{ et } n_2 = \frac{c}{v_2} \tag{4}$$

— Etant données les tensions principales σ_1 et σ_2 réciproquement perpendiculaires, entre celles-ci et les indices de réfraction existe la relation de Wertheim :

$$n_1 - n_2 = C\,(\sigma_1 - \sigma_2) \tag{5}$$

C étant une constante optique du matériel.

La différence de chemin optique entre le rayon ordinaire et celui extraordinaire est :

$$\Delta = (n_1 - n_2)\,\mathrm{e} = C\,(\sigma_1 - \sigma_2)\,\mathrm{e} \tag{6}$$

où e représente l'épaisseur de l'échantillon.

Pratiquement, il est intéressant de créer un état plan de tensions, caractérisé par des efforts unitaires suivant une seule direction. On prend ainsi en considération deux axes principaux de biréfringence 0ξ et 0η (Fig. 1).

L'étude des tensions internes s'effectue entre polaroïdes croisés, en lumière monocromatique. En admettant que la lumière incidente sur l'échantillon est une vibration armonique simple suivant la direction du polariseur :

$$V_{y_1} = a \cos\omega t, \tag{7}$$

les vibrations correspondentes aux rayons ordinaire et extraordinaire à l'entrée de l'échantillon seront :

$$V_\xi = a \cos\alpha \cos\omega t \qquad (8)$$

$$V_\eta = a \sin\alpha \cos\omega t$$

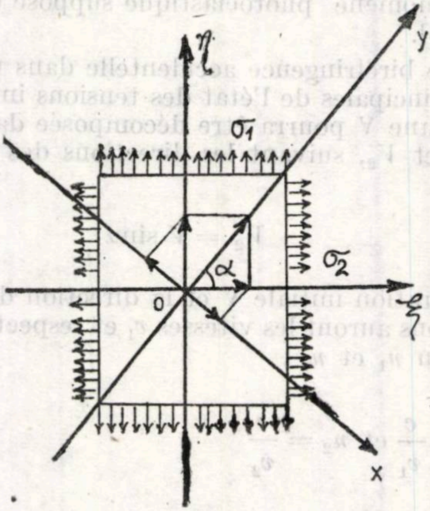

Fig. 1. L'état des tensions dans léchantillon.

Après le passage par le disque apparaitra un déphasage entre les deux rayons :

$$\varphi = 2\pi \frac{\Delta}{\lambda} \qquad (9)$$

La vibration résultante suivant l'axe de l'analyseur devient :

$$V_{x_2} = a \sin 2\alpha \sin\pi \frac{\Delta}{\lambda} \sin 2\pi \left(\frac{t}{T} - \frac{\Delta}{2\lambda} \right) \qquad (10)$$

Il en résulte que l'intensité lumineuse, à chaque point, a la valeur :

$$I = a^2 \sin^2 2\alpha \sin^2 \pi \frac{\Delta}{\lambda} \qquad (11)$$

Δ étant exprimé par la formule (6), λ représente la longueur d'onde du rayon incident, α – l'angle formé par le plan de la vibration incidente Oy et l'axe de biréfringence 0ξ.

La combinaison de l'expression de la courbe de calibrage :

$$D = \gamma \log E + b \qquad (12)$$

où :

b est une constante,
γ — la pente de la caractéristique du film,
$E = It$ — l'exposition,
I — l'intensité lumineuse au point de mesure,
t — le temps d'exposition,

avec la relation (11) où $\sin^2 2\alpha = 1$ (lumière circulaire), conduit à :

$$10 = Bt^{\gamma} A^{\gamma} \sin^{2\gamma} \frac{\pi\Delta}{\lambda} \tag{13}$$

Avec $Bt^{\gamma}A^{\gamma} = F$ — constante, et compte tenu que $\gamma = 1$, on trouve :

$$\frac{\lambda}{\pi} \arcsin \sqrt{\frac{10^D}{F}} = \Delta \tag{14}$$

Revenant à la loi de Wertheim (7), on est conduit à :

$$\sigma_1 - \sigma_2 = \frac{\lambda}{\pi\,\mathrm{Ce}} \arcsin \sqrt{\frac{10^D}{\mathrm{F}}} \tag{15}$$

Pour la déformation d'étirement suivant la direction 0η, $\sigma_2 = 0$; la constante F est déterminée à l'aide de la condition de maximum :

$$10^{D_{max}} = F.$$

On obtient alors :

$$F = 100.$$

Les variations de la tension au point de mesure sont :

$$\frac{\sigma_1''}{\sigma_1} = \frac{\arcsin \sqrt{\dfrac{10^{D''}}{100}}}{\arcsin \sqrt{\dfrac{10^{D}}{100}}} \quad \text{et} \quad \frac{\sigma_1'}{\sigma_1} = \frac{\arcsin \sqrt{\dfrac{10^{D'}}{100}}}{\arcsin \sqrt{\dfrac{10^{D}}{100}}} \tag{16}$$

où D, D', D'' et σ_1, σ_1', σ_1'' représentant respectivement les valeurs de la densité de noircissement et des tensions correspondant aux états suivants : initial, après l'irradiation et après le traitement thermique.

Mesures et résultats expérimentaux

Des feuillets rectangulaires de polyéthylène haute pression fabriqué en Roumanie („ROPOL"), avec des épaisseurs de 160 μm et 80 μm, ont été soumis à un effort de traction au long de la direction 0η (Fig. 1).

Les tensions internes ainsi crées ont été étudiées par la methode photoélastique décrite plus haut, dans la lumière d'une lampe à vapeurs de sodium.

L'effort de traction a été augmenté jusqu'à-ce que le maximum de second ordre soit aparu dans le champ photoélastique.

Les échantillons étirés ont été soumis à l'irradiation γ d'une source de Co^{60} de dose débit 0,5 Mrad/h.

Après l'irradiation les échantillons ont été délivrés des tensions élastiques.

Sur un échantillon témoin, déformé en mêmes conditions, et mentenu dans cet état durant le temps nécessaire à l'irradiation, on a mesuré le temps de relaxation des tensions internes jusqu'à zero, après l'élimination des forces externes [4]. La mesure de la tension mémorée dans l'échantillon irradié a été effectuée seulement 3 heures (le temps de disparition des tensions dans l'échantillon témoin étant 2 heures) après la cessation de l'action de la force externe, en évitant ainsi les éventulles erreurs dues à la présence de certaines forces élastiques nonrelaxées.

Après l'enregistrement de l'état rémanent des tensions, les échantillons — libres de toute tension mécanique externe — ont été mentenus pendant 10 minutes à la température de 125°C, dans une étuve.

On a effectué alors un nouveau enregistrement des tensions internes dans l'échantillon.

Les mesures ont été effectuées par voie photométrique. L'effet mémoire peut être caractérisé par la valeur de la tension rémanente rapportée à sa valeur initiale. Pour une dose donnée, on a calculé une valeur moyenne sur plusieurs points expérimentaux.

Le temps de developpement du film utilisé a été choisi de telle manière, que la pente de la partie linéaire de la caractéristique d'exposition soit $\gamma = 1$. Toute mesure de la densité de noircissement $D < 0,5$ a été considérée nulle, éliminant ainsi les erreurs dues à l'inértie de l'émulsion photographique.

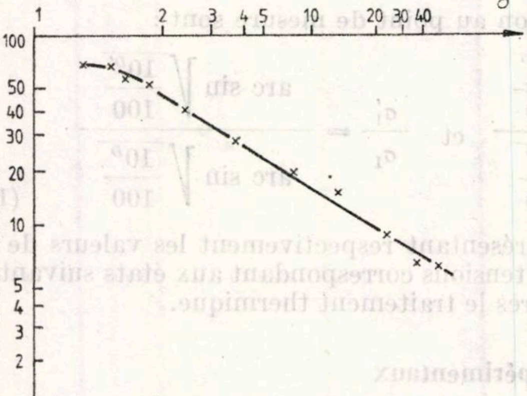

Fig. 2. Le coefficient de réticulation fonction de la dose d'irradiation pour le polyéthylène en solution dans le xylène.

L'intensité de la source et le temps d'exposition ont été réglés de façon que, pour les maximums de l'image photoélastique, le degré de noircissement corresponde à une valeur $D_{\max} = 2$.

Le coefficient de réticulation a été déterminé à l'aide de la courbe de solubilité du matériel dans le xylène (Fig. 2).

Discussion des résultats

La variation de la fraction soluble du polyéthylène de type „ROPOL", irradié, en fonction de la dose d'irradiation correspond à la loi expérimentale (1). La déviation de la linéarité constatée sur la figure 2, au voisinage de la dose de gel est due aux erreurs de mesure.

Dans la figure 3 sont représentées les tensions rémanentes de l'échantillon avant l'échauffement $\left(\frac{\sigma_1'}{\sigma_1}\right)$ et après $\left(\frac{\sigma_1''}{\sigma_1}\right)$ en fonction de la dose d'irradiation.

On observe une saturation complète des tensions appliquées, aux doses qui dépassent 55 Mrad. Cette dose correspond à un coefficient de réticulation $\delta = 35$.

On identifie ici l'effet mémoire à la conservation de certaines tensions internes qui imposent la forme de l'échantillon, conduisant à une considérable diminution du nombre d'états microscopiques possibles — conséquence des liaisons de réticulation directes et rigides propres à l'irradiation.

Le procès de réticulation par irradiation est caractérisé par le comportement rigide des liaisons formées pendant ce procès. Cela fait apparaître des propriétés nouvelles, telles que l'effet-mémoire. Cet effet étant complet après qu'une dose critique ait été atteinte, on peut lui attribuer une semnification de „seuil". La valeur que nous en avons trouvé pour le polyéthylène „ROPOL" est $r_{cr} = 55$ Mrad.

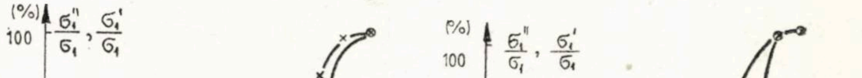

Fig. 3. Les tensions rémanentes dans l'échantillon fonction de la dose d'irradiation : a) feuillet d'épaisseur de 80 μm ; b) feuillet d'épaisseur de 160 μm ; × avant le traitement thermique ; ○ après le traitement thermique

En conclusion, on peut considérer que la généralisation du réseau réticulaire dans l'échantillon et la présence d'un coefficient de réticulation suffisamment élevé (pour empêcher la relaxation des segments) mènent à l'apparition des conditions favorables à la manifestation de l'effet-mémoire.

REFERENCES

1. A. CHARLESBY, *Atomic Radiation and Polymers*, Pergamon Pres, London, 1960.
2. M. DOLE, *The Radiation Chemistry of Macromolecules*, Academic Press, New York, 1976.
3. T. HUIDU, „Analele Universităţii Bucureşti", Matematică, XXI, 87 (1971).
4. I. E. TEODORESCU, M. FILTI, *Iradierea tehnologică*, Ed. Academiei R.S.R., Bucureşti, 1979.

Reçu, le 15 Janvier 1981

ANALELE UNIVERSITĂŢII BUCUREŞTI, FIZICA, XXX, 1981, PAG. 43–49

CONFIGURATIONAL SEQUENCE RULES IN THE POLYMERIC TACTICITY

I. C. PETREA, E. BARNA

Faculty of Physics, University of Bucharest*

C. BUNEA

Secondary School No. 7, Buzău

ABSTRACT

This paper discusses the theoretical aspects and correlations of a systematic tacticity study.

General considerations

In this paper, we shall examine the satistics of configurational sequences and their relationship to conformational preferences in several vinyl polymer chains. In order to do this, we wish to begin with a consideration of small molecules that are related in structure to vinyl polymers.

It is now well recognized that the unit monomers may exist in any or all of their particular conformations, and that NMR, for example, is a very important tool to describe microstructure and tacticity of vinyl polymer chains. ERS spectroscopy, NMR tehniques, electron microscopy X-ray diffraction and other methods can give microstrucural information about the mechanism of configurational sequences and conformational statistics of individual molecular chains. Such information, concerning the symmetry of molecules, or lack of molecular symmetry, permit a definite decision among possible conformational preferences or structures, and may also define bond angles, microstericity etc.

---

* National Centre of Physics, Măgurele P.O. Box 5211, Bucharest

In the study of configurational sequence rules we shall consider the distribution of sequences in vinyl polymer chains and their relationship to addition mechanisms. Before discussing the implication of the addition mechanisms it is important to take into consideration all the factors that are known to have an influence on the configurational sequence rules. Thus, one important aspect of configurational studies should be the consideration of structural and conformational details of single polymer molecules. The tacticity of polymers is associated with structural isomerism and stereoisomerims of polymer molecules. One can distinguishs between structural isomerism, arising from the monomers themselves and stereoisomerism, raising from the spatial arrangement of asymmetric monomeric units in a macromolecule. The influence of structural isomerism, stereoisomerims, branching and other spatial factors is a very complicated matter. Much attention has been paid to the problem of shape and microstericity of the constituent chemical units. It is to be noted that the size and shape of the configurational sequence are determined by the size and the shape of the constituent monomeric units and their local tacticity. In the case of long chain polymer it is reasonable to assume that configurational sequences contain a certain number of monomer units and that asymmetric monomers may be identically oriented (isotactic), or they may alternate in orientation (syndotactic) ; it is very easy to see that they may be randomly oriented (atactic). In a copolymer the comonomers may be in random sequences, they may be grouped in blocks ; in graft copolymers the comonomers may be arranged so that monomers of one kind constitute the main chain with different monomers in the side chains.

To simplify the ensuing discussion, we shall refer to some aspects and factors that are known to have an influence on the local tacticity of polymer molecules.

Definitions and basic rules /1–3/

Important microtacticity problems from the viewpoint of polymer structure are presented by molecules of the type 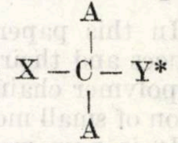 $\mathrm{X}-\overset{\mathrm{A}}{\underset{\mathrm{A}}{\mathrm{C}}}-\mathrm{Y}^*$ where X is a group (methyl, halogen, phenyl, etc.) which has a plane or axis of symmetry, and Y* — a asymmetric group (it possesses no element of symmetry). In such a molecule, the groups A (for example H, F, CF_3, CH_3, C_6H_5 etc.) will be non-equivalent, i.e., they have the same chemical shift, but are unequally coupled of another group. When the molecule has a plane of symmetry (Y* may be 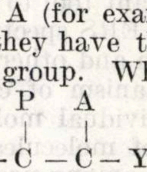 $-\overset{\mathrm{P}}{\underset{\mathrm{Q}}{\mathrm{C}}}-\overset{\mathrm{A}}{\underset{\mathrm{A}}{\mathrm{C}}}-\mathrm{Y}$) we shal refer to all such CA_2 groups in which the A groups are equivalent as homosteric, and to those in which the A groups are non-equivalent as heterosteric (diastereotopic). A molecule which is geminally heterosteric need not be asymmetric, and an asymmetric molecule may be homosteric (enantiotopic); a geminally heterosteric molecule need not be dissymmetric (if it posses a symmetry element, a two-fold axis, for example), and conversely.

If Y* is an asymmetric carbon atom $C^*-R_1R_2R_3$ for each isomer there will be three staggered conformers and in each the environments of A′ and A″ are non-equivalent.

If $X=Y^*=C^*RR'R''$ the molecule has similar asymmetric centers.

If X and Y are of the same handedness we have either the d or l diastereoisomer; when X and Y are of opposite handedness we have the meso-diasteroisomer in which the CA_2 group is heterosteric. The meso-diasteroisomer has a plane of symmetry. Such definitions and basic considerations carrie important conformational implications it is now generally agreed that these definitions and considerations can be extended to the long polymeric chains. The study of heterosteric methylene groups has almost become a characteristic field of stereochemistry in itself. Thus, a methylene group in an isotactic chain (meso-1-diastereoisomer)

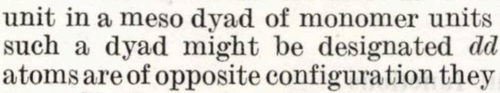

$$CH_3-\underset{R}{\overset{H}{+}}-\underset{H''}{\overset{H'}{+}}-\underset{H}{\overset{H}{+}}\ldots-\underset{H''}{\overset{H'}{+}}-\underset{R}{\overset{H}{+}}-CH_3$$

can be regarded has the center unit in a meso dyad of monomer units having the same configuration, and such a dyad might be designated *dd* or *ll*; when two asymmetric carbon atoms are of opposite configuration they are conventionally designated *d* and *l*.

Similarly, for racemic dyads (the racemic isomer has two unlike heterosteric methylene groups) in syndiotactic chain (meso-2-diastereoisomer)

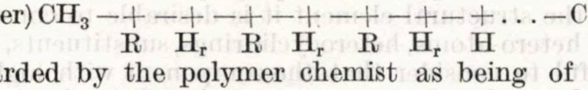

$$CH_3-\underset{R}{\overset{H}{+}}-\underset{H_r}{\overset{H_s}{+}}-\underset{R}{\overset{H}{+}}-\underset{H_r}{\overset{H_s}{+}}-\underset{R}{\overset{H}{+}}-\underset{H_r}{\overset{H_s}{+}}-\underset{H}{\overset{R}{+}}\ldots-CH_3$$

the monomer units are regarded by the polymer chemist as being of opposite configuration, whereas in the analogous sequence they have the same configuration.

In these terms, the meso dyad is designated *m* and the racemic dyad *r*; thus an isotactic triad is *mm*, a syndiotactic triad *rr*, and a heterotactic triad *mr*.

The probability of forming a mesosequence when a new monomer unit is added at the end of a growing chain can be denoted by a parameter P_m; it follows of curse, in terms of a Bernoulli-trial process, that the probability of generating an *r*-sequence is $1\text{-}P_m$ or P_r. The configurational sequences is Bernouillian if the growing chain end is not represented as having any particular stereochemistry, i.e., it is unimportant whether it is *m* or *r*. This coresponds to the fact that the monomer chain unit considered alone has no stereochemistry, but can exert a steric influence. In practice, freeradical polymerizations follow simple Bernoullian chain statistics.

If this is not the case, then the chain's configurational sequence deviates from Bernoullian distribution. Of interest in the theoretical discussion of configurational sequence rules are polymerizing systems in which the adding monomer is influenced by stereochemistry of the chain end, which may be *m* or *r*. When such propagation is possible one can define the first-order Markov sequence. If this is the case we have four probabilities characterizing the propagation steps: $P_{m/r}$, $P_{r/r}$, $P_{r/m}$ and

$P_{m/m}$. For example, $P_{r/m}$ means the probability that the monomer adds in m-fashion to an *r* chain end. However, the dimer-sequence is too simple and in this case, the object of consideration is usually a chain with the short-range intramolecular interactions only, i.e., with interactions between atoms and groups which are not far apart in configurational sequence. Much valuable information about the conformational statistics of individual macromolecules can be obtained by considering the triad frequencies and their relationships.

Strictly speaking, a triad sequence (mm, mr or rr) involves two monomer units additions and this mechanism may be characterized if we can determine conditional probabilities, in agreement with relationships $P_{m/m} + P_{m/r} = 1$ and $P_{r/r} + P_{r/m} = 1$ expressing the assumption that every additional chain unit must go either m or r. The application of high-resolution NMR spectroscopy to vinyl polymers made the experimental measurements of configurational sequence feasible and a considerable number of polymer spectra have now been examined and interpreted in these terms, including polypropylene, polystyrene, polyvinyl chloride, polyvinyl acetate, polyvinyl alcohol, polymethyl acrylate, polymethyl methacrylate, polyacrylonitrile, etc. The complete representation of a linear configurational structure allowed one to compare actual polymer chains with theoretical predictions and to correlate tacticity with other physical charycteristics.

Some typical correlations and useful functions

In the study of configurational sequences must also be considered some typical rules and useful correlations ; in polymers with 2 or more diradical components in the structural element it is desirable to consider the priority in the order of hetero-atoms, heterocyclic rings, substituents, etc.

It is generally useful to consider that the component with highest priority or seniority is given first in the structural element ; component that follow are then given in order of decreasing seniority. The order of heteroatoms in polymer chains is of considerable significance theoretically ; this observation is consistent with the assumption that heteroatoms are given priority in the order O, S, Se, Te, N, P, As, Sb, Bi, Si, Ge, Sn, Pb, B and Hg. One may also easily imagine highest priority of heterocyclic rings ; the ring with most substituents has highest priority. In configurational sequence the atoms of higher atomic weight precede those of lower atomic weight. The descending order of seniority of heteroatoms in the main chain can have a clockwise direction ; this chirality element is defined R by convention.

If the seniority of the other substituents or ligands decreases in a counter-clockwise direction, then this chirality rule is assigned the symbol S as prefix. In general, the two possible ways of arranging substituents about a central atom or a stereoisomeric center are distinguished from each other by the prefix R and S or D and L, respectivelly. For a given molecule with two central atoms one can consider four different configurative diads : RS-, RR-, SR-, and SS. If the dyads are only *m* or *r*, then the configurational sequence is termed holotactic. Polymer with one stereoisomeric center per base unit is termed monotactic ; ditactic polymers possess two stereoisomeric centers per constitutive base unit, tritactic-three, etc. We may add that the central atom is not necessarily carbon. The extension of such statements to higher sequencies, to microblocks of holotactic structure is obvious.

Let us consider a block copolymer having microblocks of isotactic and syndiotactic dyads. As it can be seen from the above statements in this case the number of isotactic dyad links is equal to that of syndiotactic dyad links, within experimental error. Development of the conformational statistics of single polymer molecules has led to the facilities to compute the configurational sequences or microblocks from their chemical sequence. Such configurational sequences will in general be formed if any stereochemical and structural chain element, once formed, tends to propagate itself preferentially but not exclusivelly. Thus, for example, we may generate a chain with a mmrr repeating unit : mmrrmmrrmmrrmm... (a third-order Markov process). The fraction f of all the mr or rm groups can be determined by NMR spectroscopy, but the sequence statistics are rather bizarre.

Each configurational sequence consisting of a number of holotactic groups may be directly considered for the evaluation of practical polymer problems on the basis of statistical concepts and of the tacticity research. It must be emphasized that even under optimum conditions in real polymeric chains the interactions between groups which remote from one another in the configurational sequence always exist. In reality polymer systems are strongly non ideal, so that is convenient to take in consideration all the factors that are known to have an influence to the microtacticity. We have to consider the ordered and disordered groups, the head-to-tail or head-to-head structure, the erythro proton and the threo proton, etc.

From the point of view of a general description of properties of tactic polymers we cannot remain within the framework of the local microconfiguration. Some attention must be paid to the physical significance of the effect of the tacticity upon the crystallinity, branching, crosslinking, etc. In the study of stereoregularity, tacticity, crystallinity of polymers and for less stereoregular chains it was necessary to have recourse to measurement of swelling behaviour, solubility properties, degree of branching, cross-link density, degree of polymerization, melting point, etc. To a first approximation the structure of polymers and their phenomenological description require a clear specification of the configurational sequence. The number average of the sequence length, the number of sequences of length j and the fraction of various groups can be adopted in important special cases, which allow the evaluation of the number-average degree of polymerization, the cross-link density, etc. Sequence rules have to observed in these special cases.

One of the most typical examples demonstrating the above discussion is independent, for example, on sequence

abaabbbaaabbabaabbbaaabbbaabbabbaabaaab . . . .

In this case, the number-aberage $(L_a)_n$ of the sequence length of monomeric unit „a" is by definition

$$(L_a)_n = \frac{\sum_j (N_a)_j (L_a)_j}{\sum_j (N_a)_j}$$

where $(N_a)_j$ is the number of sequences of length j and $(L_a)_j$ is their length As it can be seen from the above configurational sequence

$$(\bar{L}_a)_n = \frac{(3\times 1)+(4\times 2)+(3\times 3)}{3+4+3} = 2.0$$

$$(\bar{L}_b)_n = 1.9$$

Number of all the monomeric units „a" is $N_a = \sum_j (N_a)_j \, (L_a)_j$. On the other hand, can be distinguished N_b, N_{aa}, N_{ab} and N_{bb}.

The fraction of all the „ab" groups is by definition :

$$f_{ab} = \frac{N_{ab}}{N_{aa}+N_{ab}+N_{bb}} = \frac{N_{ab}}{(P_n-1)N_h}$$

Here P_n is the number-average degree of polymerization : $\dfrac{N_a+N_b}{N_h}$

If $N_a = n_a N_{Av} = m_a N_{Av}/M_a$ and $w_a = m_a/(m_a+m_b)$, $w_b = m_b/(m_a + m_b)$, then $\bar{P}_n = \bar{M}_n\left(\dfrac{w_a}{M_a}+\dfrac{w_b}{M_b}\right)$. Here, n_a is the number of moles of monomeric unit „a"; N_{Av} — Avogadro's number ; w_a and w_b — mass fractions, M_n — number-average molecular weight of the primary chain (a primary chain is the linear molecule before cross-link) ; M_a and M_b-molecular weight of monomeric units „a" and „b"', respectivelly.

Number of copolymeric enchainments is $N_h = (m_a + m_b)N_{Av}/\bar{M}_n$.

At the same time, by relating these data with laticeal and branching parameters, it is now quantitatively possible to analyze, in this circumstance, even nore special structure-property relations. Thus, can be expressed a relation between the number-average molecular weight of a network chain M_{cn} and the degree of branching $D_b D_d$. It is evident that $\bar{M}_{cn}$ is directly proportional to $\bar{M}_u$:

$$\bar{M}_{c_n} = \bar{M}_u / D_b$$

$\bar{M}_u$ is the average formula molecular weight of the monomeric unit.

By definition : $D_b = \dfrac{\text{moles of cross-linked monomeric units.}}{\text{total moles of present monomeric units.}}$

The next step is the correlation of the cross-link density C_{ld} with the branch density :

$$C_{ld} \equiv \frac{\bar{M}_{0n}}{\bar{M}_u} \cdot D_b = \bar{P}_n \cdot D_b$$

where M_{0n} is the number-average molecular weight of the primary chain.

It is intersting to note that

$$\bar{P}_n = \frac{N_a + N_b}{N_h}$$

and hence

$$C_{ld} = \frac{N_a + N_b}{N_h} \cdot D$$

This corresponds to the fact that the cross-link density depends on the number of all the monomeric units N_a, N_b and N_h. It can be concluded that the structural state approach to physical property correlations is a general one not specific to tactic polymer.

On the basis of these theoretically considerations it is posible to check the validity of other important correlations.

REFERENCES

1. F. A. BOVEY, *Polymer Conformation and Configuration*, Polytechnic Press of the Polytechnic Institute of Brooklin, New York, 1969.
2. I. C. PETREA, E. BARNA, „Analele Universității București", Fizică, XXVIII, 75 (1979)
3. B. WUNDERLICH, *Macromolecular Physics*, Academic Press, 1974.
4. H. G. ELIAS, *Macromolecules*, vol. I, Plenum Press, 1977.

ANALELE UNIVERSITĂȚII BUCUREȘTI, FIZICA, XXX, 1981, PAG. 51–57

LA FONCTION RADIALE DE DISTRIBUTION, LES NOMBRES MOYENS DE COORDINATION ET LA COMPRESSIBILITE ADIABATIQUE DES LIQUIDS (BENZÈNE)

N. FLOREA

Institutul de Construction, Bucarest

V. DIMA

Faculté de Physique, Université de Bucarest

RÉSUMÉ

On a calculé la fonction radiale de distribution $g(r)$ pour la benzene à base. des considérations statistiques sur l'état liquide. Les résultats ont été obtenus sous forme numérique et graphique. Les courbes respectives ressemblent à celles obtenues par diverses méthodes et techniques expérimentales. A l'aide de la fonction $g(r)$ in a calculé les nombres moyens de coordination et le coefficient de compressibilité adiabatique. Les valeurs du coefficient de compressibilité adiabatique sont presentées par comparaison à celles expérimentales que nous avons obtenues à base ds mesures ultraacoustiques. On a constate un accord satisfaisant entre les valeurs théoriques et celles expérimentales de la compressibilité adiabatique.

1. La fonction radiale de distribution

Dans l'étude de l'état liquide la fonction radiale de distribution g(r) présente une importance particulière parcequ'elle fournit des informations sur la structure du système étudié et permet, à la fois, le calcul de

---

* Bul. Republicii 176, Bucarest.

** Centre National de Physique, Măgurele, – Bucarest, B.P. 5211.

certaines grandeurs comme : l'energie interne, la pression, la compressibilité adiabatique, le potentiel chemiques, les nombres de coordination etc.

La fonction radiale de distribution apparaît dans la relation qui exprime la probabilité de trouver une particule entre r et r + dr par rapport à une autre particule fixe :

$$\mathrm{d}W = g(r)\,\frac{4\pi r^2\,\mathrm{d}r}{V}, \tag{1}$$

où V est le volume total du liquide.

La fonction $g(r)$ peut être déterminée soit par expériment en utilisant par exemple la méthode de la diffraction à rayons X [1], où a neutrons [2], soit théoriquement, par la solution de la suivante équation intégro-differentielle, établie à base des considérations statistiques sur l'état liquide [3] :

$$kT\,\mathrm{lng}\,(r,\lambda) + \lambda\varphi(r) + \frac{2\pi}{rv}\int_0^\infty\int_0^\lambda [g(r,\lambda) - 1]$$

$$\left\{\int_{|r-\rho|}^{r+\rho} \varphi(t)g(t\,;\,\lambda)\,t\mathrm{d}t\right\}\mathrm{d}\lambda\ \ \rho\mathrm{d}\rho = 0 \tag{2}$$

ou $\varphi(r)$ représente le potentile d'interaction moléculaire λ un paramètre qui contient la densite du système et v le volume qui revient à une molecule.

Kirkwood, Lewinson et Alder [4] ont procédé à une intégration numérique de l'équation (2). en choisant, pour décrire les interactions entre les particules, le porentiel Lennard-Jones qui accomplit les conditions suivantes :

$$\begin{aligned} &\varphi(r) = \infty & r < a \\ &\varphi(r) = 4\,\varepsilon\left[\left(\frac{a}{r}\right)^{12} - \left(\frac{a}{r}\right)^{6}\right], & r > a \end{aligned} \tag{3}$$

ou ε représente l'énergie potentielle minime et a la longueur caractéristique de la molécule.

La condition (3) montre que les particules ne peuvent pas se toucher c'est à dire pour $r < a$ $g(r)$ s'annule et pour $r \geqslant a$, la distribution des particules est décrite par $g(r)$ qui représente une solution de l'équation (2).

Pour trouver cette solution on a introduit la fonction

$$\psi(r) = r\mathrm{lng}(r), \tag{4}$$

qui se devéloppe en série d'après les puissances de $\frac{\varepsilon}{kT}$ et on obtient

$$\psi(r) = \psi_0(r) + \frac{\varepsilon}{kT}\,\psi_1(r) + \left(\frac{\varepsilon}{kT}\right)^2\psi_2(r) + \ldots \tag{5}$$

Les expressions (4) et (5) transforment l'équation (2) dans un système de trois équations intégrales en $\psi_i(r)$ avec $i = 0, 1, 2$, que Kirkwood et ses collaborateurs résoudent a l'aide d'un computer IBM. Les valeurs des functions $\psi_i(r)$ obtenues pour les diverses valeurs du parametre de la densite sont donnees sous forme numerique.

Nous avons pris ces valeurs des fonctions $\psi_i(r)$ pour calculer la fonction radiale de distribution du benzène.

Pour les parameters a et ε nous avons pris les valeurs suivantes [5]:

$$\begin{aligned} a &= 5{,}27\ \text{Å}, \\ \varepsilon &= 6{,}072\ 10^{-21}\ J. \end{aligned} \tag{6}$$

En coordonnées adimensionelles $x = \dfrac{r}{a}$ la fonction $g(r)$ s'écrit:

$$g(x) = \exp\left\{\frac{1}{x}\left[\psi_0(x) + \frac{\varepsilon}{kT}\,\psi_1(x) + \left(\frac{\varepsilon}{kT}\right)^2 \psi_2(x)\right]\right\} \tag{7}$$

En procédant à une programme en langage FORTRAN de la relation (7) et en utilisant une machine électronique de calcul FELIX 256 nous avons obtenu les valeurs de la fonction $g(x)$ pour 30 valeurs de x comprises entre 1 et 3.

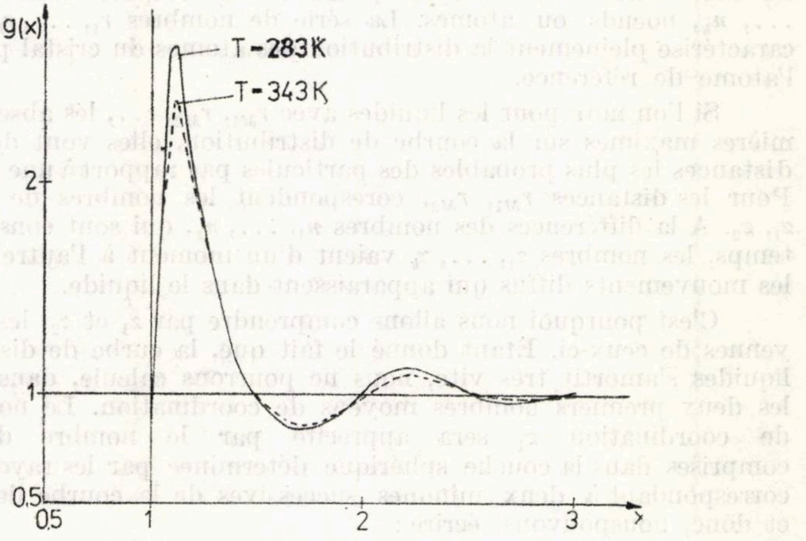

Fig. 1. La fonction $g(x)$ pour bnzène

Nous avons considéré un domain de la température, compris entre 283 et 343 °K et nous avons varié la température tous les lo degrés. Dans la figure 1 nous avons présénte les résultats sous forme graphique en tracant deux courbes de distribution pour les deux températures extremes du domaine choisi.

En analysant le diagramme de la fonction $g(x)$, nous pouvons affirmer que dans la structure du liquide on trouve des éléments d'ordre (cristallins), ainsi que des éléments de desordre (gazeux), les derniers étant prédominants à des températures proches à celle d'ebullition.

Le fait que $g(x)$ présente seulement quelques maximes plus accentuées leur amplitude s'abaissant proportionellement à la distance, indique l'existence d'un ,,ordre local'' a l'intérieur du liquide. Cet ordre s'étend sur une distance de quelques diamètres moléculaires. La continuité de la fonction $g(x)$ nous conduit à la conclusion que dans le liquide apparaît le mouvement de translation des molécules ainsi que les mouvements d'oscillation des atomes autour les noeuds.

A mesure que la température s'accroît les maximes de la fonction $g(x)$ sont moindre ce qui veut dire qu'à des températures proches à celles d'ébullition le mouvement de translation des molecules apparaît plus accentue par rapport aux oscillations autour des positions d'équilibre.

2. Le nombres moyens de coordination

Les nombres de coordination pour les liquides sont introduits par analogie aux nombres de coordination du solide cristalin [6°]. Dans le cristal on peut construire autour d'un noeud considéré comme origine, $r_1, r_2, \ldots, r_k$, des sphèrès de coordination pui passent à travers les couches successives des noeuds. Sur ces sphères on aura respectivemment $n_1, n_2, \ldots$ $\ldots, n_k$, noeuds ou atomes. La série de nombres $r_1, \ldots, r_k, n_1, \ldots, n_k$, caractérise pleinement la distribution des atomes du cristal par rapport a l'atome de référence.

Si l'on note pour les liquides avec $r_{M1}, r_{M2}, \ldots$, les abscisses des premières maximes sur la courbe de distribution, elles vont déterminer les distances les plus probables des particules par rapport à une particule fixe Pour les distances r_{M1}, r_{M2}, corespondent les nombres de coordination z_1, z_2. A la différences des nombres $n_1, \ldots, n_k$, qui sont constants tout le temps, les nombres $z_1, \ldots, z_k$ vaient d'un moment à l'autre étant donné les mouvements diffus qui apparaissent dans le liquide.

C'est pourquoi nous allons comprendre par z_1 et z_2, les valeurs moyennes de ceux-ci. Etant donné le fait que, la curbe de distribution des liquides s'amortit très vite, nous ne pourrons calcule, dans ces cas que les deux premiers nombres moyens de coordination. Le nombre moyen de coordination z_1 sera apprecité par le nombre de particules comprises dans la couche sphérique déterminée par les rayons r_{m1} et r_{m2} correspondant à deux minimes successives de la courbe de distribution et donc, nouspouvons écrire :

$$z_1 = \frac{4\pi N}{V}\int_0^{r_{m_1}} g(r)r^2\,\mathrm{d}r, \tag{8}$$

$$z_2 = \frac{4\pi N}{V}\int_{r_{m_1}}^{r_{m_2}} g(r)r^2\mathrm{d}r.$$

En passant aux coordonnées adimenssionnelles $x = \frac{r}{a}$ et prenant en considération une mole de la substance respective nous avons :

$$z_1 = \frac{4\pi a^3 N_0 \rho}{\mu} \int_1^{x_{m_1}} g(x) x^2 \mathrm{d}x,$$

$$z_2 = \frac{4\pi a^3 N_0\, \rho}{\mu} \int_{x_{m_1}}^{x_{m_2}} g(x) x^2 \mathrm{d}x. \tag{9}$$

ou μ est la masse moléculaire, N_0 le nombre d'Avogardo, *à* la densité du liquide.

Avec les valeurs que nous avons obtenues ci-dessus pour la fonction $g(x)$, nous avons calculé à l'aide d'un computer FELIX 256, les valeurs z_1 et z_2 pour le benzène aux températures auxquelles on a calculé aussi la fonction radiale de distribution.

Les résultats obtenus sont présentés sous forme graphique dans la fig. 2. On remarque sur le graphique une diminution des nombres moyens de coordination par rapport à l'augmentation de la température. Les nombres z_2 apparaisent plus grands que le nombre z_1, ce qui est d'aileurs bien naturel.

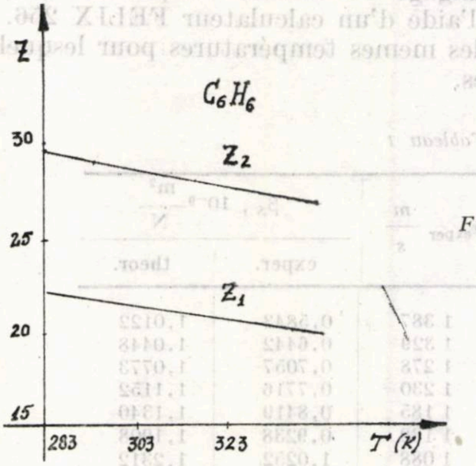

Fig. 2. Les nombres moyens de coordination pour benzène

3. Le coefficient de compressibilité des liquides

La fonction radiale de distribution permet le calcul du module adiabatique d'élasticité qui, à sont tour, est équivalent à l'inverse du coefficient de compressibilite β .

Le module adiabatique d'élasticité K est exprimé dans la théorie statistique des liquides [6] en fonction du potentiel intermoléculaire $\varphi(r)$ et de la fonction $g(r)$ ainsi :

$$K_S = \frac{1}{\beta_S} = \frac{R}{N_0}\left[\frac{T}{v} - \left(\frac{\partial T}{\partial v}\right)_S\right] + \frac{2\pi}{v}\int_0^\infty \frac{\mathrm{d}}{\mathrm{d}r}\left[\frac{1}{r^2}\ \varphi^2(r)\right] g(r) r^6\, \mathrm{d}r \qquad (10)$$

ou v c'est le volume qui revient à une molécule, T la température, R la constante générale des gaz parfaits.

En passant aux coordonées adimensionelles $x = \frac{r}{a}$ et en rendant explicite la dérivée $(\partial T\ \partial v)S$ nous avons calculé le coéfficient de compressibilité du benzène :

$$\frac{1}{\beta_S} = \frac{R\,\rho}{\mu}\left(T + \frac{\gamma - 1}{\alpha_p}\right) + \frac{16\pi N_0^2\ \rho^2 \varepsilon\, a^3}{\mu^2}\int_1^3\left(\frac{10}{x^{10}} - \frac{3}{x^4}\right) g(x)\mathrm{d}x, \qquad (11)$$

ou ρ représente la densité du liquid, α_p coefficient de dilatation isobare et γ le coefficient adiabatique.

La fonction $g(x)$ étant obtenue sous forme numérique ou graphique impose la solution numérique pour l'intégrale de la relation (11). Dans ce but nous avons transcrit en langage FORTRAN l'expression (11) et nous avons effectué les calculs à l'aide d'un calculateur FELIX 256. Ces calculs ont été effectué pour les memes températures pour lesquelles les fonctions $g(x)$ ont été calculées.

Tableau 1

T, °K	ρ, $\frac{\mathrm{Kg}}{\mathrm{m}^3}$	c_{exper} $\frac{m}{s}$	β_S, $10^{-9} \frac{\mathrm{m}^2}{\mathrm{N}}$	
			exper.	theor.
283	889,6	1 387	0,5843	1,0122
293	878,8	1 329	0,6442	1,0448
303	867,5	1 278	0,7057	1,0773
313	856,6	1 230	0,7716	1,1152
323	845,8	1 185	0,8419	1,1340
333	834,4	1 139	0,9238	1,1908
343	824,0	1 088	1,0252	1,2312

Les résultats obtenus sont presentés dans le tableau I par comparaison à ceux obtenus expérimentalement, par des mesures ultraacoustiques.

Le processus de propagation des ultrasons dans les liquides étant un processus adiabatique nous pouvons exprimer le coefficient de compressibilité adiabatique par la relation :

$$\beta_S = \frac{1}{c^2\,\rho}, \qquad (12)$$

ou ρ reprséente la densité au liquide et c la vitesse de propagation de l'ultrason dans le liquide respectif.

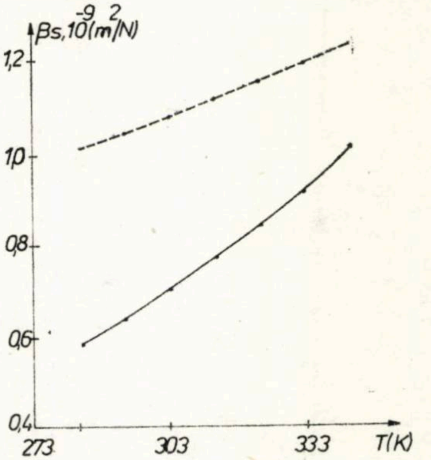

Fig. 3. La variation du coefficient de compressibilité adiabatique du benzène en fonction de la température experimentales ————, thèoriques - - - - - - -

Nous avons mesuré la vitesse de propagation des ultrasons par la méthode de l'impulsion ultrasonique et nous avons determiné à l'aide de l'expression (12) le coefficient de compressibilité adiabatique.

Dans la figure 3 nous avons representé graphiquement la variation de le β en fonction de la température.

Comme l'on peut remarquer sur le graphique, il y a un accord satisfaisant entre les valeurs théoriques et celles expérimentales. Les valeurs théoriques de la compressibilité adiabatique sont plus grandes que celles expérimentales, en obtenant dans les deux cas une augmentation approximativement linéaire, en fonction de la temperature. Le coefficient thermique de la compressibilité adiabatique $\frac{\Delta\beta_S}{\Delta T}$ est plus grand pour les valeurs expériemtales, ce qui determine le fait que l'accord entre les deux séries de valeurs soit meilleur vers des températures plus élevees. Les differences qui apparissent entre les valeurs théoriques et celles expérimentales peuvent résulter soit du potentiel adopté, qui donne de tres bons résultats pour les liquides monoatomiques, soit des approximations introduites dans la solution de l'equation (2).

REFERENCES

1. A. SCRIŞEVSKI, *Rentgenografia jidkostai*, Kiev, 1966.
2. D. G. HENSHAW, Phys. Rev., 105, 976, 1967.
3. J. KIRKWOOD, E. BOOGS, J. Chem. Phys., 10, 394, 1942.
4. J. KIRKWOOD, V. LEWINSON, B. ALDER, J. Chem. Phys., 20, 929, 1952.
5. J. HIRSCFELDER, C. CURTISS, R. BIRD, *Molecular theory of gases and liquids*, J. Wiley, New York, 1954.
6. I. FIŞER, *Statisticeskaia teoria jidkostei*, Moskva, 1961.

Received, December 18, 1980

ANALELE UNIVERSITĂŢII BUCUREŞTI, FIZICA, XXX, 1981, PAG. 59–63

A PARAMETRIC SOLUTION OF THE BINARY MOLECULAR MODELS

C. A. STĂNESCU

Faculty of Physics, Bucharest University *

ABSTRACT

Evaluation of the number of contacts between different molecules, have been made for a lattice, by a generating function method. A parametric result was obtained for the chemical potentials.

A main problem of the partition function evaluation, for a binary solution or a ferromagnetic lattice, consist in the exact or approximative estimation of the number of distinct ways, to produce a state with constant energy.

Various attempts have been made, [1 – 4], the investigators limiting their procedures to local approximations.

The present paper, is trying estimation to this respestive number of ways, $g(a, b, n_{ab})$, for all the lattice places simultaneousy. The result yelds without any further approximation to the quasichemical solution.

Let us take into account a lattice, having the coordination parameter z and with N sites. We have : a, A-type molecules and b, B-type molecules. We make the notations w_{aa}, w_{ab}, w_{bb} for interaction energies, (nearest neighbours only), and n_{aa}, n_{ab}, n_{bb}, for the number of contacts in the whole lattice between $A - A$, respectively $A - B$ and $B - B$ neighbouring molecules.

The energy of a single state for this situation is :

$$E(n_{ab}) = n_{aa}w_{aa} + n_{ab}w_{ab} + n_{bb}w_{bb} \tag{1}$$

This sum can be reduced to :

$$E = \frac{z(aw_{aa} + bw_{bb})}{2} + \frac{n_{ab}}{2}(2w_{ab} - w_{aa} - w_{bb}) \tag{2}$$

---

* National Centre of Physics, P.O. Box 5211, Măgurele, Bucharest.

because :

$$n_{aa} = \frac{1}{2}(za - n_{ab}) \text{ and } n_{bb} = \frac{1}{2}(zb - n_{ab}) \tag{3}$$

Our problem is now reduced to the estimation of the number of distinct ways to realise n_{ab} contacts betweens A and B molecules in the latice previously described. We can notice that no latice dimensionality occurs.

Let us consider a_i the A molecules which have i B-type nearest neighbours and b_j the B molecules with j A-type nearest neighbours. Evidently :

$$n_{aa} = \frac{1}{2}\sum_i (za - i)a_i\,; \qquad n_{bb} = \frac{1}{2}\sum_i (z - j)b_j \tag{3}$$

$$a = \sum_i a_i\,; \qquad b = \sum_j b_j \tag{4a — 4e}$$

$$n_{ab} = \sum_i i a_i = \sum_j j b_j \qquad 0 \leqslant i, j \leqslant z$$

The energy can be written now :

$$E = \frac{1}{2}\left[w_{aa}\sum_i (z - i)a_i + w_{ab}\sum_{i,j}(ia_i + jb_j) + w_{bb}\sum_j (z - j)b_j\right] \tag{5}$$

The problem is now, to estimate the number of ways in which we can mix $a_0, a_1, a_2, \ldots b_0, b_1, \ldots b_z$ molecules A and B (distinct ways, only), on the conditions $4a - 4e$.

For a complete evaluation it is necessary to consider all the possible values of the sets $(a_0, a_1, \ldots b_z)$, satisfying relations $4a - 4e$.

But this number is :

$$g(a, b, n_{ab}) = \sum_{a_0}\sum_{a_1}\cdots\sum_{b_0}\cdots\sum_{b_z}\frac{a!\,b!}{a_0!\,a_1!\,a_2!\ldots b_{z-1}!\,b_z!} \tag{6}$$

sum taken only for those values of the fraction which satisfy the restrictive conditions $4c - 4e$. The formula is a product of two so called polynomial coefficients, generated evidently by the two polynom product :

$$P(x)P(y) = (1 + x + x^2 + \ldots + x^z)^a (1 + y + y^2 + \ldots + y^z)^b \tag{7}$$

preserving only those terms having the same exponent for variables x and y, in our case the coefficients of $x^{n_{ab}}y^{n_{aa}}$.

The partition function is now :

$$Z = \sum_{n_{ab}} g(a, b, n_{ab}) \exp\left\{\frac{-1}{2kT}\left[z(aw_{aa} + bw_{bb}) + n_{ab}(2w_{ab} - w_{aa} - w_{bb})\right]\right\} \tag{8}$$

and from the preceeding remarks we can easily see that it is generated by the product :

$$P_1(x)P_1(y) = (1 + e^{u}x + e^{2u}x^2 + \ldots e^{zu}x^{z})^{a}\,(1 + e^{u}y + \ldots + e^{zu}y^{z})^{b} \qquad (9)$$

with :

$$u = -\frac{1}{4kT}\,(2w_{ab} - w_{aa} - w_{bb}) \qquad (10)$$

and retaining also only those terms which have identical exponents for x and y.

These terms can be obtained by appropriate derivation and :

$$Z = \exp\left(\frac{-\,zaw_{aa} - zbw_{bb}}{2kT}\right)\frac{1}{(n\,!)^2}\sum_{n}\frac{\partial^{u}}{\partial x^{n}}\,\frac{\partial^{n}}{\partial y^{n}}\,[(\sum_{k} e^{ku}x^{k})^{a}(\sum_{1} e^{lu}y^{ll})]\Big|_{x,\,y=0} \qquad (11)$$

which is not the unique way to write this result.

We can remark here that the derivatives can be calculated by the residues formula, using for example the steepest descent method.

In a similar way the grand partition function can be calculated. A transposition can be made into the Ising model lattices.

We try to calculate the partition function and we use for this purpose a method which is equivalent to the maximum term method (or the maximum eigenvalue) in a matriceal description.

We must also retain the restrictive conditions 4c — 4e which mean to keep the number of components constant in the lattice and to take the same number of direct interactions A to B as the number of interactions B to A.

We shall use the conditions of conditioned extremum and we use the Stirling formula, for approximate factorials.

The free energy successively is :

$$F = -\,kT \ln Z \qquad (12)$$

$$F = -\,kT \ln \sum_{a_0}\sum_{a_1}\cdots\sum_{b_z}\frac{a!\;b!}{a_0!\,a_1!\ldots b_z!}\exp\left[\frac{-\,n_{ab}(2w_{ab} - w_{aa} - w_{bb})}{2kT}\right] - $$

$$-\,\frac{z}{2}\,(aw_{aa} - bw_{bb}) \qquad (13)$$

If we evidentiate the maximum term the free energy will become :

$$F = -\,kT \ln \frac{a!\,b!}{a_0!\,a_1!\,\ldots\,b_z!}\left[-\,n_{ab}\left(w_{ab} - \frac{w_{aa} + w_{bb}}{2}\right) - \right.$$

$$\left. -\,\frac{z}{2}\,(aw_{aa} + bw_{bb}) \right. \qquad (14)$$

together with the extremum conditions. These will imply a function f, which contain the Lagrange multiplicators.

$$f = F + p(a - \sum_i a_i) + q(b - \sum_j b_j) +$$

$$+ r(n_{ab} - \sum_i i a_i) + s(n_{ab} - \sum_j j b_j) \qquad (15)$$

together with another $2z + 3$ extremum conditions:

$$\frac{\partial f}{\partial n_{ab}} = 0 \qquad (16 - 18)$$

$$\frac{\partial f}{\partial a_i} = 0, \quad \frac{\partial f}{\partial b_j} = 0, \quad i, j = 0.\ 1,\ 2,\ \dots z$$

p, q, r, s are multiplicators.

These relations become successively:

$$\frac{w_{aa} + w_{bb}}{2} - w_{ab} + r + s = 0 \qquad (19-21)$$

$$a_i = \exp\left(\frac{p + r_i}{kT}\right), \quad b_j = \exp\left(\frac{q + sj}{kT}\right) \qquad i, j, = 0, 1 \dots z$$

and if we use again the relations $4c - 4e$, we find out:

$$a_i = a \frac{1 - t}{1 - t^{z+1}} t^i, \ b_j = b \frac{1 - v}{1 - v^{z+1}} v^j, \ i,\ j = 0,\ 1, \dots z \qquad (22-23)$$

here t and v are given by:

$$kT \ln t + kT \ln v = w_{ab} - \frac{w_{aa} + w_{bb}}{2} \qquad (24 - 25)$$

$$a \frac{z t^{z+2} - (z + 1) t^{z+1} + t}{(1 - t)(1 - t^{z+1})} = b \frac{z v^{z+2} - (z + 1) v^{z+1} + v}{(1 - v)\,(1 - v^{z+1})}$$

The relation 25 was obtained deriving 4e.

Replacing in the free energy (14) and in $4a - 4e$ the relations 22 — 25 we find:

$$F = -kTA \ln \frac{t - 1}{t^{z-1} - 1} - kTb \ln \frac{v - 1}{v^{z+1} - 1} + a w_{aa} - b w_{bb} \qquad (26)$$

This is a parametric representation of the free nergy, which lead easily to the chemical potentials.

If we derive relation 24 and multiply it by relation 25, finaly we have:

$$\mu_a = kT \ln(1 - t) - kT \ln(1 - t^{z+1}) - w_{aa} \tag{27}$$

$$\mu_b = kT \ln(1 - v) - kT \ln(1 - v^{z+1}) - w_{bb} \tag{28}$$

These are parametric representations which can also shape us out the functional dependence of chemical potentials in a latticeal model if we estimate the configurations in the manner represented here.

Further series developments will lead us to the critical conditions.

The model and the method can be extended to a model with variable coordination parameter, which is more natural. This will be perhaps a new attempt to describe phase transitions.

Extension to ternary or more complicated sistems can be made and also to more than nearest neighbours, but no essential features occurs. Supplementary, difficulties arise in calculs and in the restrictive conditions $4c - 4e$, concerning the values taked by the indepedent variables.

REFERENCES

1. I. PRIGOGINE, *Molecular Theory of Solutions*, North Holland, Amsterdam, 1957.
2. I. SYOZI, *Transformation of Ising Models*, in C. DOMB, M. S. GREEN, *Phase Transitions and Critical Phenomena*, vol. I, 269, Academic Press, New York, 1972.
3. H. N. V. TEMPERLEY, *Two-dimensional Ising Models*, idem as the reference, 2, pg. 227.
4. R. H. FOWLER, *Statistical Mechanics*, Cambridge Univ. Press, 1966.

Received, Mars 9, 1981

ANALELE UNIVERSITĂŢII BUCUREŞTI, FIZICA, XXX, 1981, PAG. 65–70

CRYSTAL GROWTH MECHANISMS IN SOLUTIONS

H. V. ALEXANDRU and I. DIMA

Faculty of Physics, University of Bucharest *

ABSTRACT

Crystal growth kinetic of ammonium dihydrogen phosphate (ADP) and Rochelle salt crystals in solutions is analysed vs. surface diffusion model. Microscopic parameters and activation energies has been estimated according to the model. On a thermodynamic basis it is concluded that at small supersaturations the surface diffusion mechanism playes the essential role for ADP, while the volume diffusion mechanism becomes important at large supersaturations for Rochelle salt crystals.

Introduction

The crystal growth mechanism is now investigated on the basis of experimental growth kinetic, according to some models, or by computer simulations. Both ways have to be checked vs. real growth. Generally, the "driving force" in crystal growth from the fluid phase is taken the relative supersaturation $\sigma = \frac{C}{C_0} - 1$ where C — actual concentration, C_0 — equillibrium concentration

The surface diffusion model, first time proposed by Burton, Cabrera and Frank [1], for the growth from the vapour phase, has been adapted by Bennema [2] for solutions growth. The volume diffusion growth model, also proposed by BCF [1], represents an alternative choise for crystal growth from solutions

---

* National Centre of Physics, PO Box 5211, Măgurele, Bucharest

Experimental

The growth kinetic of ADP singlecrystal at pH 4.8 has been measured using a weighing technique. Briefly, a double walled system for growing — dissolution measuremets of rapidely adjustable temperature (accuracy of 0,01°C) has been used and overal growth rate has been precisely determined following the crystal weight [3], [4]. Corrections for saturation temperature sliding due to crystal growth and solvent evaporation has been made [4] and gowing — disolution ratas has been fitted with the BCF ideal curves [1] — [4] eq. (1).

Rochelle salt crystals with linear dimensions up to 10cm have been grown in dynamic regime, using a planetary rotation mechanism (about 60 r.p.m.). The ,,c" linear dimension, i.e. R (001) has been measured vs. supersaturation, using a cathetometer (0.05 mm accuracy) [5].

Both type of data have been represented according to the BCF ecuation :

$$R = C\,\frac{\sigma^2}{\sigma_1}\ \mathrm{th}\,\frac{\sigma_1}{\sigma} \tag{1}$$

where characteristic constants C and σ_1 are presented in table 1.

Table 1

Crystal	C (mm/h)	1	Observations
ADP [4]	3.5	$2.4\cdot10^{-2}$	overal, growth
ADP [4]	4.5	$2{,}1\cdot10^{-2}$	overal, dissolution
RS [5]	8.0	$8.5\cdot10^{-2}$	001) face, growth
RS [5]	10.0	$8.5\cdot10^{-2}$	idem slightly impurified
RS [5]	9.8	$24.0\cdot10^{-2}$	(idem havy impurification

Results

The surface diffusion model for solutions growth, according to the Eyring's one particle model, as presented by Bennema [2], supposes an activated mechanism in three steps (fig. 1) :

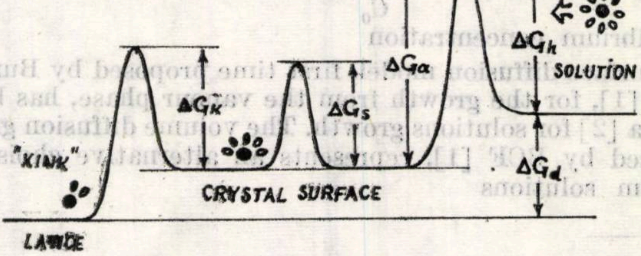

Fig. 1.

a) The growth unity (GU) hydrated (solvated) in soution, requires ΔG_h activation energy to enter the adsorbed layer.

b) In the mean lifetime in the surface layer, GU diffuse to the steps on the crystal surface, every jump requires ΔG_s activation energy, or after this time GU return to the bulk with an activation energy ΔG_a.

c) The *GU* integration to the kink (step), requires an activation energy ΔG_k, for final dehydraton of *GU* and of the kink, fig. 1.

1°. The mean free path (diffusion length) of growth unity (*GU*) in the adsorbed layer on the crystal surface is [2], [3]:

$$\lambda_s = \frac{9.5}{\varepsilon} \frac{\gamma \, a}{KT \, \sigma_1} \tag{2}$$

where : ε — the efficiency of the dominating group of dislocati on the crystal surface which creats the steps, γ — edge free energy par dislocations *GU* in the step, a — the linear dimension of *GU*, σ_1 — *BCF* constant (table 1). In accordance with Alexandru [3] we have found :

$$\lambda_s^{ADP} = (40 \div 50)a, \quad \lambda_s^{RS} \simeq 200a \tag{3}$$

2°. The dehydratation energy [2], [3] is :

$$\Delta G_h = RT \ln \left(\frac{c_0 \, \beta \, \nu \, \Lambda \, N_0 \Omega}{C} \right) \tag{4}$$

where c_0, β — constants $\simeq 1$, $\nu = KT/h$ frequency factor, $\Lambda \simeq 10$ Å thicknes of adsorbed layer, N_0 — concentration of *GU* in solution, Ω — — *GU's* volume in the crystal latice, C — *BCF* characteristic constant (table 1). We have found :

$$\Delta G_h^{ADP} = 12.4 \text{ Kcal/nol}, \quad \Delta G_h^{RS} = 11 \text{ Kcal/mol} \tag{5}$$

3°. The activation energy of the *GU* to return to the solution volume is :

$$\Delta G_a = \Delta G_h + RT \ln(N_{s0}/N_0) \tag{6}$$

where N_{s0} — concentration of *GU* in the adsorbed layer according to Alexandru [3], can be estimated as :

$$N_{s0}/N_0 = 1 + 50 \, \rho_{cr}/C_0 \tag{7}$$

where : ρ_{cr} — crystal density, C_0 — solution concentration (g/100 g solvent). We have found :

$$\Delta G_a^{ADP} = 12.8 \text{ Kcal/mol}, \quad \Delta G_a^{RS} = 11.2 \text{ Kcal/mol} \tag{8}$$

4°. The surface diffusion jump of GU on the crystal surface need an activation energy [2], [3] :

$$\Delta G_s = \Delta G_a - 2RT\ln(\lambda_s/a) \tag{9}$$

that is:

$$\Delta G_s^{ADP} = 8.1 \text{ Kcal/mol}, \quad \Delta G_s^{RS} = 4{,}8 \text{ Kcal/mol} \tag{10}$$

5°. The activation energy ΔG_k cannot be estimated in the frame of the model. Some superior limit have been estimated as proposed by Bennema using the condition for retardation factor $\beta \mapsto 1$. A more reliable value has been estimated by Alexandru [3] using Chernov's model for the surface diffusion in the presence of impurities [6]. For the Rochelle salt crystals grown in solution impurified with bakelite particles ($\sim 10\ \mu$), it has been found [3]:

$$\Delta G_k^{RS} = \Delta G_s^{RS} - RT\ln(\lambda_s/a) = 1.6 \text{ Kcal/mol} \tag{11}$$

Discussions

On the basis of estimated data we can asume for ADP crystal grown from solutions, the surface diffusion mechanism plays the essential role. According to Mullin [7], the activation energy for volume diffusion in *ADP* solutions is $\Delta G_v^{ADP} = 2.4$ Kcal/mol, while the surface diffusion requires a much larger value eq. (10): $\Delta G_s^{ADP} = 8.1$ Kcal/mol. So, the volume diffusion transport is not rate determining.

It has been demonstrated by Alexandru [3], that the volume diffusion model for ADP leads to a parabolic dependence of the growth rate on supersaturation, and the absolute value of this rate is negligeable small vs. experimentally measured rate. On the other hand, direct integration of GU from the volume, as a paralel process to the surface diffusion one, from a thermodynamic point of view is not competitive. Indeed, for direct integration GU has to overcame a barrier at least $\Delta G_h + \Delta G_k$, vs. ΔG_h in the second process.

Spiral growth mechanism for *ADP* crystal has been many times revealed [8], [9]. Dominating centers of growth, created by cooperating spiral dislocations on a (010) face of ADP crystals (static growth, normal pH) can be seen in fig. 2. Rounded steps and kinematic waves could be many times observed both in static and dynamic regime. In fig. 2, spreding out layers are not symmetrical because of crystal efilation along [001] direction.

For the Rochell salt crystal altough the surface diffusion model gives a resonable description at small supersaturations as demonstrated by Alexandru [3], at large supersaturations $\sigma = 0.1 - 0.2$, volume integration becomes competitive as a parallel process (amount about 20 — — 30% from the total rate).

Using the Arhenius temperature type dependence of C constant, eq. (4), for $T = 41°C$ data of Alexandru [5] and $T = 21°C$ data of Levina and Belustin [10], the activation energy for growth (the dehydration energy) has been estimated as:

$$\Delta G_h^{RS} = R\frac{T_1T_2}{T_1 - T_2}\ln(C_1/C_2) \simeq 4 \text{ Kcal/mol} \qquad (12)$$

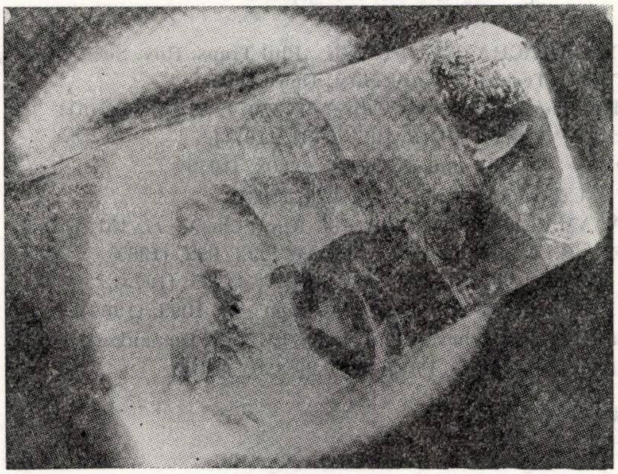

Fig. 2

A more realistic evaluation, using the growing kinetic data of Blaga [11] for Rochelle salt crystal, measured in similar conditions to Alexandru [5] gives:

$$\Delta G_h^{RS} = 6.1 \text{ Kcal/mol}$$

This discrepancy to the previouslly estimated value, eq. (5) shows that the surface diffusion mechanism does not control the growth process at high supersaturations.

On a thermodynamic basis we can assume that the volume integration may be competitive to surface integration as long as $\Delta G_k^{RS} = 1.6$Kcal/ /mol, eq. (11), is considerable smaller than ΔG_h^{RS} eq. (5). Indeed, both processes have energetical barriers $\Delta G_h + \Delta G_k$ and ΔG_h comparable to overcame and volume integration does not remain negligeable.

Although steps on (001) faces of Rochelle salt crystals have been many times observed [12] and dislocation mechanism operate, it is possible that high ordering in the adsorbed layer, or association degree of molecules in solution to be very large for *RS*, as approching temperature of fusion $T_f \simeq 56°$C

Conclusions.

1. Microscopic growing parameters and activation energies for growth of *ADP* and *RS* crystals have been estimated.

2. The growth of *ADP* crystals at small supersaturations ($\sigma \lesssim 5\%$) is surface diffusion controled.

3. For the RS crystal the volume integration at large supersaturations $\sigma \sim (10-20)$ % become competitive to the surface diffusion mechanism.

REFERENCES

1. W. K. BURTON, N. CABRCRA, F. C. FRANK „Phil Trans. Roy. Soc." *A 243*, 299 (1951).
2. P. BENNEMA, *Thèsis*, Technical University, Delft 1965.
3. H. V. ALEXANDRU, Thèsis, Bucharest University, 1974, (in Romanian)
4. H. V. ALEXANDRU, "J. Crystal Growth" *9*, 151, (1971).
5. H. V. ALEXANDRU- "Kristall und Technik" *8*, 803, (1973).
6. A. A. GHERNOV, "Uspeh. Fiz. Nauk", *73*, 275, (1961).
7. J. W. MULLIN, A. AMATAVIVADHANA, "J. Appl. Chem" *17*, 151, (1967).
8. J. L. TORGESSEN, R. W. JACKSON, „Science" *148*, 952, (1965).
9. R. J. DAVEY, J. W. MILLIN, "J. Crystal Growth", *29*, 45, (1975).
10. I. M. LEVINA, A. V. BELUSTIN, *"Kristallografiya"* *14*, 1093, (1969).
11. I. BLAGA, *Batcheler Thèsis*, Bucharest University 1975, (in Romanian).
12. H. V. ALEXANDRU, "Rev. Rom. Physique", *19*, 241, (1974).

Received, January, 12, 1981

ANALELE UNIVERSITĂŢII BUCUREŞTI, FIZICA, XXX, 1981, PAG. 71–74

OPTICAL CONSTANTS OF BISMUTH TRIOXIDE THIN FILMS

V. DOLOCAN

Faculty of Physics, University of Bucharest *

ELENA DOLOCAN

Physical and Technological Institute of Materials, Bucharest **

ABSTRACT

The optical transmision in flash evaporated bismuth trioxide thin films was studied in the visible and infrare drange 0.4 – 2.2 μm. Experimental data on the wavelength dependence of the refractive index and the extinction coefficient are presented. The dispersion of the refractive index follows a single oscillator model.

1. Introduction

In recent years the optical properties of materials are intensively studied for their applications [1 ÷ 5]. The tetragonal phase of bismuth trioxide has an optic energy gap of 3.6 eV [1] at room temperature, very close to the energy gap of CdS, a very useful material for solar cells. It was the aim of this work to determinate the real and imaginary parts of the complex refractive index by measuring the optical absorption in Bi_2O_3 thin films. The Bi_2O_3 films with thicknesses in the range 0.29 – 1.08 μm were obtained by thermal oxidation at 300 – 400°C of bismuth films produced by flash evaporation on a glass slide. Films formed in this way were orange-yellow in appearance, microcrystalline and had fairly uniform

---

* National Centre of Physics, PO BOX 5211, Măgurele-Bucharest

** National Centre of Physics, PO Box 5207, Măgurele-Bucharest

thickness. The optical properties were studied by measuring the transmission T of the sample between $\lambda = 0.4\ \mu$ m and $\lambda = 2.2\mu$m using a Beckmann Model *DU* spectrophotometer.

2. Transmission spectra

The transmission spectra for six typical samples of Bi_2O_3 deposited on glass are represented in Fig. 1. In the transparence region of these layers the variation of transsmision is due mainly to interference phenomena; the transmission exhibits interferential patterns. The optical constants were determined from the anvelope curves T_{max} and T_{min} as shown by the dashed lines in Fig. 1. Let us consider a thin film with a complex refractive index, $\eta = n - ik$. In the transparence region the following formula are adequate [5]

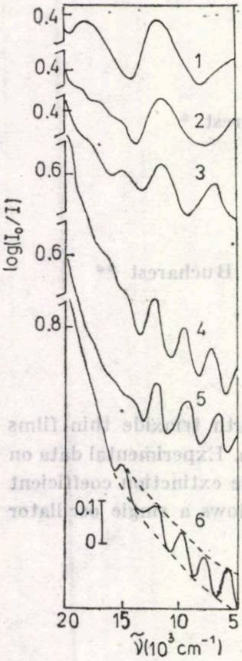

Fig. 1. Transmission specta of polycristalline Bi O₃ thin films

$$n = [N^2 + (N^2 - n_0^2\, n_1^2)^{1/2}] \tag{1}$$

where

$$N = \frac{n_0^2 + n_1^2}{2} + 2 n_0\, n_1\, \frac{T_{max} - T_{min}}{T_{max} \cdot T_{min}} \tag{2}$$

$n_0 = 1$ is the refractive index of air and $n_1 = 1.5$ is the refractive index of the glass substrate. The thickness d of the layer can be Calculated from two maxima or two minima, using

$$d = \frac{M\, \lambda_1\, \lambda_2}{2[n(\lambda_2)\lambda_1 - n(\lambda_1)\lambda_2]} \tag{3}$$

where M is the number of oscillations between the two extrema ($M = 1$ between two consecutive maxima or minima); λ_1, $n\ (\lambda_1)$ and $\lambda_2, n(\lambda_2)$ are the coresponding wavelengths and indices of refraction. The thicknesses of the samples corresponding to Fig. 1 were found to be the following: (1) 0.29 μm; (2) 0.33μm, (3) 0.46 μm, (4) 0,77 μm, (5) 0.79 μm, (6) 1.08 μm, The extinction coefficient k was calculated from the relation

$$\beta = \exp\,(-4\pi k\, d/\lambda) \tag{4}$$

where

$$\beta = \frac{C_1[1 - (T_{max}/T_{min})^{1/2}]}{C_2[1 + (T_{max}/T_{min})^{1/2}]}$$

$$C_1 = (n + n_0)(n_1 + n)$$

$$C_2 = (n - n_0)\,(n_1 - n)$$

From Fig. 2 it is observed that the index of refraction and extinction coefficient decrease with wavelength increasing. The values of n are in accordance with that derived from the wavelength position of the interference maxima [1]

$$nd = m\frac{\lambda}{4}$$

where d is the thickness of the film and m the order of the interference; m is even at the maxima and odd at the minima. For the curve 6 the order of the interference maxima are 4, 6, 8, 10. For longer wavelengths ($\lambda > > 1.4\mu$m) the single oscilator model may be used for the dispersion relation of the refractive index [1, 6]

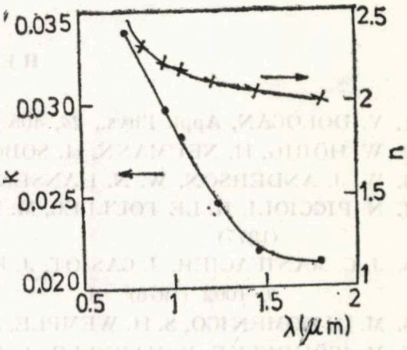

Fig. 2. Wavelength dependence of refractive index n and extinction coefficient$k$

$$n^2 - 1 = \frac{S_0\lambda_0^2}{1 - (\lambda_0/\lambda)^2}$$

where λ_0 is an average oscillator position and S_0 is an average oscillator strength. The oscillator strength S_0 is derived from the slope of the straight line $1/(n^2 - 1) = f(1/\lambda^2)$ in Fig. 3 while λ_0 follows from the infinite-wavelength intercept. The data obtained are the following: $S_0 = 1.16 \times_0$ $\times 10^{13}$ m^{-2}; $E_0 = hc\ /e\ \lambda_0 = 1.9eV$, $E_0/S_0 = 2.55 \times 10^{-13}$ eV m^2; E_0/S, is named the refractive index dispersion parametr. h is Planck's constant c is the speed of the light.

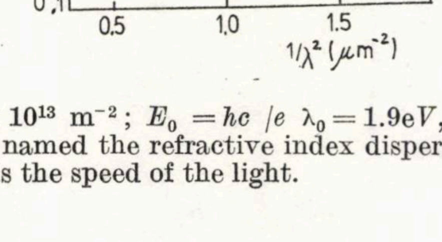

Fig. 3. $1./(n^2 - 1)$ as a function on $1/\lambda^2$

3. Conclusions

The value of $n = 2.1$ for Bi_2O_3 shows that this material may be optical matching between a luminescent material with a greater refractive index and air or between two materials with more different refractive indices.

The dispersion of the refractive index in the Bi_2O_3 thin films follows a single oscillator model. The value of refractive index dispersion parameter E/S is a constant independent of the material. Our obtained results are in agreement with the results for other materials [7]

REFERENCES

1. V. DOLOCAN, Appl. Phys., *16*, 405 (1978)
2. W. HÖRIG, H. NEUMANN, H. SOBOTA, Thin Solid Films, *48*, 67 (1978)
3. W. J. ANDERSON, W. N. HANSEN, J. Opt. Soc. Am., *67*, 1051 (1977)
4. N. PICCIOLI, R. LE TOULLEC, M. MEJATTI, M. BALKANSKI, Appl. Optics, *16*, 1236 (1977)
5. J. C. MANIFACIER, J. CASIOT, J. P. FILLARD, J. of Physics E : Scientific Instruments, *9*, 1002 (1976)
6. M. DI DOMENICO, S. H. WEMPLE, J. Appl. Phys., *40*, 720 (1969)
7. M. WÖHRECKE, V. MARELLO, A. ONTON, J. Appl. Phys., *48*, 1748 (1977)

ANALELE UNIVERSITĂŢII BUCUREŞTI, FIZICA, XXX, 1981, PAG. 75–81

THE ELECTROPHYSICAL PROPERTIES OF PbTe AND CdTe THIN FILMS

MOHAMED ISMAIL ABD EL ATI

Faculty of Science, Physics *

I. SPÂNULESCU, I. DIMA

Faculty of Physics, University of Bucharest **

ABSTRACT

The crystalline structure and some electrical properties of PbTe and CdTe thin films were studied. It is found that these properties depend on the stoichiometry and preparation conditions of the samples.

1. Introduction

In the last 10 – 15 years the study of the electrophysical and structural properties of thin films semiconductor materials was intensified according with finding more and more applications in electronics, optics, radiations dozimetry, optoelectronics, energetics etc. Among them a great interest is presented by the study of A^2B^6, A^4B^6, A^3B^5 semiconductor compounds, especially for radiation detectors, solar cells and optoelectronic devices.

In this paper some electrical and structural properties of PbTe and CdTe thin films obtained in various experimental conditions, are investigated.

2. Experimental

PbTe and CdTe thin films have been obtained by thermal evaporation in vacuum or in argon atmosphere using a method similar to that described in [1, 2]. As substrate some optically polished glass and quartz little plates have been used and they were heated at 25 to 300°C varying temperatures for PbTe and 30 to 400°C for CdTe. The evaporation temperature was varied between 300 and 850°C for both of the substances and the air or inert gas pressure value in the evaporation chamber was modified between 5.10^{-2} and 10^{-5} Torr.

---

* Permanent adress: Egypt, Tanta, Faculty of Science, Physics.

** National Centre of Physics, Măgurele, Bucharest, Romania P.O. Box 5211.

For faze composition analysis as a function of stoichiometric composition in the CdTe case, simultaneausly with the basic substance evaporation, one of the components (Te or Cd) was evaporated too, for different substrate temperatures.

The thickness of the obtained samples varied between 0.05 and 4.0 μm, and were measured using an interference microscope. For these samples the electrical resistivity as a function of substrate temperature and layers thickness, the sign of charge and the mobility of the carriers and also the temperature dependence of the resistivity were measured.

The crystalline structure of the samples was investigated by X-ray diffraction (the powder method) and by electron diffraction, using the transmission method and the electron beam reflexion by the surface layers of the thin films method.

3. Results and discussion

3.1. The crystalline structure of PbTe and CdTe thin films

The X-ray and electron diffraction structural analysis showed that the crystalline structure of PbTe and CdTe thin films have an essential dependence of samples obtaining conditions, especially of the nature, cleaning and the temperature of the substrate and also of the residual gases pressure value in the evaporation chamber.

As it have been showed in other previous papers [3 — 5], the crystalline structure of PbTe and CdTe thin films become better if the substrate temperature is increasing and if the pressure value in the evaporation chamber is decreasing. Also, it can be observed a significant growing of the crystallites and their prefferential orientation reported to certain crystallographic axis (fig. 1b) especially in [111] direction and sometimes in [100] direction.

By X-ray analysis it was established that PbTe crystallizes in the cubic system having a NaCl type lattice with the lattice period equal to (fig. 1, a)

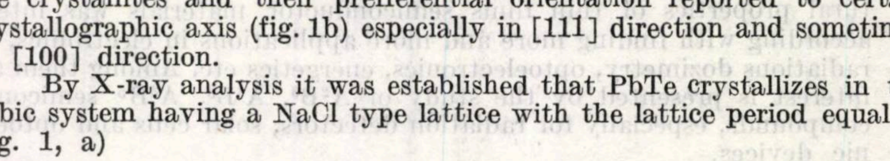

Fig. 1. a — X-ray pattern of PbTe thin film obtained on the substarte heated up to 250°C;

$$a = (6,439 \pm 0.007)\text{Å}$$

When the substrate temperature is getting higher ($t \gtrsim 200 - 250$°C) the crystalline structure of the PbTe crystallites is improving and it can be observed also a certain orientation of them in [111] direction. On very clean substrates, submited to a thermal treatment in vacuum for 30 minutes at 35°C, at high substrate temperature (300 – 350°C) and low pressure in the evaporation chamber ($p \approx 5.10^{-6} - 5.10^{-7}$ Torr), PbTe thin films with a structure near to that of a monocrystal can be obtained [6].

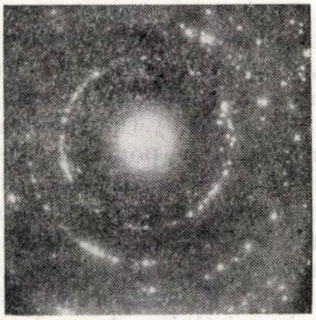

Fig. 1.b – Electron diffrction pattern of PbTe thin film obtained on substrate heated up to 200°C.

A big influence on the CdTe thin films structure has the layer's composition deviation from the stoichiometric one. As it was shown in [1,3 –8] for this substance like for ZnTe, ZnSe, CdS etc. characterisated by non-stoichiometric atoms excess presence, by modifying the stoichiometric composition can be obtained several structural modifications.

In the CdTe case, if Cd is evaporated simultaneously with the main substance, then in the obtained films a big number of hexagonal structure cystallites appear and grow, (fig. 2, *b*). The substrate temperature must bre generally enough high ($t > 220$°C), and the gases pressure in the chamber must vary between 2.10^{-2} and 10^{-4} Torr. If in the some experimental conditions only the main substance (CdTe) is evaporated, the obtained films contain only cubical structure crystallites (fig. 2, *a*).

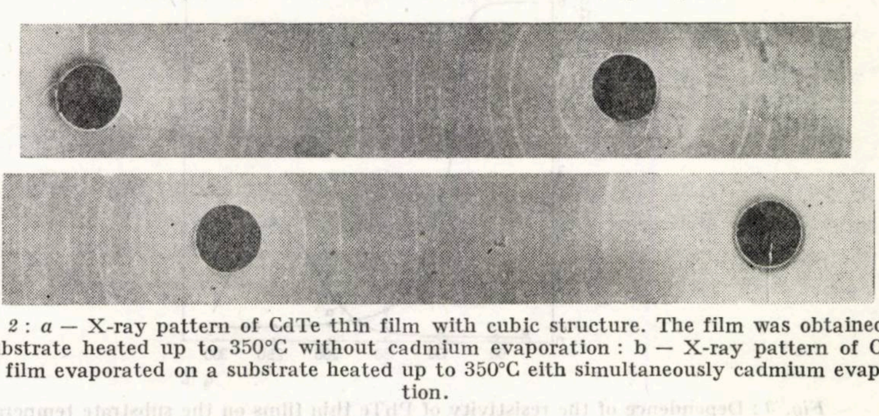

Fig. 2 : *a* – X-ray pattern of CdTe thin film with cubic structure. The film was obtained on a substrate heated up to 350°C without cadmium evaporation : b – X-ray pattern of CdTe thin film evaporated on a substrate heated up to 350°C eith simultaneously cadmium evaporation.

The lattice parameters of the crystallites contained in the studied thin films has been calculated taking into account the absorption correction. For the cubical structure CdTe crystal it was found the value

$$a = (6.474 \pm 0.005) \text{Å},$$

and for the hexagonal structure crystals the following values were obtained

$$a = (4.572 \pm 0.005)\text{Å}$$
$$c = (7.485 \pm 0.005)\text{Å}.$$

3.2. Electrical properties

The experiments showed that the electrical properties of the PbTe and CdTe thin films, as their crystalline structure have a strong dependence on the preparation conditions of samples. The greatest influence on these properties is exercited by the substrate temperature in the layer's condensing moment and the evaporation temperature. In the CdTe case it was observed that the obtained layer's resistance depends on the angle between the atomomo-lecular beam and the surface of the substrate, and also on the stoichiometric composition of the sample.

For the studied samples, the electrical resistivity ranged between 0.1 and $6.10^1\Omega$. cm for PbTe and between 1.0 and $10^7\Omega$. cm for CdTe. The PbTe thin films' resistivity dependence on the substrate temperature is represented in Fig. 3 (curve 1), for samples obtained from substances thermally nondegassed in vacuum (before evaporation) and respectively for the case when the initial substance have been before thermally treated in vacuum (fig. 3, curve 2)

From figure 3, it can be observed that for substrate temperature not too high, in the case of samples obtained from vacuum thermal untreated substance, low resistivity thin films are obtained, while for higher temperatures (above 200°C) greater resistivity thin films are obtained (fig. 3, curve 1). High resistivity samples are also obtained in the case, when then initial substance has been previously thermally treated in vacuum for 30′ at 450 – 500°C (Fig. 3, curve 2).

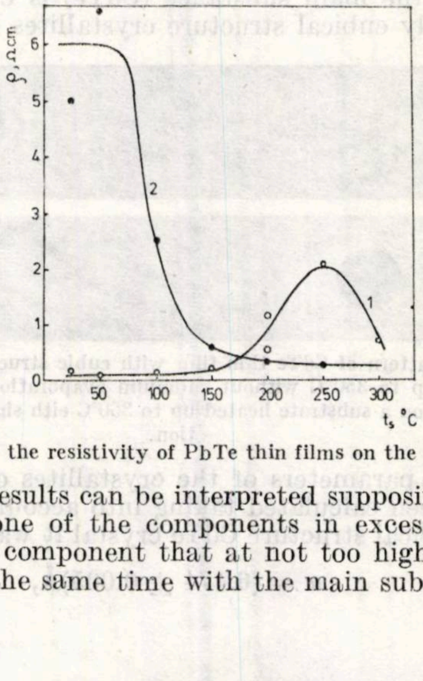

Fig. 3 : Dependence of the resistivity of PbTe thin films on the substrate temperature.

The obtained results can be interpreted supposing that in the initial substance there is one of the components in excess from the stoichiometric composition, component that at not too high substrate temperatures is deposed in the same time with the main substance, implying the layer's electrical dependence decreasing. For higher substrate temperatures ($t_s > 250°C$) a part of the excess component is back „evaporated" from the heated surface of the substrate and the composition of the sample becomes closer by the stoichiometric one [1, 3 – 6]. The same result is also obtained if the PbTe thin films are prepared from substance previously treated in vacuum at temperatures enough high for escaping the easy volatile component.

For higher substrate temperature ($t_s \gtrsim 300°C$ for PbTe and $t_s \gtrsim 400°C$ for CdTe) it can be observed a decreasing of the thin films resistivity, that can be explained by samples crystalline structure improving. It is not impossible that the high heated substrate deposed thin films' resistence decreasing to be caused in the same time by the excess presence of one or the other of the components, appeared by substance dissociating just on the very hot surface of the substrate [1 – 6].

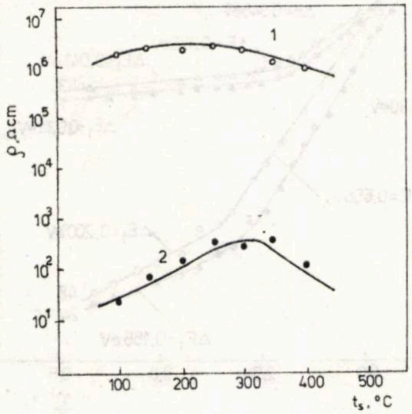

Fig. 4. Dependence of the resistivity of CdTe thin films on the substrate temperature : 1 — for normal incidence : 2 — for the oblique incidence.

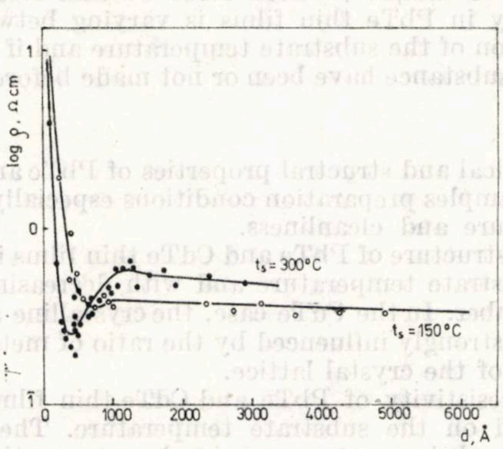

Fig. 5. Dependence of the resistivity of PbTe thin films on the samples thickness.

For CdTe case it was observed that the layers' resistivity depends by the evaporation angle (between the molecular-atomic beam and the support's surface) as it can be seen in fig. 4. For normal incidence high resistivity thin films are generally obtained (fig. 4, curve 1), while for a 10 — 80° angle low resistivity CdTe films are generally obtained (fig. 4, curve 2).

For PbTe thin films there were also measured the dependences of the electrical resistivity of the samples thickness (fig. 5), of the conductivity on temperature (fig. 6), and the carriers' mobility. It was found that the activation energy corresponding to the forbidden gap ΔE_g for PbTe is varying from sample to sample between 0.345 eV and 0.630 eV (fig. 6). The carriers' mobility in PbTe thin films is varying between 0.01 and 19 cm^2/Vs as a function of the substrate temperature and if vacuum thermal treatment of the substance have been or not made before evaporation.

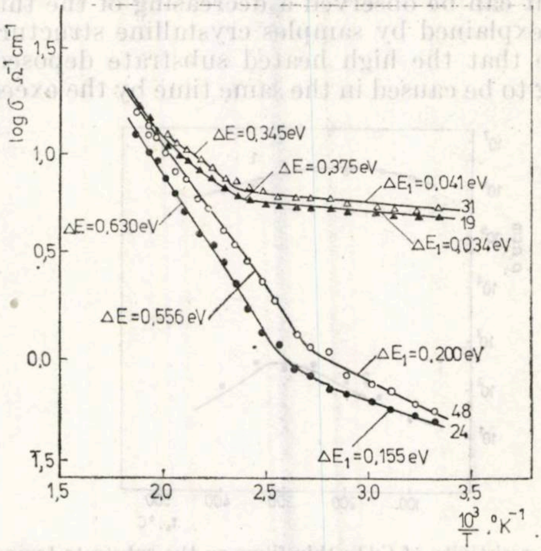

Fig. 6. **Dependence of the PbTe thin films conductivity on temperature, in vacuum, for samples obtained at different substrate temperature : $48 - t = 25°C$; $24 - t = 50_1 C\nu$ $19 - t = 250°C$; $31 - t = 300°C$.**

4. Conclusions

The electrophysical and structral properties of PbTe and CdTe films strongly depend on samples preparation conditions especially on substrate temperature, its nature and cleanliness.

The crystalline structure of PbTe and CdTe thin films improves with increasing of the substrate temperature and with decreasing pressure in the evaporation chamber. In the CdTe case, the crystalline structure and structural phases are strongly influenced by the ratio of metallic and nonmetallic components of the crystal lattice.

The electrical resistivity of PbTe and CdTe thin films and carrier mobility also depend on the substrate temperature. The results were different if the initial substances were previously vacuum thermal treated or if they were not. In the case of CdTe the electrical resistivity of thin films also depend on the angle between the atomo-molecular beam and the substrate surface.

REFERENCES

1. I. SPÂNULESCU, *Thesis*, Moscow, 1964.
2. I. SPÂNULESCU, Automatica şi Electronica, *9*, 163 (1965).
3. I. SPÂNULESCU-CARNARU, Phys. stat. sol. *18*, 769, (1966).
4. I. SPÂNULESCU-CARNARU, Phys. stat. sol. *15*, 761 (1966).
5. I. SPÂNULESCU-CARNARU, "Analele Universităţii Bucureşti", seria Fizică, XVI, *27* (1966).
6. I. SPÂNULESCU-CARNARU, I. DRAGHICI, Thin Solid Films, 3, 119 (1969).
7. I. DIMA, *Thesis*, Moscow, 1964.
8. I. DIMA, I. BORSAN, Phys. stat. sol., *23*, K 119 (1967).

PHOTOELECTRICAL PROPERTIES OF INDIUM MONOSELENIDE

HAMDIA I. ZAYED*, **I. MUNTEANU and I. DIMA**

Faculty of Physics, University of Bucharest **

ABSTRACT

The electrical and photoelectrical properties of polycrystalline and amorphous InSe have been investigated. From the study of the photoconduction in polycrystalline InSe it results that can be realized photodetectors which are sensitive in the spectral range within 0,6 and 1,6 μm. By thermal evaporation in vacuum it was realized heterostructures of the type CdS-aInSe. In the case when this isotype heterojunctions are illuminated through the CdS layer it is observed that the photoresponse changes its sign. Also it is shown that after thermal treatment the amorphous layer aInSe is transformed to polycrystalline and the maximum of the spectral photoresponse is shifted from 1,85 to 1,20 eV when the isotype heterojunctions are illuminated through the InSe layer.

1. Introduction

In the last few years it is observed a greater interest in the semiconductor compounds from the group $A^{III} - B^{IV}$ which show interesting photoelectrical properties and could be used as active medium for generation of laser radiation in the visible and near infrared regions. From this group of semiconductor compounds is InSe of which photoelectrical properties are the subject of this paper.

The monocrystalline InSe crystallize in hexagonal structure whose symmetry properties are described by the space group D^4_{6h}. The crystals have a lamellar structure and the layers of In and Se are arranged in the order Se-In-In-Se. Because of the fact that the chemical bonds between the layers (Se-Se) are predominantly of the Van der Waals type and weaker than the covalent bonds inside the layers, the monocrystals are easy clivage in the plane perpendicular to the C_6 symmetry axis.

---

* **Permanent address: University of Ein Shams Faculty of Women, Department of Physics, Cairo, Egypt.**

** **National Centre of Physics, Bucharest-Măgurele, P.O. Box 5211, Romania.**

The energy gap of InSe is approximatively 1,2 eV at 300°K [1 – 3] and because the charge carriers have relatively high mobilities in the plane perpendicular to the C_6 axis ($\cong 10^2 - 10^3$ cm^2/V s) it results that this semiconductor compounds presents interest for the photovoltaic conversion of solar energy. Although the studies in this direction are still in the beginning. The rsults obtained in [4 – 8] are promising and recently it is shown [9] that it can be realised Schottky diodes based on InSe with an efficiency of 5 – 6% in the photovoltaic conversion of solar energy.

The electrical and photoelectrical properties of InSe are much les studied in comparison with other semiconductor compounds from the group A^{III} B^{IV} (for example GaSe, GaS or GaTe). In the literature practically does not exist data referring to the physical properties of the polycrystalline or amorphous InSe. Because of these reasons the studies done in this direction present a big interest in the idea of using this semiconductor material not only for the photovoltaic conversion of solar energy but also for the realization of some electronic devices.

It is the aim of the present work to present some electrical and photoelectrical properties of polycrystalline and amorphous InSe. From the study of the photoconductivity of polycrystalline InSe it is shown that can be realized photodetectors which are sensitive in a spectral range between 0,6 and 1,6 μm. The amorphous thin layers of InSe were obtained by the method of thermal evaporation in vacuum. It was then realized heterostructures of the type CdS-aInSe. The maximum of the spectral distribution of the photoresponse when these structures are illuminated through the layer of aInSe are located at the wave length $\lambda = 0,67$ μm. If these structures are illuminated through the CdS layer then it is observed that the photoresponse changes its sign. Further it is shown that after thermal treatments of aInSe it transforms to polycrystalline InSe and the maximum of the photoresponse shifts from 1,85 to 1,2eV when the heterojunctions are illuminated through the InSe layer.

2. Photoconductivity of the polycrystalline InSe

The semiconductor compound of InSe was obtained by the direct synthesis of the In and Se of high purity (99,999%). In and Se, in stoichiometric composition, was introduced in a quartz tube evacuated to 10^{-5} mmHg. The synthesis of InSe was made at 800°C during a period of time of 40 hours. By slow cooling (50° C/hour) it was obtained a polycrystalline material with microcrystals of the order of millimeters. From such ingot was cut samples with dimensions of $3 \times 2 \times 1$ mm^2. The ohmic contacts was realized from In by thermal evaporation in vacuum. The experimental results showed that in the dark or for different intensities of the incident radiation the I – V characteristics are ohmic (Fig. 1). Also it was observed that the photocurrent varies linearly with the intensity of the incident radiation.

As it is shown in Fig. 2, the spectral distribution of the photecurrent presents a maximum for λ = 1,05 μm and corresponds to a width of forbidden gap of polycrystalline InSe, $E_g = 1{,}181$ eV. Comparing these results with those obtained in literatures [1–3,10], we observe the following particularities :

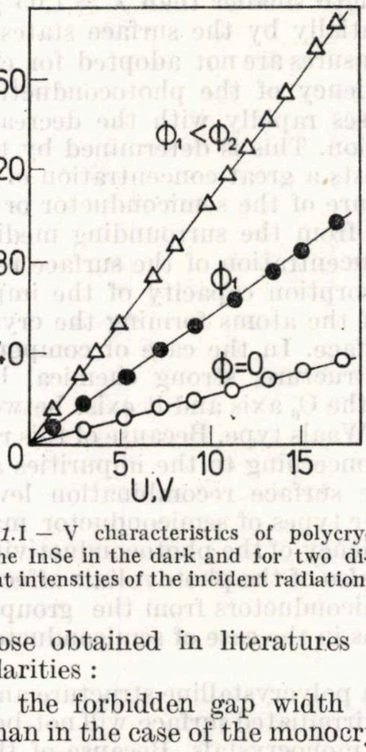

Fig. 1. I – V characteristics of polycrystalline InSe in the dark and for two different intensities of the incident radiation.

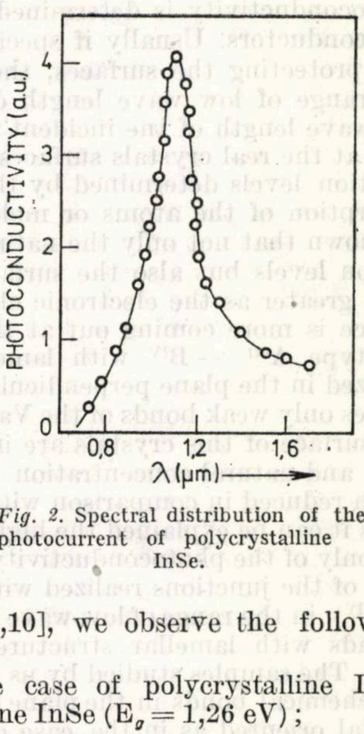

Fig. 2. Spectral distribution of the photocurrent of polycrystalline InSe.

— the forbidden gap width in the case of polycrystalline InSe is less than in the case of the monocrystalline InSe ($E_g = 1{,}26$ eV) ;

— the photoconductivity descreases rapidly to wave length less than λ = 1,1 μm but in the case of the monocrystals the spectral sensitivity is extended to wave lengths of the order λ = 0,35 μm [11].

The semiempirical calculation for the band structures of InSe [12,13] do not give complete information about the structure of threshold absorption. In the photoluminescence spectrum of InSe at the liquid nitrogen temperature it was observed one band at 1,1 μm and another one at 0,936 μm (14, 15). In the analysis of the absorption spectrum in [16] was shown that at the room temperature the width of the indirect forbidden gap is $E_g^i = 1{,}187$ eV. In the monocrystalline InSe, as it results from the spectral distribution of the absorption coefficient [10, 11] or of photoconductivity [17] and of photovoltaic efect in junctions based on InSe (9), in the vecinity of the direct absorption threshold is always the excitonic absorption even at the room temperature.

The samples studied by us have a polycrystalline structure so that the excitonic photoconductivity at the room temperature practically is inexistent. The maximum of the spectral distribution of the photoconductivity, observed at the wave length of the incident radiation $\lambda = 1{,}05\ \mu m$, it will be attribute to the indirect transitions and so for the width of the indirect forbidden gap of InSe it is obtained $E_g^i = 1{,}181$ eV. This result is in concordance with the value obtained in [6] from the analysis of the absorption spectrum of monocrystalline InSe.

The second particularity which we find it can be explained if we consider that in the range of wave length smaller than $\lambda = 1{,}05\ \mu m$ the photoconductivity is determined essentially by the surface states of the semiconductors. Usually if special measures are not adopted for cleaning and protecting the surfaces, the efficiency of the photoconductivity in the range of low wave length decreases rapidly with the decreasing of the wave length of tne incident radiation. This is determined by the fact that at the real crystals surfaces it exists a great concentration of recombination levels determined by the nature of the semiconductor or by the adsorption of the atoms or molecules from the surrounding medium. It is known that not only the natural concentration of the surface recombination levels but also the surface adsorption capacity of the impurities is so greater as the electronic cloud of the atoms forming the crystalline lattice is more coming out at the surface. In the case of compounds of the type $A^{III} - B^{IV}$ with lamellar structure, strong chemical bond is realized in the plane perpendicular on the C_6 axis and it exist between the planes only weak bonds of the Van der Waals type. Because of this reasons, the surface of this crystals are inert concerning to the impurities adsorption and natural concentration of the surface recombination levels is. much reduced in comparison with other types of semiconductor materials Thus it can be explained the high afficiency of the photoconductivity (and not only of the photoconductivity but also of the photovoltaic affect in the ashe of the junctions realized with semiconductors from the group $A^{III} - B^{IV}$) in the range of low wave lengths in the case of semiconductor compounds with lamellar structure.

The samples studied by us have a polycrystalline structure and thus, the chemical bonds in the plane of the irradiated surface will not be preferential oriented as in the case of the monocrystals. Because of this reason the concentration of the surface recombination levels is higher and effective depth of penetraing in sample of light with low wave length is smaller than in the case of monocrystals. Thus, it can be explained why the efficiency of the photoconductivity in the range of low wave lengths is much more reduced in the case of semiconductor compounds from the $A^{III} - B^{IV}$ group wihch have a polycrystalline structure.

3. Photoelectric properties of (n)CdS–(n)InSe isotype heterostructures

The structures of the type (n) CdS–(n) InSe was obtained by thermal evaporation in vacuum ($\cong 10^{-5}$ mmHg). The support temperature in the case of the evaporation of CdS was 200°C. Over the CdS layer was evaporated InSe. Substrate temperature during deposition of InSe were monitored by means of a thermocouple and was about 30°C. Source-to--substrate distance was 15 cm, with the vapor flow normal to the substrate surface. The InSe layers which are obtained in this conditions have amorphous structure and stoichiometric composition [18]. For realizing the ohmic contact with InSe another thin layer of In or Ag was deposited.

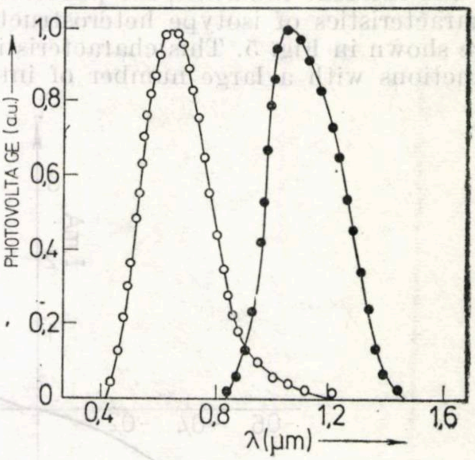

Fig. 3. Spectral distribution of the photoresponse befor (open circles) and after the effect of thermal treatment (full circles).

The geometry of such a structure is presented in the upper corner from the right in Fig. 4. The obtained heterojunctions was treated thermally at 200°C two hours long. The spectral characteristics of the photoresponse before and after the thermal treatment in the case of illumination through the InSe layer are shown in Fig. 3. We remark the fact that after thermal treatment the maximum of the spectral distribution of the photovoltage

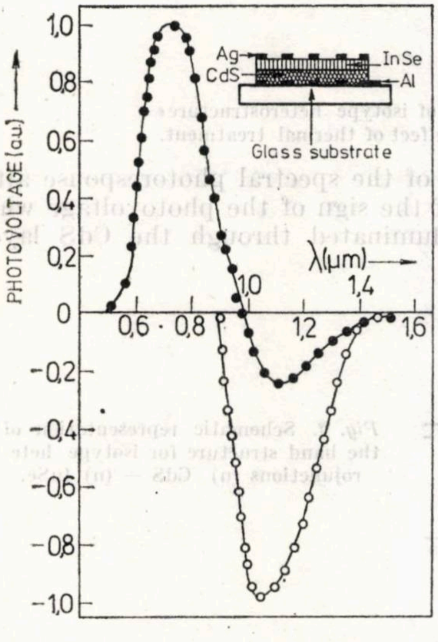

Fig. 4. Spectral distribution of the photoresponsse in the case of CdS—InSe structure after thermal treatment : ○ — sample irradiated through the InSe layer ; ● —sample irradiated through the CdS layer.

is shifted from wave length of 0,67 μm to 1,046 μm. The spectral distribution of the photoresponse in the case of the illumination through the CdS layer is shown in Fig. 4. We observe that with increasing the wave length of the incident radiation, the photoresponse changes its sign. The I – V characteristics of isotype heterostructures, after the thermal treatment, are shown in Fig. 5. This characteristics are specific for isotype heterojunctions with a large number of interface states.

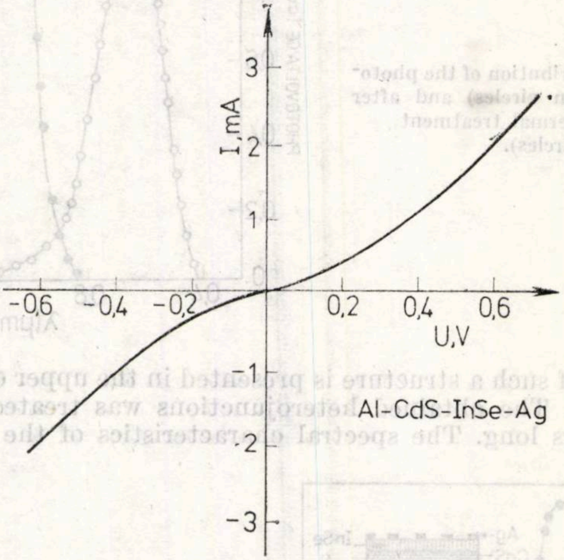

Fig. 5. I – V characteristics of isotype heterostructures (n) CdS – (n) InSe after the effect of thermal treatment.

For explaning the modification of the spectral photoresponse after thermal treatment and the change of the sign of the photovoltage when these isotype heterojunctions are illuminated through the CdS layer, we must take into account not only the nature of the semiconductors which form the isotype heterojunction but also their structural particularities. By means of a thermal probe it was found that the InSe layer is

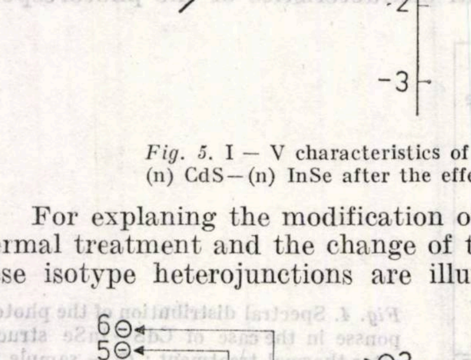

Fig. 6. Schematic representation of the band structure for isotype heterojunctions (n) CdS – (n) InSe.

of n-type not only before but also after thermal treatment. Before the thermal traeatment the InSe layer is amophous (aInSe), and because of the high densities of the interface states, the electrons from the conduction bands will be captured on this states so that the energy bands in CdS and also in InSe will be currved up. The schematic representation of the band structure for isotype heterojunctions (n)CdS-(n)InSe is shown in Fig. 6. In the same figure are shown the various excitation processes contributing to generation of photoresponse. It does not exist in literature dates concerning the width of the forbidden gap of amorphous InSe. From the spectral distribution of the photoresponse, as it is shown in Fig. 3, the forbidden gap width of amorphous InSe is equal to approximately 1,85 eV. By following, the incident radiation of wave lengths less than 0,67 μm in the case of illumination of the heterostructures through the aInSe layer will be absorbed in this layer and will generate charge carriers in the layer of CdS. Thus the photovoltage which appares will be determined only by charge carriers generated by the incident radiation absorbed in amorphous InSe.

The shift of photovoltaic response toward the greater wave length after thermal treatment is determined by the recrystallization of amorphous InSe layer. As it is observed from Fig. 3, the maximum of the photoresponse is at the wavelength $\lambda = 1{,}046$ μm and corresponds to a forbidden gap width $E_g = 1{,}185$ eV of crystallized InSe.

As it is shown in [19,20] the photoelectrical properties of the isotype heterojunctions can be explained by a structure model formed by two Schottky diodes connected back-to-back. This model is plausible in the case of isotype heterostructres studied by us because the lattice mismatch of the two semiconductor materials produce a large number of interface states. These interface states determine double depletion layers and the heterojunctions can be represented as two Schottky diodes back-to-back. A typical energy band diagram of such a double depleted type of n-n heterojunction and the various processes which contribute to photocurrent are shown in Fig. 6.

For the I — V characteristics of these two Schottky diodes the following relations can be written

$$I_1 = I_{s1}\,[\exp\,(a_1 V_1) - 1\,] - I_{f1} \tag{1}$$

and

$$I_2 = -I_{s2}\,[\exp(-a_2\,V_2) - 1] + I_{f2} \tag{2}$$

where I_{f1} and I_{f2} are the photocurrents generated by incidental radiation on the Schottky diodes 1 and 2 respectively. The expressions $I_{s1}\,[\exp(a_1 V_1) - 1]$ and $I_{s2}[1 - \exp(-a_2 V_2)]$ represents the dark majority current densities across the heterojunction when a voltage $V = V_1 + V_2$ is applied. From relations (1) and (2), for the open-circuit photovoltage we have

$$V_{0c} = \frac{1}{a_1}\ln\left(1 + \frac{I_{f1}}{I_{s1}}\right) - \frac{1}{a_2}\ln\left(1 + \frac{I_{f2}}{I_{s2}}\right) \tag{3}$$

In the case of a weak photoresponse, when $I_{f1} < I_{s1}$ and $I_{f2} < I_{s2}$, from relation (3) we obtained

$$V_{0c} = \frac{I_{f1}}{a_1 I_{s1}} - \frac{I_{f2}}{a_2 I_{s2}} \tag{4}$$

In conditions of a short-circuit $I_1 = I_2 = I_{0c}$, $V_1 + V_2 = 0$ and $a_1 V_1 \ll 1$, $a_2 V_2 \ll 1$. Thus, considering $\exp\,(a_2 V_2) - 1 \cong a_2 V_2$ and $\exp\,(a_1 V_1) - 1 \cong a_1 V_1$, for the short-cicuit photocurrent density we have

$$I_{sc} = \frac{I_{f2}\, I_{s1}\, a_1 - I_{f1}\, I_{s2} a_2}{I_{s1} a_1 + I_{s2}\, a_2} \tag{5}$$

From the relation (4) it can be observed that at small wave length, when the charge carriers are generated in the semiconductor with large forbidden gap (Fig. 6), the photoresponse will be positive. At greater wave lengths, when it happens the generation of charge carriers in the semiconductor with smaller energy gap and when in the relation (4) the second term is predominante, the photoresponse will changes its sign. The photoresponse changes its sign when the following relation is satisfied

$$I_{f1}\, I_{s2}\, a_2 = I_{f2}\, I_{s1}\, a_1 \tag{6}$$

As it results from Fig. 4, the change of the photoresponse sign happens at a certain wavelength of the incident radiation which can be modfied as a function of the applied voltage. It can be seen from this figure that there exists a unique wavelength for which there is no photovoltage at a given bias. Baised on this effect it can be made null detcting pyrometer with a high sensitivity.

The results obtained in this paper put in evidence the fact that the InSe not only in polycristalline form but also in amorphous one has some interesting properties and can be used for obtaining electronic or optoelectronic devices.

Received, 2 December 1980

REFERENCES

1. R. W. DAMON, R. W. REDINGTON, Phys. Rev. *96*, 1498 (1954).
2. G. B. ABDULLAEV, M. KH. ALIEVA. A. Z. MAMEDOVA, Phys. Stat. Sol. *25*, 75 (1968).
3. M. V. ANDRIYASHIK, M. YU. SAKHNOVSKII, V. B. TIMOFEEV, A. S. YAKIMOVA, Phys. Stat. Sol. *28*, 277 (1968).
4. V. L. BAKUMENKO, Z. D. KOVALYUK, L. N. KURBATOV, V. F. CHISHKO, Fiz. Tekh. Poluprovodn. *10*, 1045 (1976).
5. T. MATSUSHITA, T. T. NANG, M. OKUDA, A. SUZUKI, Japan, J. Appl. Phys. *15*, 901 (1976).

6. T. T. NANG, T. MATSUSHITA, M. OKUDA, SUZUKI, Japan. J. Appl. Phys. *16*, 253 (1977).

7. A. SEGURA, J. M. BESSON, A. CHEVY, M. S. MARTINI, Il Nuovo Cimento, *38B*, 345 (1977).

8. A. SEGURA, J. P. GUESDON, J. M. BESSON, Rev. Phys. Appliquée, *14*, 253 (1979).

9. A. SEGURA, A. CHEVY, J. P. GUEDSON, J. M. BESSON, Solar Energy Materials, *2*, 159 (1979/1980).

10. J. CAMASSEL, P. MERLE, H. MATHIEU, A. CHEVY, Phys. Rev. B *17*, 4718 (1978).

11. D. B. ANANINA, V. L. BAKUMENKO, L. N. KURBATOV, V. F. CHISHKO, Fiz. Tech. Poluprovodn. *10*, 2374 (1976).

12. J. V. MC CANNY, R. B. MURRAY, J. Phys. *C10*, 1211 (1977).

13. V. K. BAZHENOV, D. I. MARVAKOV, A. G. PETUKHOV, Fiz. Tekh. Poluprovodn. *13*, 1482 (1979).

14. L. N. KURBATOV, A. I. DIROCHKA. V. L. BAKUMENKO, Z. D. KOVALYUK, Fiz. Tverd. Tela, *12*, 3634 (1970).

15. V. L. BAKUMENKO, A. I. DIROCHKA, Z. D. KOVALYUK, L. N. KURBATOV, D. V. SOBOLEV, V. F. CHISHKO, Fiz. Tekh. Poluprovodn. *8*, 1016 (1974).

16. M. V. ANDRIYASHIK, M. YU. SAKHNOVSKII, V. B. TIMOFEEV, A. S. YAKIMOVA, Phys. Stat. Sol. *28*, 277 (1968).

17. G. B. ABDULLAEV, V. I. TAGIROV, A. G. KYAZYM-ZADE, M. M. PANAKHOV, V. L. SALMANOV, Fiz. Tekh. Poluprovodn. *14*, 1842 (1980).

18. YU. G. POLTAVSTEV, V. P. ZAKHAROV, T. V. REMIZOVICH, Krystallografiya, *18*, 1109 (1973).

19. A. KUNIOKA, Y. SAKAI, Japan. J. Appl. Phys., *7*, 1138 (1968).

20. A. G. MILLNES, D. L. FEUCHT, *Heterojunctions and Metal Semiconductor Junctions*, Academic Press, New York – London, 1972.

ANALELE UNIVERSITĂŢII BUCUREŞTI, FIZICA, XXX, 1981, PAG. 93–99

CRYSTAL FIELD SPLITTING OF THE GROUND LEVEL $^4I_{9/2}$ OF Nd^{3+} : YAG

C. CIUCU

Faculty of Physics, University of Bucharest *

S. GEORGESCU

Institute for Physics and Technology for Radiation Devices**

ABSTRACT

A crystal field analysis is applied to the ground level of Nd^{3+} in YAG. Being well isolated from the next ones, two simplifications can be made : the use of the Russell-Saunders coupling and the neglecting of the J mixing. The wavefunctions obtained can be used to evaluate the giromagnetic factors.

1. Introduction

The development and technical improvement of many laser systems during recent years have made necessary to use the best theoretical techniques, currently available, to analyse reported spectra in a consistent way to obtain a description of the rare earth ions behaviour in different host materials. Theoretical techniques that have had great application in the interpretation of the spectroscopic properties of the simpler elements have proved often to be quite inadequate for the rare earths.

In the case of the rare earths the crystal field splittings are a few hundred cm^{-1}, the spin-orbit effects on the order of a thousand cm^{-1}, and the electrostatic effects on the order of ten thousand cm^{-1}. Thus, in the case of rare earth ions, considering the crystal field to be a perturbation on the free ion levels has a certain amount of justification.

In this paper, after a review of theoretical techniques used in the interpretation of the spectroscopic data, we apply them to obtain the crystal field splittings and the wavefunctions of the ground level $^4I_{9/2}$ of Nd^{3+} ion in YAG. These wavefunctions can be used to evaluate other observabls as giromagnetic factors.

---

* National Centre of Physics, PO BOX 5211, Măgurele, Bucharest

** National Centre of Physics, PO BOX 5206, Măgurele, Bucharest

II. Review of theory

II. 1 Free ion

The ground configuration of trivalent rare-earth (R^{+3}) is $(Xe)4f^N$. The total Hamiltonian of a system, consisting of a rare earth ion situated in the electric field produced by surrounding lattice ions, can be written in the form

$$H = E^1 e_1 + E^2 e_2 + E^3 e_3 + \xi \sum l_i s_i + \alpha L(L+1) +$$

$$+ \beta G(G_2) + \gamma G(R_7) + H_{ss}(M^0, M^2, M^4) + H_{s00}(M^0, M^2, M^4) +$$

$$H_{s00}(M^0, M^2, M^4) + H_{ci}(P_2, P_4, P_6) + \sum t_i T_i + H_{cf}$$

The first three terms are the electrostatic interaction cast in a form due to Racah (1). The E^k are combinations of Slater integrals wich are treated as adjustable parameters and the $e_k's$ are angular operators which have been tabulated by Nielson and Koster (2). The fourth term is the spin-orbit interaction with ξ being an adjustable parameter. The next three terms are two-body configuration interaction terms; α, β and γ are adjustable parameters and $G(G_2)$ and $G(R_7)$ ar eigenvalues of Casimir's operators for the groups G_2 and R_7 (3). The terms H_{ss}, H_{s00} and H_{00} represent the spin-spin, spin-other-orbit and orbit-orbit interactions. They are functions of the so called Marvin integral M^0, M^2, M^4 (4). The term H_{ci} stands for the electrostatically correlated spin-spin interactions (5, 6), P^2, P^4 and P^6 being essentially radial integrals. The terms in T^i are effective three-body interactions (7).

The above Hamiltonian can be split into two parts:

$$H = H_0 + H_{cf} \tag{2}$$

where H_0 is the free ion Hamiltonian, for which the eigenvalue problem is assumed solved (8, 9) and H_{cf} describes the perturbation generated by the crystal field.

The Hamiltonian H_0 is diagonalized in the Russell-Saunders basis, its eigenvectors being liniar combinations of Russell-Saunders coupled states $|f^N SL>$:

$$|f^N[SL]J> = \sum A(S, L)\,|f^N SLJ> \tag{3}$$

In these "intermediate coupled" states the quantum numbers S and L, although convenient for purposes of labelling, are not "good" and are enclosed in square brackets. So, the spectroscopic notation $^4I_{9/2}$ means that the term ^4I has the largest contribution to this level.

In the case of rare earth ions the crystal field interaction is weak compared to H_0 due to strong screening of deep-lying $4f$-electronic shells from the crystal fields.

A free ion level with total angular momentum J is $(2J + 1)$ — fold degenerate. This degeneracy is removed by the crystal field interaction. Crystal field splitting has two aspects : one concerns the symmetry of the problem, namely, the number of levels into which the free ion J levels are split in a crystal field of a given symmetry ; the second concerns the size of the crystal field splitting. Whereas the first topic is now completely understood, the second is being actively researched, and the various mechanisms that determine the magnitude of the crystal field splitting are by no means completely understood.

II. Crystal field

a. Simmetry consideration

When an atom or ion is located, not in the free space, but in a crystal, it is subjected to various inhomogeneous electric fields which destroy the isotropy of free space. Thus the symmetry group is reduced from that of the full three-dimensional rotation group plus inversion to some finite group of rotations through finite angles and perhaps also reflections.

Each J-value of the free atom will span a $(2J + 1)$ — dimensional representation of R_3. This representation may be descomposed into irreducible representations of the subgroup associated with a particular point symmetry. If there is an odd number of electrons J is half integral and we have deal with representations of the full rotation group which are double-valued. Within the farmework of double-group method, introduced by Bethe (10) we can handle the half integral J's by the same procedure as was developed for the ordinary case (integral J).

Tables for reductions of irreducible representations D_J of R_3 to the irreducible representations of the thirty-two crystallographic point groups have been given by Koster et al (11). An inspection of these tables shows that for half integral values of J all the groups other than cubic give rise to $J + 1/2$ levels. This is in accordance with the well known theorem of Kramers (10) wich states that all energy levels of a system containing an odd number of electrons must be at least double degenerate regardless of how the symmetry, is, provided that there are no magnetic fields. This is due to another esential symmetry to be considered, namely, time reversal symmetry.

b. Quantitative evaluations of splitting

In order to consider the splitting of degenerate levels of rare-earth ions in a crystal field quantitatively, one must solve the secular equation of perturbation theory, namely :

$$|< JM \,|\, V_{cf} \,|\, J'M' > - \,\lambda\, \delta_{JJ'} \delta_{MM'} | = 0 \tag{4}$$

wich involves the evaluation of the matrix elements of the crystaline field between free ion states.

The crystal field potential acting on the electrons of a rare-earth ion can be represented in the form :

$$V_{cf} = \sum_{k=0}^{\infty} \sum_{q=-k}^{+k} \sum_{i} B_q^k (C_q^k)_i = \sum V_q^k \tag{5}$$

where the summation involving i is over all electrons of interest and

$$C_q^k = (4\pi/2k+1)^{1/2}\, Y_k^q \tag{6}$$

The quantities B_q^k are regarded as simply coefficients of expaneion to be determined empirically from the experimental data ; Y_q^k are spherical harmonics. The use of group theory permits the determination of which spherical harmonics will be significant in the expansion of the crystal field potential (12). First of all, as long as we have deal with a single configuration, k must be even. Secondly, all matrix elements are ultimately reduced to integrals involving on-electron, functions, the angular part of which are expressible as spherical harmonics. The triangular condition for spherical harmonics demands that $k \leqslant 21 = 6$, fo the case of f-electrons. Hence we need consider only spherical potentials V_0^0, V_q^2, V_q^4, V_q^6. The term V_0^0 simply shifts the whole Stark levels a constant amount and will be ignored. The number of nonzero terms is then further restricted by the point symmetry at the site of the rare earth ion.

We shall now deal with the calculation of the angular part of the crystal field matrix elements

$$<f^N\tau SLJM\,|V_{cf}|\,f^N\tau' S'L'J'M'> =$$

$$= \sum B_q^k <f^N\tau SLJM\,|U_q^k|\,f^N\tau' SL'J'M'> <f\,\|C^k\|\,f> \tag{7}$$

(since V_{cf} is an electrical interaction, it cannot act on spin and therefore $S = S'$). Here we used the nomalized U_q^k. To get the proper normalization ($<f\,\|U^k\|\,f> = 1$) we have multiply by $<f\,\|C^k\|\,f>$. Applying the Wigner-Eckart theorem, the matrix element becomes

$$<f^N\tau SLJM\,|U_q^k|\,f^N\tau' SL'J'M'> =$$

$$= (-1)^{J-M} \begin{pmatrix} J & k & J' \\ -M & q & M' \end{pmatrix} <f^N\tau SLJ\,\|U^k\|\,f^N\tau' SL'J'> \tag{8}$$

$\begin{pmatrix} J & k & J' \\ -M & q & M' \end{pmatrix}$ is the standard 3-j simbol tabulated by Rotenbeg et al (13). $<f^N\tau SLJ\,\|U^k\|\,f^N\tau' SL'J'>$ is called a reduced matrix element. This reduced matrix element can be further reduced

$$<f^N\tau SLJ \parallel U^k \parallel f^N\tau' SL'J'> = \qquad (9)$$

$$= (-1)^{S+L+J+k}\sqrt{(2J+1)\,(2J'+1)}\begin{Bmatrix} J & J' & k \\ L' & L & S \end{Bmatrix} <f^N\tau SL \parallel U^k \parallel f^N\tau' SL'>$$

The factor within braces is a 6-*j* symbol also tabulated in the Rotenberg's tables (13). $<f^N\tau SL \parallel U^k \parallel f\tau^N SL'>$ is frequently called a double reduced matrix element and can be found in the tables of Nielson and Koster (2).

These formulas are the most general ones. The matrix elements are diagonal only in S, and the formula make it possible to evaluate matrix elements of the crystal field Hamiltonian between states of different *J* as well.

III. The crystal field splitting of the ground level $^4I_{9/2}$ of Nd^{3+} in YAG

The crystal $Y_3AL_5O_{12}$ (YAG) posses a cubic symmetry (space group O_h^{10}-Ia3d). The site symmetry of Y^{3+} (wich is substituted by Nd^{3+}) is D_2. For the symmetry the double-valued representations of R_3 are descomposed according to (11):

$$D_J^{\pm} \rightarrow (J + 1/2)\,\Gamma_5 \qquad (10)$$

The crystal field Hamiltonian for this symmetry is:

$$H_{cf} = \sum V_q^k = \sum B_q^k\,(\,C_q^k + C_{-q}^{\,k}) \qquad (11)$$

$$k = 2,\ 4,\ 6\ ;\ q = 0,\ 2,\ 4,\ 6\ ;\ q \leqslant k$$

The matrix elements of the tensor operators C_q^k between the states of $^4I_{9/2}$ were calculated using Eqs. (7), (8) (and (9) and the tables of Rotenberg et al (13) for 3-j and 6-*j* symbols and of Nielson and Koster (2) for double reduced matrix elements. For $^4I_{9/2}$ level the Russell-Saunders coupling is a good aproximation wich permits to sinplify the calculations. Also, the ground level is well separated from the next one, so the J-mixing can be neglected.

The matrix elements depend on the parameters B_q^k; these parameters may be chosen to minimize the rms deviation between theoretical and experimental energy level schemes. The crystal field parameters for Nd^{3+} in YAG have been calculated by several authors (14, 15, 16). We used the following parameters (16) (in cm^{-1}):

$$B_0^2 = -336\ ;\ B_2^2 = 209\ ;\ B_0^4 = -2872\ ;\ B_2^4 = 14\ ;\ B_4^4 = 1159\ ;$$

$$B_0^6 = 992 : B_2^6 = -339\ ;\ B_4^6 = 1611\ ;\ B_6^6 = 133$$

The diagnolization of crystal field matrix yields following eigenvalues (normalized to the lowest crystal field level) : O, 139, 191, 318, 857 (experimental values are 0, 134, 197, 411, 848).

The eigenbectors corresponding to the lowest level are :

$$\left\{\begin{array}{c} -0{,}639\left|-\frac{9}{2}\right\rangle -0{,}011\left|-\frac{5}{2}\right\rangle + 0{,}743\left|-\frac{1}{2}\right\rangle + 0{,}082\left|+\frac{3}{2}\right\rangle \\ -0{,}173\left|+\frac{7}{2}\right. \\ \\ M \to -M \end{array}\right.$$

These eigenvectors are superpositions of states with $M + mq$, with m integer. For D_2 symmetry $q = 2$. So, M is no longer a good quantum number. Hellwege (3) introduced the crystal quantum number μ, wich is that' M of the set of $M's$ mixed by crystal field wich is the smallest in absolute magnitude.

IV. Conclusions

The separation of the full Hamiltonian into two parts : "free ion' and crystal field gives the possibility to solve the problem of rare earth ion embeded in a crystal. The intermediate coupling parameters are sometimes juggled, along with the B_q^k, to produce a best fit. Wybourne (3) has stressed the danger inherent in letting the complete set of parameters ("free ion" parameters and B_q^k) vary simultaneously in a least squares fit to the energies of all the states since, the B_q^k tend to accommodate the inadequacies of the treatment of the free ion levels, with the result that although the calculation of the free ion levels will be improved, the crystal field splittings of the levels will be badly represented.

Using the set of crystal field parameters published by Nekvasil (16) and making two simplifications (*LS* coupling and negect of J-mixing) the wavefunctions for the ground level are obtained. These wavefunctions can be used to calculate the giromagnetic factors.

An inspection of these functions shows that the M-states are well mixed. This mixing supports one of the hypothesis of Judd-Ofelt, theory, namely, the uniform population of M-states.

REFERENCES

1. G. RACAH, Phys. Rev., *76*, 1352 (1949)
2. C. W. NIELSON and G. F. KOSTER, *Spectroscopic Coefficients for p^n, d^n, and f^n Configurations* (The MIT Press, Cambridge. Mass. 1963)
3. B. G. WYBOURNE, *Spectroscopic Properties of Rare Earths* (Interscience, New York, 1965)
4. H. H. MARVIN, Phys., Rev., *71*, 102 (1947)
5. K. RAJNAK and B. G. WYBOURNE, Phys. Rev., *134*, A596 (1964)

6. B. R. JUDD, H. M. CROSSWHITE and H. CROSSWHITE, Phys. Rev. 169, 130 (1989).
7. B. R. JUDD, Phys. Rev., *141*, 4 (1966)
8. B. G. WYBOURNE, J. Chem. Phys., *34*, 279 (1961)
9. C. CIUCU, S. GEORGESCU and V. LUPEI, Rev. Roum. Phys. (1981 in press)
10. M. TINKHAM, *Group Theory and Quantum Mechanics*, Mc Graw-Hill, 1964
11. G. F. KOSTER, J. O. DIMMOCK, R. G. WHEELER and H. STATZ, *Properties of the Thirty-two Point Groups*, (The M.I.T. Press, Cambridge, Massachusetts, 1963).
12. J. L. PRATHER, *Atomic Energy Levels in Crystals*, Nat. Bur. Standards, Monogr. 19 (1961)
13. M. ROTENBERG, R. BIVINS, M. METROPOLIS and J. WOOTEN Jr., *The 3-j and 6-j Symbols*, Technology, Press, M.I.T. (1959)
14. B. C. TOFIELD, H. P. WEBER, T. C. DAMEN, and P. F. LIAO, J. Solid State Chem., *12*, 207 (1975)
15. J. A. KONINGSTEIN and J. E. GEUSIC, Phys. Rev., *136A*, 711, (1964)
16. V. NEKVASIL, J. Phys. C : Solid State Phys., 7*L*, 246, (1974)

Received January 8, 1981

ANALELE UNIVERSITĂŢII BUCUREŞTI, FIZICA, XXX, 1981, PAG. 101–105

FLUORIMETRIC EVALUATION OF TYROSINE CONTENT OF SOLUBILIZED COLLAGEN

V. GHEORGHE, GABRIELA ANGEL,

Faculty of Physics, University of Bucharest*

VIORICA TRANDAFIR

Institute for Leather and Shoe Research, Bucharest

OLGA IONESCU

Secondary School of Mathematiques and Physics, No. 4, Bucharest

ABSTRACT

The fluorescent properties of a series of neutral hydrolysates of collagen have been investigated. Using the method of Jankowski-Siemion, there have been determined the number of tyrosyl residues per molecule, n_{tyr}. The variation of n_{tyr} is correlated with the molecular weight i.e. the hydrolysis time.

Introduction

Collagen, a largely insoluble protein, is the major structural component of the animal body. Due to complex biochemical and microbiological investigations, today is known the almost complete picture of the amino acid composition of collagens of different origin [1]. It is well documented that collagen do not contain tryptophan and contains only a few tyrosyl and phenylalanyl residues. These residues are the most important fluorophores of collagen, though there has been attempts to

---

* National Centre of Physics, P.O.Box 5211, Măgurele, Bucharest

put into evidence the fluorescent contribution of the peptidic bond and of the double bond involved in carbonylic group [2]. Further, it has been reported a specific collagen fluorescence with the maximum of excitation at $\lambda_{ex} = 325$ nm and emission maximum near 410 nm, attributed to a structural element formed by crosslinking and designated by the authors "pyridinoline" (3).

There is a certain disagreement in the literature in connection with the fluorescence of collagen mostly due to the different experimental conditions involved (pH, temperature, concentration, which due influence the luminiscence) and also due to disregarding the possibility of phosphorescent deexcitation.

In our experiments there have been investigated some hydrolysis products of collagen. These hydrolysates, used mostly for medical and biotechnological purposes, have to be characterited in a complex manner befor using them. The present paper contains part of our results regarding the collagen hydrolysates. Among our scopes were the study of the luminescent properties of collagen hydrolysates and dosage of the aromatic amino acids, which certainly are the most important fluorophores of it. Such studies have a preparing character in view of using fluorescent markers for studying the uptake of hydrolysates by the living organisms.

Materials and Methods

Our experiments were performed on a series of collagen hydrolysates obtained by neutral hydrolysis of 2, 4, 6, 8 hours and labeled respectively NH2, NH4, NH6, NH8 (5).

Fluorescence spectra were recorded with an Aminco-Bowman spectrophotofluorimeter; pH was controlled with a Radiometer PHM63 pH-meter using a combined electrode. Molecular weights were determined by viscosimetric method.

For the dosage of tyrosine and tryptophan we used the method of Jankowski and Siemion (4). This method, based on the inner filter effect, permits the nondestructive determination of the tyrosine content of proteins not containing tryptophan and of the tryptophan content, independently of the amount of tyrosine present. In our case, the method permits to check the purity of the hydrolysates with respect to tryptophan containing proteic impurities.

Appropriate amounts of each hydrolysate were disolved in 0.2 M phosphate-citrate buffer, pH 5.4, in order to obtain concentrations of 0.10 mM, 0.15 mM, 0.20 mN, 0,40 mM, 0.60 mM, 0.70 mM and 1 mM. Emission spectra were recorded at these concentrations. The excitation beams were of 280 nm and 285 nm for tyrosine and of 295 mn and 300 nm for tryptophan detection. Figures 1—4 presents the variation of the maximum emission intensity versus concentration for $\lambda^1_{ex} = 280$ nm and $\lambda^2_{ex} = 285$ nm in the case of NH2, NH4, NH6, NH8.

As reference materials for dosage, we used tyrosine and tryptophan standards as indicated by Jankowski-Siemion (4).

Table 1. shows the molecular weights, the cros spoints of the Jankowski-Siemion diagrams and the number of tyrosyl re sidues, as determined in the present investigation.

Results and Discussions

The hydrolysis process consists in several steps which results in disaggregating the collagenous macromolecular assemblies. After the removal of noncollagenous components follows: 1) the disaggregation of collagen fibrils; 2) irreversible melting of the helical structure; 3) irreversible rupture of some interchain bonds; 4) irreversible rupture of some peptide linkages at certain points of the back-bone.

Following the hydrolysis process, it resulted a series of hydrolysates with the mean molecular weight distributed in the range 30,000–100,000, in function of hydrolysis duration, according to table 1.

Table. 1

Molecular characteristics of the collagen hydrolysates ; MW-molecular weight ; N,-approximate number of resides per molecule ; x-abscisa of the crosspoint in the Jankowski-Siemion diagram ; *n* — number of tyrosyl residues per molecule.

Hydrolysate	MW	N	x	n
NH2	100,000	1,000	1.26	1.82
NH4	70,000	700	1.36	1.72
NH6	40,000	400	1.40	1.60
NH8	30,000	300	1.47	1.57

The excitation spectra of collagen hydrolysates were similar, with a single peak at 285 nm (for emission set at 350 nm) suggesting the presence of tyrosylic chromophores.

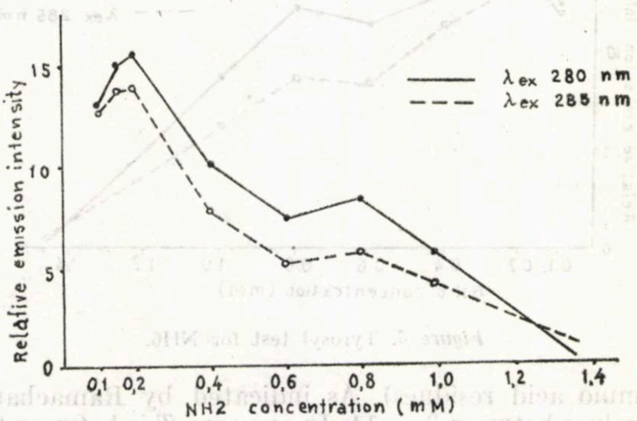

Figure 1. Tyrosyl test for NH2.

The curves of the maximum emission intensity versus concentration, for excitation with 295 nm and 300 nm, do not intersect for none of the hydrolysates, that is they do not contain tryptophyl residues. This is in accordance with our expectancies as collagen do not contain Trp and our material should be free of noncollagenous, accidentally Trp containing proteins.

To accomplish the tyrosine dosage, we recorded the emission spectra for decreasing concentrations in the range 1 mM –0.1 mM, for all hydrolysates. The Jankowski-Siemion diagrams for tyrosine dosage are presented in figures 1 – 4. From the crosspoints we obtained the number of tyrosyl residues per molecule, n_{tyr}, as indicated in table 1. From table 1. it is obvious that as the mean molecular weight decreases, n_{tyr} decreases too. The values of n_{tyr} obtained from our experiments can be correlated with the values indicated in literature for T(number of tyrosyl residues per 1,000 amino acid residues). As indicated by Ramachandran (1), T has usually values between 3 – 11. In our case T is between 2 – 5. These lower values of T can be explained by the destructive preparative procedure involved in our experiments.

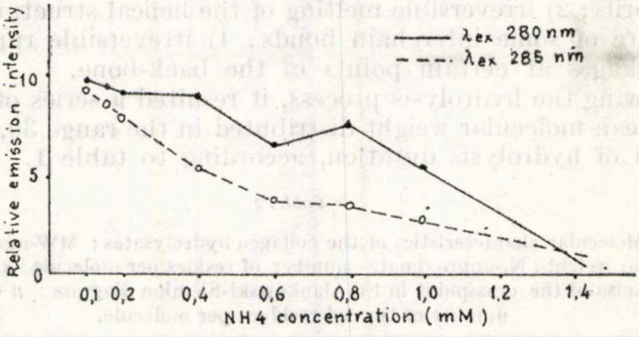

Figure 2. Tyrosyl test for NH4.

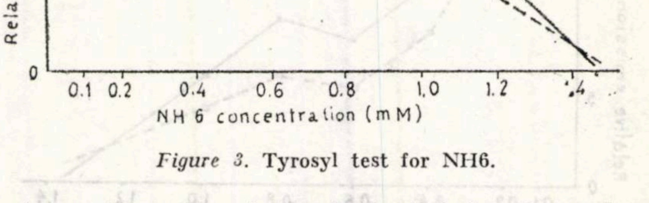

Figure 3. Tyrosyl test for NH6.

One can observe on the curves presented in figures 1 – 4, that all of them show a relative minimum of emission intensity at concentration of 0.6 mM. We advance the hypothesis that at this concentration some kind of aggregation could occure. This has to be checked in further experiments.

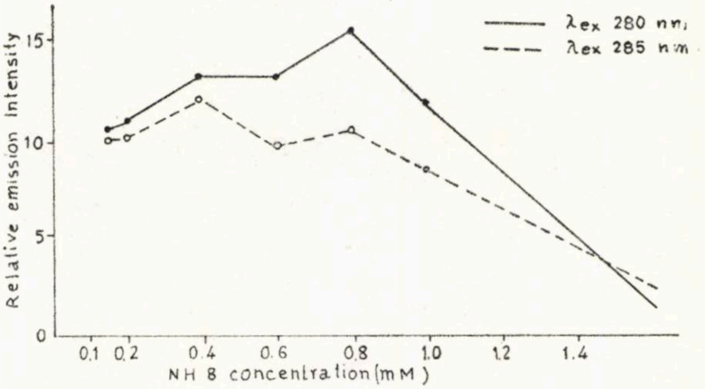

Figure 4. Tyrosyl test for NH8.

Conclusions

1. Our collagen hydrolysates do not contain Tryptophan.
2. The hydrolysates contain tyrosyl residues ; we were able to determine n_{tyr} with the method of Jankowski and Siemion.
3. n_{tyr} decreases as the mean molecular weight decreases.
4. It seems probable that at concentration of 0.6 mM occures a phenomenon of aggregation.

REFERENCES

1. G. N. RAMACHANDRAN, *Treatise on Collagen*, Acad. Press. New York, 1967
2. H. KALLMAN, V. KRASNAUSKY, P. PERSON, Photochem. Photobiol., 8, 65, (1968)
3. D. FUJIMOTO, K. AKIBA, N. NAKAMURA, Biochem. Biophys. Res. Comm., *76*, 1124 (1977)
4. A. JANKOWSKI, I. SIEMION, Acta Biochim. Polon., *24*, 1 . (1977)
5. V. TRANDAFIR, *Session of Central Institute of Biology*, 19 dec. 1979, Bucharest

Received, 21 January 1981

ANALELE UNIVERSITĂŢII BUCUREŞTI, FIZICA XXX, 1981, PAG. 107–114

A NEW METHOD FOR DETECTING THE SECOND DERIVATIVE IN INNELASTIC ELECTRON TUNNELING SPECTROSCOPY

S. I. SPÂNULESCU

Research Apparatus and Equipment Entréprise – Bucharest *

V. GHEORGHE, I. SPÂNULESCU

Faculty of Physics, University of Bucharest **

ABSTRACT

This paper presents a new experimental method aplying the innelastic electron tunneling spectroscopy (IETS). As the fields of interest for IETS are continuously increasing [5, 6] it seems to be very important that it's practical using to become as easy as possible. The electronic techniques can give some solutions in this problem as it will be seen further.

1. Introduction

In last few years a new method of spectroscopy has been developed according with the increasing field of analysis necessary in modern physics. The Innelastic Electron Tunneling Spectroscopy (IETS) seems to be the best method actually known, permitting a large variety of applications.

All the advantages specified in the literature are [3, 7] in many cases inadequalitely because of the experimental difficulties implied by the method.

The phenomena implied in IETS consist in exciting atomic and molecular vibration in a studied material by a tunneling electron current passing through [4]. The sample is formed by dopping an alluminium oxid layer on Al support with the investigated substances and adding above the second electrod (lead, usually) [3]. This "sandwich" has a resistance of $10^2 - 10^3\,\Omega$ and the current through this is composed by two fractions : an elastic tunneling electron part and an inelastic one. In the point where the energy of the electrons is equaly with the vibration energy of an atoms group, the excitation appears and supplimentary inelastic tunneling current is added. In the exterior circuit it has the effect of increasing the sample conductance. So the current-voltage characteristics is not lineray, as shown in fig. 1.

---

* Str. Fabricii nr. 47, sect. 7, Bucharest – Romania

** National Centre of Physics, P.O.Box 5211 Măgurele, Bucharest, Romania

The conductance presents in the breaking point a step (fig. 2).

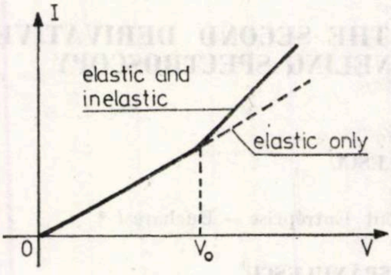

Fig. 1.

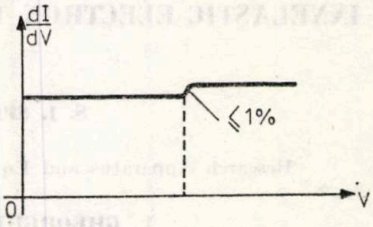

Fig. 2.

The amplitude of the step is under 1 % and so this is practically very difficult to be observed. That is why the methods of IETS use the second derivative $\frac{d^2I}{dV^2}$ shown in fig. 3, that appears like a peak, easy to be localised.

A real sample presents a large number of breaking points (or peaks in th second derivative) according to the multitude of vibration modes of the studied molecules. It is evident that each substance, each group of atoms have their own position of the peaks so that they can be recognised in a spectrum using the tables (fig. 4).

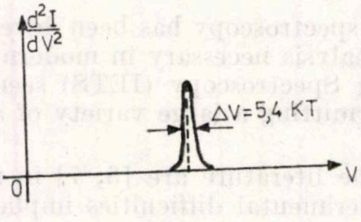

Fig. 3.

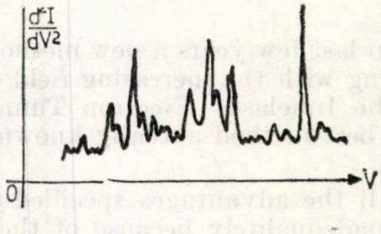

Fig. 4

The method actually used in IETS is based on the distortions introduced by the nonlinear characterstics of the sample to a sinnusoidal signal with an adjustable average value. It can be demonstrated in Fourier analysis that in certain conditions (current generator at the input) the second harmonics obtained is proportional with the second derivative $\frac{d^2I}{dV^2}$. Unfortunatelly, the signal to be detected is extremely low, $10^{-8} - 10^{-9}$ V, while the usual noise level of the electronic devices is

$10^{-4} - 10^{-7}\ V$. This implies very expensive installations including high performances filters and lock-in amplifiers. Also the modulation of the spectral line enlarges it by a factor of 10 to 100 and for good resolution liquid hellium temperatures are required [2 – 7].

2. The new method

There is no general use electronic device able to provide $\mathrm{d}I/\mathrm{d}V$; the only derivative circuit is the operational amplifier diferentiator (fig. 5)

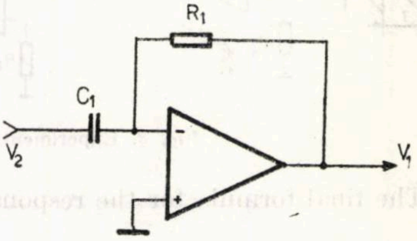

Fig. 5. **Basical differentiator circuit**

that gives $\frac{\mathrm{d}V}{\mathrm{d}t}$. We can obtain the second derivative $\frac{\mathrm{d}^2V}{\mathrm{d}t^2}$ by cascading two diferentiators:

$$v_1 = -R_1C_1\frac{\mathrm{d}v_2}{\mathrm{d}t}; \quad v_2 = R_1R_1'C_1C_1'\frac{\mathrm{d}^2v_3}{\mathrm{d}t^2}.$$

Using also a converter current-voltage at the input we have:

$$v_3 = R_3I; \quad v_1 = R_1R_1'C_3C_1C_1'\frac{\mathrm{d}^2I}{\mathrm{d}t^2}.$$

If the voltage has a time dependence $V = V(t)$ the current will be also time dependent $I = I[V(t)]$. The derivative $\frac{\mathrm{d}^2I}{\mathrm{d}t^2}$ becomes:

$$\frac{\mathrm{d}^2I}{\mathrm{d}t^2} = \frac{\mathrm{d}}{\mathrm{d}t}\left[\frac{\mathrm{d}I(V)}{\mathrm{d}t}\right] = \frac{\mathrm{d}}{\mathrm{d}t}\left[\frac{\mathrm{d}I}{\mathrm{d}V}\cdot\frac{\mathrm{d}V}{\mathrm{d}t}\right].$$

If the voltage is lineary increasing in time:

$$V(t) = V_0\frac{t}{T} = V_0\cdot\frac{\omega_0}{2\pi}\cdot t$$

$$\frac{\mathrm{d}V}{\mathrm{d}t} = V_0\frac{\omega_0}{2\pi}$$

we obtain:

$$\frac{\mathrm{d}^2 I}{\mathrm{d}t^2} = \frac{\mathrm{d}}{\mathrm{d}t}\left[\frac{\mathrm{d}I}{\mathrm{d}V} \cdot V_0 \cdot \frac{\omega_0}{2\pi}\right] = V_0^2 \frac{\omega_0}{4\pi^2} \cdot \frac{\mathrm{d}^2 I}{\mathrm{d}V^2}.$$

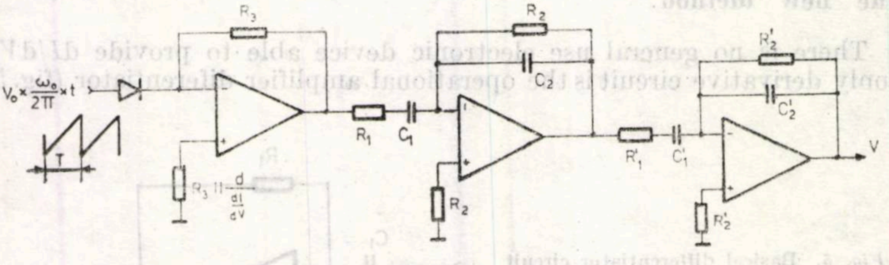

Fig. 6. Experimental circuit set-up

The final formula for the response of the circuit given in fig. 6 will be:

$$v = V_0^2 \cdot \frac{\omega_0^2}{4\pi^2} R_1 R_1' R_3 C_1 C_1' \frac{\mathrm{d}^2 I}{\mathrm{d}V^2}.$$

3. Errors and perturbations in the systhem

As we can expect. the output signal will be altered by the noise and the imperfections of the devices. For a given operational amplifier it is specified in the literature the noise voltage at the input as $e_{0n}(\omega)$, $[nV/\sqrt{\mathrm{Hz}}]$. The total noise at the input is:

$$e_n^2 = \frac{1}{2\pi^2}\int_0^{\omega_{\max}} e_{0n}^2(\omega)\,\mathrm{d}\omega. \tag{3.1}$$

At the output the noise will be:

$$N^2 = \frac{1}{2\pi}\int_0^{\omega_{\max}} A^2(\omega)\, e_{0n}(\omega)\,\mathrm{d}\omega.$$

The practical differentiator has the ideal amplification $A(\omega) = \omega RC$ only for a limited range of frequencies. As it is known for making the device stable the ideal transfer function $H(s) = -sRC$ will become:

$$H(s) = \frac{-sR_2C_1}{(1 + sR_1C_1)(1 + sR_2C_2)}$$

as in fig. 7 and fig. 8.

For limiting as much as possible the noise we shall reduce to zero the horizontal region, thus $R_1C_1 = R_2C_2$. In these conditions the asimptotic characteristics of frequency are

$$A_1(\omega) = -R_2C_1\omega \text{ for } \omega \leqslant \omega_C = \frac{1}{R_1C_1}$$

$$A_2(\omega) = -R_2C_1\frac{\omega_c^2}{\omega} = -\frac{R_2}{R_1^2C_1\omega} \text{ for } \omega > \omega_c.$$

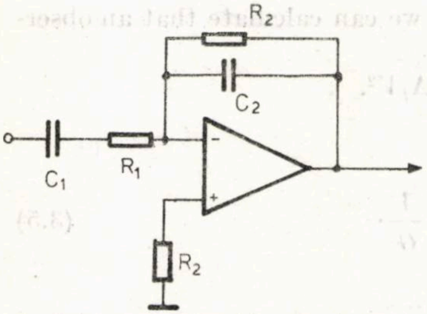

Fig. 7. Practical differentiator circuit

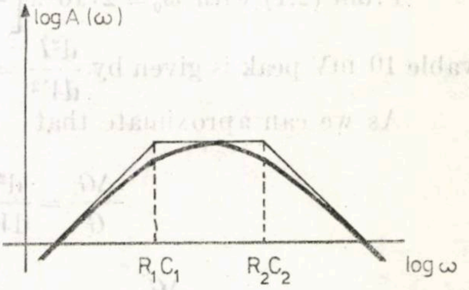

Fig. 8. Practical differentiator frequency response

As the real amplifications are allways less than those above, the noise at the output is:

$$N^2 \leqslant \frac{1}{2\pi}(R_2C_1)^4\int_0^{\omega_c}\omega^4 e_n^2(\omega)\,d\omega + \frac{1}{2\pi}\cdot\frac{R_2^4}{(R_1^2C_1)^4}\int_{\omega_c}^{\infty}\frac{e_n(\omega)}{\omega^4}\,d\omega \quad (3.3)$$

where e_n^2 is the noise voltage at the input of the first differentiator containing the noise of the converter: $e_{nc}^2 = A_c^2 e_{0n}^2$

As $A_c = R_3\dfrac{dI}{dV}$ we have:

$$e_n^2(\omega) = e_{0n}^2(\omega)\left[1 + R_3^2\left(\frac{dI}{dV}\right)^2\right].$$

Taking $e_{0n} = \max\limits_{\omega\in(0,\infty)}[e_{0n}(\omega)]$ we shall have:

$$N^2 \leqslant \frac{1}{2\pi}e_{0n}^2\left[1 + R_3^2\left(\frac{dI}{dV}\right)^2\right]\cdot\frac{8}{15}\omega_c\left(\frac{R^2}{R_1}\right)^4. \quad (3.4)$$

As an example for some reasonable values :

$$e_{0n} = 2\cdot 10^{-8}\, V/\sqrt{Hz}\,;\ R_3 = 1/\frac{\mathrm{d}I}{\mathrm{d}V} = 1\,\mathrm{K}\Omega\,;\ R_2 = 100\,\mathrm{k}\Omega\,;\ \frac{R_2}{R_1} =$$

$$= 100\,;\ C_1 = 10\mu F,$$

we obtain :

$$N \leqslant 2{,}53\ \ \mathrm{m}V.$$

From (2.1) with $\omega_0 = 2\cdot 10^2\pi\left[\frac{\mathrm{rad}}{\mathrm{s}}\right]$ we can calculate that an observable 10 mV peak is given by $\frac{\mathrm{d}^2I}{\mathrm{d}V^2} = 10^{-7}\mathrm{A}/V^2$.

As we can aproximate that

$$\frac{\Delta G}{G} = \frac{\mathrm{d}^2I}{\mathrm{d}V^2}\, VG\, \frac{1}{G}\cdot \tag{3.5}$$

the conductance step $\frac{\Delta G}{G}$ that gives this peak in liquid nitrogen ($\Delta V = 5.4\ \mathrm{k}T$) is : $\frac{\Delta G}{G} = 5\cdot 10^{-6}\%$ for the usual $G = 10^{-2}$ mho. This value is very good in comparison with the actual method that detects steps of about 0·1% — 0,5%. But, of course, some other phenomena come to limit the sensitivity of the device. One of them appears if we study the influence of R_3 to the signal to noise ratio.

From (2.1), (3.4) and (3.5) we have :

$$\frac{v_0}{N} = \frac{KR_3^2G}{\sqrt{1 + (R_3G)^2}}$$

where

$$K = \frac{R_2^2C_1^2\,\frac{V_0^2}{T^2}\,\frac{\Delta G}{G}\cdot\frac{1}{\Delta V}}{2\cdot\sqrt{\frac{\omega_c}{15\pi}}\cdot\left(\frac{R_2}{R_1}\right)^2}\cdot$$

We now see that

$$\frac{\mathrm{d}}{\mathrm{d}R_3}\left(\frac{v_0}{N}\right) = \frac{R_3KG[2 + (R_3G)^2]}{[1 + (R_3G)^2]^{2/3}} > 0,$$

and so the performances will increase unlimited with R_3; of course this is impossible, so we must have a limit for this resistor. This is evidently given by the nonlinearities of the operational amplifier that may be written in the first approximation as:

$$A = A_0 + \frac{\mathrm{d}A}{\mathrm{d}i}\,\mathrm{d}i \text{ -- open loop amplification}$$

$$z_i = z_{i_0} + \frac{\mathrm{d}z_i}{\mathrm{d}i}\,\mathrm{d}i \text{ -- input impedance.}$$

So the conversion factor α from the relation $I = \alpha v$ becomes variable, as:

$$\alpha \approx \left(\frac{1}{R_3} + \frac{1}{A_0 Z_{i_0}}\right) - \frac{1}{A_0 Z_{i_0}} \cdot \left(\frac{1}{Z_{i_0}} \cdot \frac{\mathrm{d}Z_i}{\mathrm{d}i}\,\mathrm{d}i + \frac{1}{A_0}\,\frac{\mathrm{d}A_i}{\mathrm{d}i}\,\mathrm{d}i\right)$$

and the relative error introduced is:

$$\varepsilon_\alpha \approx R_3 \frac{1}{A_0 Z_{i_0}} \cdot \left(\frac{1}{Z_{i_0}}\,\frac{\mathrm{d}Z_i}{\mathrm{d}i}\,\mathrm{d}i + \frac{1}{A_0}\,\frac{\mathrm{d}A_i}{\mathrm{d}i}\,\mathrm{d}i\right).$$

that imposes the upper limit for the R_3.

The differentiators also intoduce errors especially due to the finite open loop gain of the operational amplifiers. The differential equation that describes the real case is:

$$u_0 = -\frac{A_0}{A_0 - 1} RC \frac{\mathrm{d}u_i}{\mathrm{d}t} + \frac{R^2C^2}{A_0 - 1}\,\frac{\mathrm{d}^2 u_i}{\mathrm{d}t^2} \xrightarrow[A_0 \to \infty]{} - RC \frac{\mathrm{d}u_i}{\mathrm{d}t^2}.$$

Even in the practical differentiator given in figure 7 the higher order derivatives will appear:

$$u_0 = -R_2 C_1 \frac{A_0}{A_0 - 1}\,\frac{\mathrm{d}u_i}{\mathrm{d}t} + \frac{R_2^2 C_1}{A_0 - 1}\,[C_1 - (A_0 - 1) C_2]\,\frac{\mathrm{d}^2 u_i}{\mathrm{d}t^2}.$$

A good rejection of these terms is obtained for a value of C_2 enough high to have $C_2 = \frac{C_1}{A_1(\omega) - 1}$. But, on the other hand, it is known that for a transfer function as in (3.2.) the response to a step function is not an ideal Dirac function, being (fig. 9):

$$u_0(t) = \frac{R_2 C_1}{R_2 C_2 + R_1 C_1}\left(\mathrm{e}^{-\frac{t}{R_2 C_2}} - \mathrm{e}^{-\frac{t}{R_1 C_1}}\right).$$

All these effects must be taken into account when practical design of such an installation is made.

Our experiments revealed that a corect compromise between the parameters can be obtained from case to case by correctly choosing ω_0. With μA471 amplifiers and the given values for the components the niose level in the output was about 6 mV peak to peak. Using a classic $Al-Al_2O_3-Pb$ sandwich we could observe on the oscilloscope some C_6H_6 and CH_3OH spectra in liquid nitrogen similar to those given in the literature [7]. For a $\frac{\Delta G}{G} = 10^{-5}\%$ electronically simulated step in conductance, the output signal was about 24 mV.

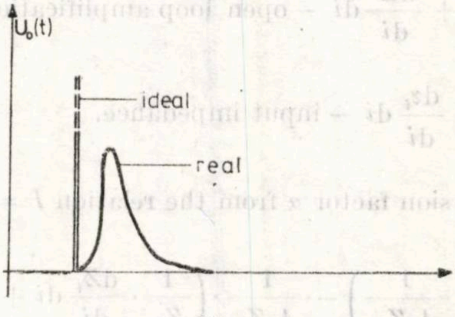

Fig. 9.

4. Conclusions

The actually experimental techniques in IETS are rather far from the best possible. The new method is a step in improving the performances of this spectroscopy making it more accesible and having a large area of further development. For the presented installations, the noise and perturbations levels were theoretically calculated and the correspondance with the experiments was good. Their effects must be taken into account, making a resonable compromise between the installation's parameters for properly using the advantges of the new method.

REFERENCES

1. L. ESAKI, Phys. Rev. *109*, 60 (1957).
2. I. GIAVAER, Phys. Rev. *5*, 147 (1960).
3. R. C. JAKLEVIC, J. LAMBE, Phys. Rev. *17*, 1139 (1966).
4. D. J. SCALAPINO, S. M. MARCUS, Phys. Rev. *18*, 497 (1967).
5. A. YELON, etc. Surd. Sci. *43*, 353 (1974).
6. J. T. HALL. P. K. HANSMA, M. PARIKH, Science 188, 1304 (1076).
7. J. BARDEEN, Phys. Rev. *6*, 57 (1961).
8. J. KIRTELY, D. J. SCALAPINO, P. K. HANSMA, Phys. Rev. 14, 3177 (1976)

BUDAPESTI MŰSZAKI EGYETEM KÖZPONTI KÖNYVTÁRA 1848

Abonamentele în țară se pot contracta la oficiile P.T.T.R., agenții poștali și factorii poștali.

Cititorii din străinătate se pot abona, adresîndu-se la ILEXIM Departamentul Export-Import Presă, P.O. Box 136—137, telex: 11229, București str. 13 Decembrie nr. 3.

c. 1237 – I. P. „INFORMAŢIA"

Lei 22